Alma Mater Studiorum - Università di Bologna

SCUOLA DI SCIENZE

Dipartimento di Chimica Industriale "Toso Montanari"

Corso di Laurea Magistrale in

Chimica Industriale

Classe LM-71 - Scienze e Tecnologie della Chimica Industriale

Cadmium Telluride Magic-Sized Clusters and Superstructures

Tesi di laurea sperimentale

CANDIDATO

Claudia Spallacci

RELATORE

Prof.ssa Cristina Femoni

CORRELATORE

Dr. Celso de Mello Donegà

Anno Accademico 2019-2020

ABSTRACT

The aim of the present work is to gain new insights into the formation mechanism of CdTe magic-sized clusters (MSCs) at low temperatures, as well as on their evolution towards 1D and 2D nanostructures and assemblies thereof, under mild reaction conditions. The reaction system included toluene as solvent, octylamine as primary alkylamine, trioctylphosphine-Te as chalcogenide precursor and $Cd(oleate)_2$ as metal precursor. UV-Vis absorption spectroscopy and transmission electron microscopy (TEM) were used to analyze samples containing concentrations of octylamine of 0.2, 0.8 and 2 M: well-defined, sharp absorption peaks were observed, with peaks maxima at 449, 417 and 373 nm respectively, and 1D structures with a string-like appearance were displayed in the TEM images. Investigating peaks growth, step-wise peaks shift to lower energies and reverse, step-wise peak shift to higher energies allowed to propose a model to describe the system, based on interconnected $[CdTe]_x$ cluster units originating an amine-capped, 1-dimensional, polymer-like structure, in which different degrees of electronic coupling between the clusters are held responsible for the different absorption transitions. The many parameters involved in the synthesis procedure were then investigated, starting from the Cd:Te ratio, the role of the amine, the use of different phosphine-Te and Cd precursors. The results allowed to gain important information of the reaction mechanism, as well as on the different behavior of the species featuring the sharp absorption peaks in each case. Using $Cd(acetate)_2$ as metal precursor, 2D structures were found to evolve from the MSCs solutions over time, and their tendency to self-assemble was then analyzed employing two amines of different alkyl chain length, octylamine (C-8) and oleylamine (C-18). Their co-presence led to the formation of free-floating triangular nanosheets, which tend to readily aggregate if only octylamine is present in solution.

ABSTRACT (ITA)

Lo scopo di questo elaborato di tesi sperimentale è quello di investigare il meccanismo di formazione di magic-sized clusters (MSCs) di CdTe, così come la loro evoluzione in nanostrutture 1- e 2-dimensionali e in aggregati delle stesse, a temperatura ambiente (o poco superiore). Il sistema di reazione comprende toluene come solvente, ottilammina come ammina primaria, triottilfosfina-Te e oleato di Cd come precursori di Tellurio e Cadmio, rispettivamente. Spettroscopia di assorbimento UV-Vis e microscopia a trasmissione elettronica (TEM) sono state usate per analizzare campioni contenenti concentrazioni di ottilammina pari a 0.2, 0.8 e 2 M: sono stati osservati picchi stretti e ben definiti, con massimi rispettivamente a 449, 417 e 373 nm. Le immagini TEM mostrano strutture 1-dimensionali che appaiono come lunghi filamenti. Esaminando la crescita dell'intensità di picchi e il loro shift in modo discreto verso energie minori o maggiori, ha permesso di proporre un modello per descrivere il sistema, in cui unità di [CdTe] clusters interconnesse originano una struttura 1-dimensionale simil-polimerica rivestita di ammine, nella quale vari gradi di coupling elettronico sono responsabili delle diverse transizioni negli spettri di assorbimento. I numerosi parametri coinvolti nella sintesi, come il rapporto Cd:Te, il ruolo dell'ammina, e l'uso di diversi precursori di Te e di Cd, sono stati esaminati più approfonditamente. I risultati ottenuti hanno permesso di comprendere meglio il meccanismo di reazione, così come il diverso comportamento delle specie che danno origine ai picchi di assorbimento ad energie ben definite. Usando acetato di Cd come precursore, è stata osservata l'evoluzione di nanostrutture 2-dimensionali dalle soluzioni contenenti i MSCs nel tempo, e la loro tendenza ad auto-assemblarsi è stata analizzata utilizzando due ammine di diversa lunghezza, ottilammina (C-8) e oleilammina (C-18). La loro co-presenza ha portato alla formazione di nanosheets triangolari separati tra loro, che tendono ad aggregarsi quando in soluzione è presente solo ottilammina.

Contents

1. Introduction

One of the more dynamic and multidisciplinary research field of the last decades is the study of colloidal semiconductor nanocrystals (NCs). The increasing interest in these materials stems primarily from their distinctive feature of having size- and shape-dependent optoelectronic properties, combined with easy surface manipulation and solution processing. Because of these properties, nanomaterials are promising for various applications in many fields, such as in light emitting devices (LEDs), solar cells, luminescent solar concentrators (LSCs), optoelectronics, sensing, thermoelectrics, catalysis and biomedical sciences. [1] Worldwide research activity has resulted in a remarkable degree of control over the composition, size, and shape of colloidal semiconductor NCs, allowing for the investigation of zero-dimensional, one-dimensional and two-dimensional morphologies such as quantum dots (QDs), nanowires (NWs), and nanoplatelets (NPLs), respectively. The latter gained increasing popularity since the discovery of the unexpected properties of graphene in 2004, [2] which pushed research not only on graphene itself, but also on other 2D materials, such as transition metal dichalcogenides and colloidal 2D NCs.

The aforementioned properties of semiconductor nanocrystals arise from the so-called "quantum confinement" effect, which sets in when their dimensions become comparable or smaller than the exciton Bohr radius, a characteristic length that account for the spatial extension of the excitonic wave function in the material (where "exciton" is the term which indicates a localized, mobile excited state represented by a bound electron-hole pair in a semiconductor). One of the direct consequences of quantum confinement is that the band gap between the conduction and valence band of a semiconductor becomes size dependent, increasing with decreasing size of the nanocrystal, thus allowing tailoring of material optoelectronic properties. The extent of quantum confinement effect in nanocrystals of comparable sizes is strongly dependent on their composition, since the exciton Bohr radius ranges from ~2 to ~50 nm depending on the semiconductor.

One of the most interesting outcomes of the research on semiconductor nanocrystals has been the discovery of the so-called magic-size clusters (MSCs). Their properties strongly differ from those of conventional NCs, even though they have been accounted as intermediates in the formation of NCs.[3] MSCs experience strong 3D quantum confinement owing to the very small sizes (< 2 nm, < 100 atoms) that are usually significantly smaller than the exciton Bohr radius, which causes an increase in the exciton transition energy and correspondingly a blueshift of the peaks in the optical absorption and emission spectra. Well-defined, narrow absorption peaks have been observed at high energies in the early stages of NCs growth and have been ascribed to the formation of clusters of well-defined stoichiometry, size, and shape, located in local minima of the potential energy landscape. [4] Despite the intensive research work over the past few years, a general agreement on the exact composition, structure, or formation mechanism of MSCs has not yet been reached. Further investigation both on the nature and formation pathways of MSCs, and on their role in the synthesis of 2D colloidal NCs would provide an essential knowledge to better control and engineer these materials, which have been shown to possess remarkable optical properties. In the field of MSCs and corresponding colloidal 2D NCs, the most investigated ones belong to the II-VI semiconductors family, with II = Zn, Cd and VI = S, Se, Te.

The aim of the present work is to gain new insights into the formation mechanism of CdTe magic-sized clusters at low temperatures, as well as on the evolution towards 1D and 2D nanostructures and assemblies thereof, under mild reaction conditions.

This Thesis is divided into five chapters, the first being the Introduction. Chapter 2 provides an essential theoretical background on confining effects in semiconductor nanocrystals, nucleation and growth theories of nanoparticles, and present the current state-of-the-art on the topic of magic-sized clusters and their role in the formation of 2D nanocrystals, by revising the most recent literature. The synthesis protocols and methodologies of analysis and characterizations are described in detail in Chapter 3. The experimental results are illustrated and extensively discussed in Chapter 4: in particular, Section 4.1 is focused on room-temperature synthesis of CdTe magic-sized clusters, and

presents a thorough study of the many parameters involved, leading to the proposal of a model involving non-classical pathways of nucleation and growth, while Section 4.2 is dedicated to the investigation of 2D structures and larger assemblies, which follow the MSCs evolution. In Chapter 5, conclusions are drawn on the formation of CdTe MSCs and their superstructures as investigated in this work, and further perspectives for future work are considered.

2. Theoretical background

2.1. Size effects on semiconductor nanoparticles

Nanomaterials possess the distinctive feature of having physical and chemical properties that are size dependent. At the nanoscale, it possible to engineer the properties of a material of definite chemical composition, by tailoring the size and shape, and the way in which individual nanostructures are further assembled. The origin of the size dependence of nanomaterials properties can be traced to two fundamental nanoscale effects: first, the fraction of surface atoms (*i.e.* surface/volume ratio) increases with decreasing size and becomes significantly large in nanoparticles, and secondly, the limited dimensions lead to spatial confinement effects, that have consequences on different physical properties depending on the material (metal, semiconductor,…). [5] The scaling effect, common for all nanomaterials, increases the free energy of the system and makes it more reactive and dynamic, thus modifying a number of properties (e.g. solubility, melting and evaporation temperatures, plasticity etc.). On the other hand, the second effect is material dependent. In this Thesis, the discussion will be limited to spatial confinement effect in semiconductors, better known as quantum confinement, which induces changes in the optical and electronic properties of the nanostructures. In the case of nanoparticles of semiconductors, this can be noticed when their dimensions become comparable or smaller than the spatial extension of excitons (i.e. electron-hole pairs), also known as the exciton Bohr radius (a_0). In the quantum confinement regime, the exciton wave function is perturbed, and this induces changes in the electronic structure of the material and determines different optical properties that manifest in the size-dependent absorption (and photoluminescence) spectra of semiconductor NPs.

2.1.1 - Electronic structure of bulk semiconductors

To better understand the impact of size reduction in semiconductor nanostructures, it is useful to first consider the electronic structure of bulk semiconductor materials. Electrons in a semiconductor experience a periodic potential caused by the atoms in the crystal lattice. This potential causes an important change in the dispersion relation

describing the energy levels for electrons: when the wavelength of the electron is about twice the lattice spacing, the electron waves will experience Bragg reflections due to the periodic potential of the lattice, occurring at specific locations (i.e. $k = n\pi/a$, where k is the wave vector of the wavefunction). The result of these reflections are energy gaps in the dispersion relation, often referred to as band gaps. In a 3D crystal lattice, the periodicity is not the same in the three dimensions, so the electron will experience different Bragg reflections when travelling in different directions, leading to multiple band gaps and thus to a more complex band structure. The energy bands can be occupied by electrons and the degree of occupation will determine the electronic properties of the solid. The highest occupied energy band is called the valence band (VB) and the lowest unoccupied energy band is referred to as conduction band (CB). The energy difference between the VB and CB is referred to as the fundamental band gap. For semiconductors, the fundamental energy gap is smaller than 4 eV, which allows electrons to be thermally excited from the VB to the CB at sufficiently high temperatures. When an electron from the valence band gets sufficient energy to overcome the energy gap, usually by the absorption of a photon, and is promoted to the conduction band, a "hole" (i.e. a *quasi*-particle correlated with the VB from which an electron is removed) is left behind. Due to their charge, electrons and holes are denoted as charge carriers, and interact via a Coulomb potential, forming electron-hole pairs that can be described as *quasi*-particles (the 'excitons'). The most probable distance between the electron and the hole in an exciton is given by the so-called exciton Bohr radius (a_0), which ranges from ~2 to ~50 nm depending on the semiconductor. The exciton Bohr radius provides a very useful length scale to describe the spatial extension of excitons in semiconductors and allows to predict at what nanoparticle size different materials will start to experience the effects of quantum confinement.

2.1.2 - Electronic properties of semiconductor nanocrystals

As introduced above, when the dimensions of a material are decreased until the nanoscale ($\leq$ 100 nm) is reached, its intrinsic properties start to change and may be strikingly different from those of its bulk counterparts. The electronic structure of a semiconductor nanocrystal changes and becomes size (and shape) dependent when its

dimensions become comparable to the exciton Bohr radius of the bulk material. In these conditions, the exciton energy levels are affected due to the spatial confinement of the exciton wave function. The exciton Bohr radius a_0 provides a very convenient length scale to evaluate the impact of quantum confinement on the properties of semiconductor nanocrystals, because quantum confinement effects will occur at different dimensions for different semiconductors, since the exciton Bohr radius varies widely within the semiconductor materials.

Quantum confinement leads to two important consequences in semiconductor nanocrystals: firstly, the band gap becomes larger with decreasing size (scaling as D^{-2} if the Coulomb interaction is negligible) and secondly, discrete energy levels (with different quantum numbers) arise at the band-edges of both the conduction band and valence band.

A useful way to describe the electronic structure of nanocrystals is by considering them as large molecules, their energy levels as molecular orbitals (MOs) obtained by Linear Combination of Atomic Orbitals (LCAO) (Figure 2.1). In the simplest example of the homodiatomic H_2 molecule, from the combination between two atomic orbitals (AOs), two MOs arise, delocalized over both atoms. The bonding MO is lower in energy with respect to the individual AOs, while the anti-bonding MO is higher in energy. To minimize the energy, the two electrons originally occupying the AOs, will occupy the bonding MO and the anti-bonding MO will be left empty. In general, the highest occupied and lowest unoccupied molecular orbital are referred to as HOMO and LUMO, respectively. For a sufficiently large number of atoms, hence of atomic orbitals (AOs) combining to form MOs (*i.e.* in the bulk material), the energy levels become so numerous and so closely spaced that a *quasi*-continuum (*i.e.*, an energy band) is formed both from the bonding and from the anti-bonding MOs, analogous to the valence and conduction bands described in the above paragraph. A semiconductor nanocrystal instead, consists of a few tens to a few thousand atoms, forming as many MOs from the linear combination of their atomic valence orbitals. Therefore, its electronic structure will be characterized by energy bands with a large density of levels at intermediate

energy values and more sparse, discrete energy levels near the band edges, where the density of MOs states is small. Moreover, the HOMO-LUMO energy gap will be larger than in the bulk and size-dependent, increasing with decreasing size of the nanocrystal (Figure 2.1).
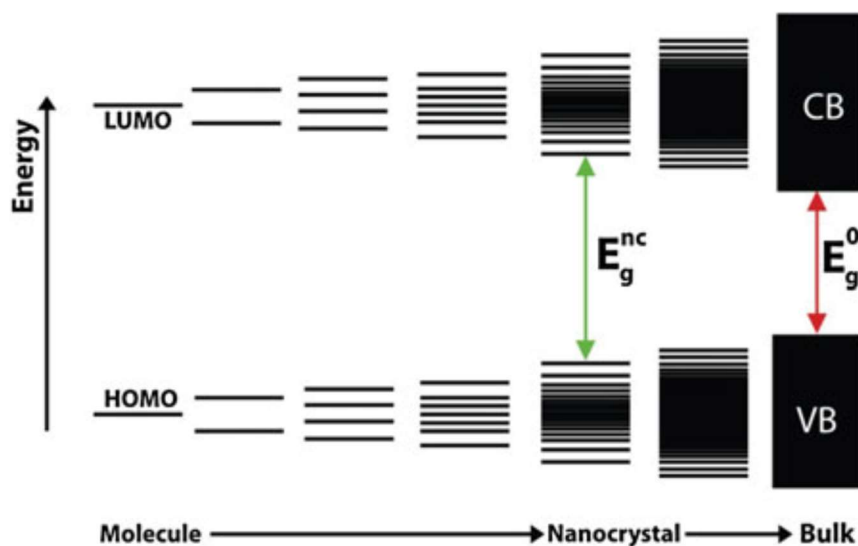

Figure 2.1. Evolution of the energy level structure from a hypothetical diatomic molecule (extreme left) to a bulk semiconductor (extreme right). E_g^{nc} and E_g^0 indicate the energy gap between the highest occupied molecular orbital (HOMO) and the lowest unoccupied molecular orbital (LUMO) for a nanocrystal and bulk. Reprinted with permission from Ref. [6]

Quantum confinement effects are reflected in the optical absorption (and photoluminescence, PL) spectra of semiconductors: since, as discussed above, the optical band gap of nanocrystals can be tuned by simply changing their size, the onset of the absorption (and the maximum of the PL) and therefore the perceived color are size-dependent (Figure 2.2). Additionally, the energy spacing between the discrete levels at the edges of the valence and conduction bands is in the order of hundreds of meV, and therefore optical transitions between these levels can be clearly resolved in the optical absorption spectrum. The lowest energy optical transition can be assigned to the $1S_h$ to $1S_e$-level (h denotes the hole and e the electron), the second transition to the $1P_h$ to $1P_e$ level, and so on (Figure 2.3).
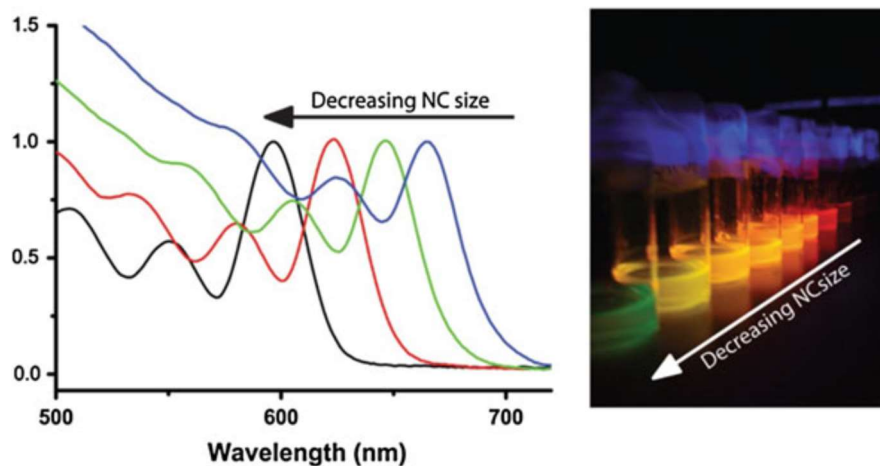
Figure 2.2. (Left) Absorption spectra of colloidal suspensions of CdTe nanocrystal (NC) quantum dots of different sizes. (Right) Photograph of vials containing colloidal suspensions of CdTe QDs of different sizes under UV excitation. Reprinted with permission from Ref. [6]
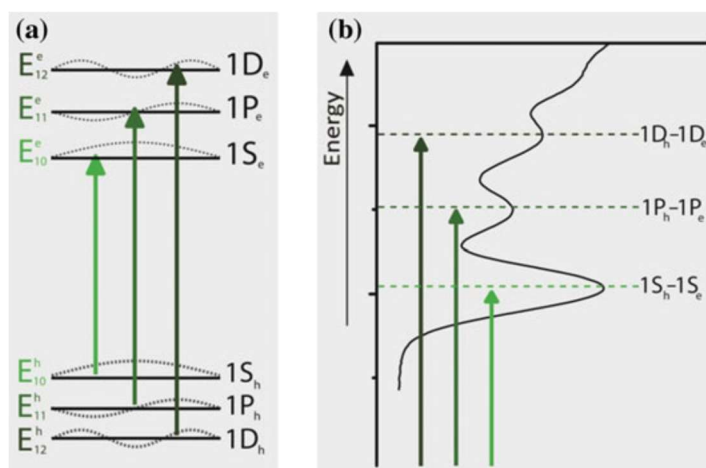
Figure 2.3. (a) Three lowest electron and hole energy levels in a semiconductor nanocrystal quantum dot. Allowed optical transitions are given by the arrows. (b) Assignment of the transitions in the absorption spectrum of colloidal CdTe quantum dots. Reprinted with permission from Ref. [6]

If the confinement is the same in all directions, the nanocrystal can better be represented as a zero-dimensional spherical potential well (i.e., a quantum dot, QD). Nevertheless, it is also possible to have non-spherical QDs, provided all dimensions are small enough with respect to a_0. In such a case, the electronic structure of the QD will still be characterized by a series of discrete energy levels (Fig. 2.4). The degree of quantum confinement may also vary along different directions depending on the nanostructure shape. If only the diameter of an anisotropic NC is sufficiently small to induce quantum

confinement, the exciton will experience a 2-dimensional confinement and the nanocrystal will then be referred to as a Quantum Wire or Quantum Rod, depending on its relative aspect ratio (wires are significantly longer than a_0, while rods have lengths smaller than a few a_0). If the exciton is confined only in the thickness direction, a Quantum Well is formed (1-dimensional confinement).
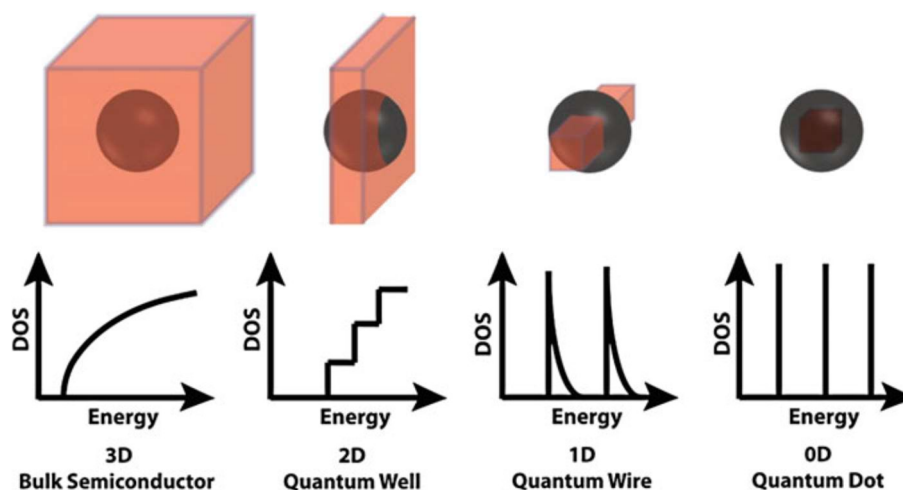
Figure 2.4. Schematic illustration of the energy level structure of semiconductor nanostructures with reduced dimensionality. The exciton Bohr diameter is represented by the sphere while DOS gives the density of states.

2.2. Nanocrystals formation

A colloidal crystalline nanoparticle can be described as a multifaceted inorganic nanocrystal coated with amphiphilic organic ligands, forming the surfactant layer. The properties of this hybrid system are thus dictated not only by the individual characteristics of the inorganic core and the organic shell, but also by their relative interactions, which play a very important role in the synthesis process. The complex interplay of the interactions between the atoms composing the nanocrystal, those between the surface atoms and the polar head of the organic surfactant molecules, and the intermolecular interactions between the surfactant molecules at the surface and in

solution, is the driving force behind the remarkable control achieved over the composition, size, and shape of NPs.

2.2.1 - Nucleation and growth of nanoparticles

Despite the large amount of publications on colloidal NCs synthesis, the underlying mechanism leading to nucleation and growth is still a matter of debate. This subsection illustrates the model of classical nucleation and growth, emphasizes its limitations to describe real systems due to some unrealistic assumptions and offers alternative non-classical paths to explain the many exceptions.

Prior to the formation of nuclei, the induction or pre-nucleation period encompasses the series of chemical reactions that bring to the formation of "monomers" (basic unit of crystal, f.i. [CdTe] stabilized by ligand molecules). This stage ends when the monomer concentration exceeds a critical value of supersaturation (temperature dependent), and nucleation occurs.

In the classical nucleation theory (CNT), the high thermodynamic energy barrier for homogeneous nucleation originates from the high surface to volume ratio of the nuclei. Given that the surface energy per area, γ, and the bulk energy per volume, ΔG_v, are assumed to be constant, the total change in free energy change, ΔG, resulting from homogeneous nucleation is written as:

$$\Delta G_{hom}(r) = 4\pi r^2 \gamma + 4/3\pi r^3 \Delta G_v \qquad (1)$$

where r is the radius of a spherical nucleus. From the condition $d[\Delta G_{hom}(r)]/dr = 0$, the critical radius, $r^* = -2\gamma/\Delta G_v$, is derived. Only the nuclei with $r \geq r^*$ can spontaneously grow into larger particles ($d[\Delta G_{hom}(r)]/dr < 0$), whereas those with $r < r^*$ will redissolve in the solution. In nonclassical nucleation theory on the contrary, γ and ΔG_v are not constant with respect to particle size. Instead, there are intermediate structures with lower surface and/or bulk energy, which provide alternative pathways to circumvent the high energy barrier of homogeneous nucleation (Figure 2.5).
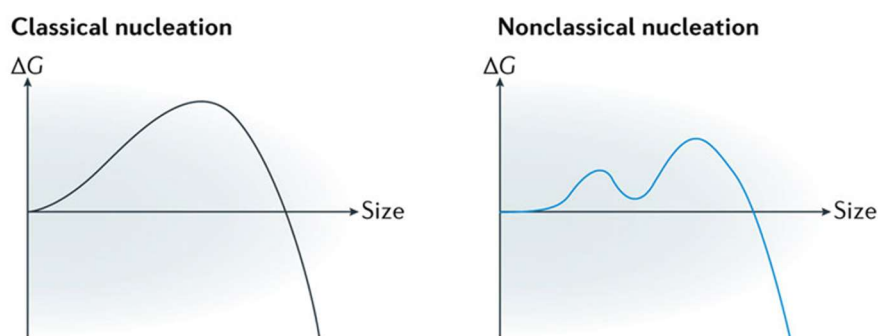
Figure 2.5. Examples of simplified free energy diagrams displaying classical (left) and non-classical (right) nucleation pathways with increasing size. Reprinted from Ref [7].

These alternative pathways can involve the formations of clusters with particular stability due to their geometrical and/or electronic configuration, which corresponds to local minima in the potential energy landscape (lower bulk free energy), or a two-step nucleation via amorphous nuclei, or nuclei with crystalline core and amorphous shell (lower surface free energy because of the disordered interface). Another non-classical nucleation pathway, whose origin is kinetic rather than thermodynamic, is the aggregation of subcritical nuclei ($r < r*$). According to CNT, these nuclei should redissolve but if their dissolution rate is much slower than their collision rate, nucleation can still occur at low supersaturation, in an equivalent of "tunneling" through the free energy barrier. [7]

Analogously, alongside classical growth, which proceeds via sequential addition of monomer units to the growing nanoparticles, non-classical growth pathways exist. The latter proceed via assembly and merging of nanoparticles and can result in highly anisotropic nanostructures.

2.2.2 - Colloidal synthesis of nanocrystals

Colloidal synthesis of nanoparticles is carried out in liquid phase under conditions that allow the growth to be controlled and arrested when the size is still in the nanoscale. In the case of II-VI semiconductor nanoparticles, this is achieved by reacting precursors, which contain metals and chalcogenides (*e.g.* organometallic compounds or inorganic salts), at sufficiently high temperatures and/or concentrations in the presence of

11

coordinating ligands (amphiphilic molecules). The (thermal) decomposition of the precursors results in a high concentration of metal and chalcogenide ions (atoms) over a short period of time, which leads to nucleation followed by growth of the NPs. Ligands, introduced as solvent (e.g. alkylamines), as part of the precursor compound (e.g. Cd oleate) or as additives (e.g. alkylamines, carboxylic and phosphonic acids, thiols…), serve and essential role in NPs synthesis, since they control both the nucleation and the growth rates. The binding strength of ligand-metal/chalcogenide determines the decomposition rate of the precursors and the binding dynamics of the ligand to the NP surface.

Absorption spectroscopy represents a valuable technique to follow nanocrystals growth, since, as mentioned above, the electronic structure of semiconductor NCs is size dependent (band gap decreasing with increasing particle size). As NCs grow, the lowest energy absorption peak shifts *continuously* toward lower energies, as a consequence of increasing size.
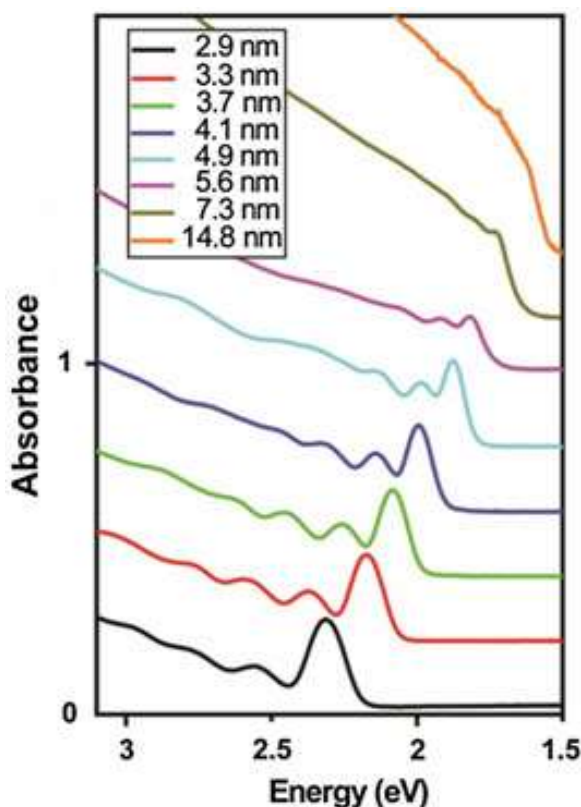
Figure 2.6. UV-vis absorption spectra of colloidal CdTe nanocrystals of increasing size.

Under some circumstances, sharp and narrow peaks have been observed in the early stages of the NC growth, which have been ascribed to the presence of clusters with well-defined geometry and/or electronic configuration, composed of tens to a hundred atoms and often referred to as "magic-sized clusters" (MSCs). MSCs are characterized by a much higher thermodynamic stability with respect to slightly larger or slightly smaller clusters, and the growth in the "magic-size regime" (i.e. diameter d ≤ 2 nm) has been observed to proceed in a *stepwise* fashion, from a higher energy peak to the next, towards lower energies, before eventually turning into the continuous growth of regular NCs. [8] As a result of their ultrasmall dimensions, magic-size clusters experience strong quantum confinement as their size is significantly smaller than the exciton Bohr radius (viz, a_0 = 7.3 nm for CdTe). Their exciton transition energies remarkably increase compared to the bulk and correspond to a marked blueshift of their peaks in the optical absorption and emission spectra. [9]

2.2.3 - Colloidal nanocrystals vs Magic-sized clusters

Although magic-sized nanoclusters can share similar properties with small nanocrystals, two fundamental features lead to their different classification.[4] The first one is the remarkably narrow absorption peaks observed for magic-sized clusters, compared to the broader peaks which small nanocrystals display. The narrow absorption peaks have been attributed to the fact that MSCs consist of a small number of atoms in a well-defined geometry, thus their optical feature do not suffer from inhomogeneous broadening caused by size distribution and display small values of full widths at half maximum (fwhm). In contrast, small nanocrystals have an unavoidable size distribution that depends on the synthetic conditions, leading to the inhomogeneous broadening of the peaks.

The second distinguishing feature is the growth of magic-sized clusters compared to ultrasmall nanocrystals. Ultrasmall nanocrystals grow continuously, displaying a continuous red shift of the absorption peak, while the growth in the case of magic-sized clusters is observed to progress stepwise (Figure 2.7). If followed with UV-Vis absorption spectroscopy, the higher energy peaks decrease in intensity, while red-shifted

peaks arise and increase in intensity over time. This behavior has been previously attributed to the formation of clusters of increasing size which, due to their well-defined stoichiometry, size, and shape, are placed in deep, local minima in the potential energy landscape. [10] Nevertheless, a general agreement on the formation mechanisms as well as on the exact structures of these species has not been yet reached.
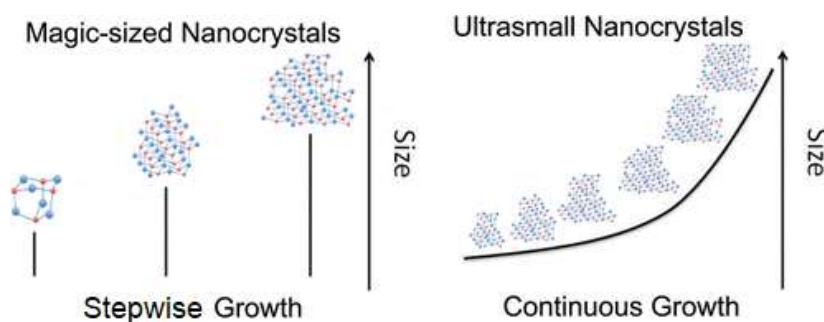
Figure 2.7. Schematic description of the stepwise growth attributed to MSCs compared to conventional NCs continuous growth. Adapted from Ref. [4].

2.2.4 - Formation pathways of MSCs

Since the existence of MSCs is attributed to the presence of local minima in the energy landscape, synthetic protocols need to provide conditions under which these are metastable (e.g. low temperatures, presence of mesophase that constrain the growth). [11] Isolation from the reaction mixture after rapid quenching of the growth reaction has been followed by dedicated synthetic routes to form MSCs under much milder conditions. However, it is still under debate if the same species form in these two synthetic approaches, which can be generally distinguished as: (i) high temperatures with negatively charged ligands (carboxylates, phosphonic acids) and (ii) low temperatures with neutral ligands (alkylamines). Even if the absorption peaks fall at similar positions, in (i) they are attributed to non-stoichiometric (Cd-terminated) nanoclusters, with zinc blende crystal structure, while in (ii) they are ascribed to stoichiometric nanoclusters, with cage-like or slightly elongated tubular structure.

Since in this Thesis, the latter synthetic routes were employed, the discussion will be limited to these species in the rest of the paragraph. The lack of reliable *in situ* analyses

on the required time scales has led to the proposal of many different formation mechanisms, however a general distinction can be made between two main views.

The first approach supports the evolution of MSCs species from preassembled, amorphous precursor compounds, at room temperature (or slightly above), according to a two-step non-classical nucleation pathway. [12][13] The presence of the amorphous precursors has been detected by MALDI-TOF mass spectrometry, and their conversion to MSCs involves changes in surface capping, suggesting that clusters families with the same core composition but different external structure or shape can occupy different potential energy local minima. In particular, the evolution between several CdTe species has been previously reported, following the sequence: CdTe-371 →CdTe-417 → CdTe-448 → CdTe-371(doublet), where each species is denoted by the lowest energy peak position, expressed in nm. The observed trend cannot be unambiguously explained by stepwise increasing sizes, since the final species has the same absorption edge as the initial one (the intensity ratio between the first two excitonic transitions is however very different). The authors proposed the possibility of these clusters sharing the same core composition but differing in the outer structure or shape. It is worth mentioning that the differences in absorption spectra are strongly correlated with the concentration of ligands. Reversible isomerization between CdS magic-sized clusters has also been reported to be promoted by temperature and ligand shell configuration, as observed by the interconversion between well-distinct absorption peaks. [14][15]

The second approach is based on the role of mesostructures. Mesophases are partially ordered structures and are characterized by well-defined peaks in small-angle X-ray scattering (SAXS), [16] and/or optical birefringence. Buhro and co-workers reported that, at lower temperatures, MSCs form within a lamellar surfactant mesophase or liquid crystalline structure that is composed of the precursors. [17] Robinson *et al.* suggest their presence as organic-inorganic templates in which the clusters can grow, [18] while Liu, Y.-H *et al.* support the formation of MSCs tubular assemblies, held together by dipole interactions between the inorganic clusters. [19] A template effect has also been used to describe the non-classical growth of a 1D coordination polymer, in which ligands

function as bridges between the constituent MSCs. [20] In several cases, the presence of a ligand-promoted mesostructure has also been found responsible for the evolution of 0D (nanoclusters) into 2D structures (i.e. nanosheets, nanoplatelets, nanobelts). [21][22]

These two formation mechanisms are probably not at all separated, but rather interrelated and co-existing in these systems, representing two aspects of the same complex series of events, which cannot be described by a classical approach.

A general theory for the non-classical nucleation and growth of magic-sized clusters is needed, which, taking into consideration all the different "players", succeeds in explaining the origin of their metastability, their optical properties and the observed interconversion between their narrow absorption features, in relation to the cluster structures.

3. Experimental Section

3.1. Materials

The experimental work was performed in a Korea Kiyon glovebox under N_2, with H_2O and O_2 levels of 0.0 and 0.1 ppm, respectively. The antechamber was evacuated once when taking items out of the glovebox and three times when bringing items into the glovebox.

The chemicals used for the experimental work described in the next section were bought from Sigma Aldrich unless otherwise stated. The following solvents were used: toluene (Alfa Aesar anhydrous, 99.8%; packaged under Argon), 1-octadecene (ODE, technical grade, 90%; degassed on a Schlenk line), n-hexane (Fischer Scientific, anhydrous), tetrahydrofuran (THF, anhydrous, 99.9%), dibutyl ether (DBE, anhydrous, 99.3%), tetrachloroethylene (TCE, anhydrous, $\geq$ 99.9%), hexadecane (HDE, 99%), methyl acetate (anhydrous, 99.5%), ethyl acetate (anhydrous, 99.8%). The selected alkylamines were: butylamine (99.5%), amylamine (99%), hexylamine (99%), heptylamine (99%), octylamine (OTA, 99%), di-n-octylamine (97%), tri-n-octylamine (98%), dodecylamine (98%), octadecylamine (technical grade, 90%), oleylamine (OLAm, degassed on a Schlenk line, $\geq$ 98%). The reagents used for the synthesis of the Cd precursors were: Cd oxide (99.99%), Cd(acetate)$_2$ (anhydrous, 99.995%), CdMe$_2$, oleic acid (technical grade, 90%), stearic acid (95%). Tellurium powder (-30 mesh, 99.997% trace metals basis) was used for the synthesis of the chalcogenide precursors, dissolved in either trioctylphosphine (TOP, technical grade, 90%), triphenylphosphine (TPP, 99%), tributylphosphine (TBP, 99%), triphenylphosphite (TPT, 97%), diphenylphosphine (DPP, 98%), chlorodiphenylphosphine (ClDPP, 96%) or diterbutylphosphine (DTP, 98%). Other chemicals used during the experimental work were didodecyldimethylammonium bromide (DDAB, 98%), ammonium bromide (NH$_4$Br, 98%), hexadecyltrimethylammonium bromide (HTAB, $\geq$ 99%), hexadecyltrimethylammonium chloride (HTAC, $\geq$ 98%), sodium myristate ($\geq$ 99%).

3.2. Experimental methods

3.2.1 - Preparation of the Cd- and Te-precursors

Cadmium oleate: 0.1 M Cd(oleate)$_2$ in octadecene (ODE) was synthesized by heating 1.284 g of CdO (0.01 mol), 11.299 g of oleic acid (0.04 mol) in 100 mL of ODE at 220 °C on a Schlenck line under N$_2$ for 2 h until all the CdO was dissolved. Then this solution was cooled to 100 °C and degassed under vacuum for 2 h.

Cadmium stearate: 0.1 M Cd(stearate)$_2$ in octadecene (ODE) was synthesized by heating 0.624 g of CdO (0.005 mol), 5.690 g of stearic acid (0.02 mol) in 50 mL of ODE at 240 °C on a Schlenck line under N$_2$ for 2 h until all the CdO was dissolved. Then this solution was cooled to 100 °C and degassed under vacuum for 2 h.

Cadmium acetate: Three different Cadmium acetate precursors were synthetized by dissolving under stirring 115 mg of Cd(acetate)$_2$ (anhydrous, 99.995%) in 5 mL of either octylamine, oleylamine or a 1:1 mixture of the two, in order to obtain 0.1 M solutions.

Non-stoichiometric Tellurium precursor solutions (TOP-Te, TBP-Te, DPP-Te): Three different phosphine-Te precursors were synthetized by dissolving under stirring Te powder (31.9 mg, 0.25 mmol) in 5 mL of either trioctylphosphine (TOP), tributylphosphine (TBP) or diphenylphosphine (DPP) respectively, in order to reach a final concentration of 0.05M of Te in solution. In the case of DPP, the solution was heated to 40-50°C for one hour in order to achieve dissolution.

Stoichiometric TOP-Te precursor solution (TOP-Te 1:1): A stoichiometric 0.1 M TOP-Te solution was prepared under stirring, by dissolving 68 mg of Te powder (theoretical amount: 63.8 mg, 0.5 mmol) and 185 mg of TOP (0.5 mmol) in 4.78 mL of toluene at 50°C for 1 hour. The solution was then filtered with a syringe to remove unreacted Te powder. The resulting solution was then diluted in order to reach a concentration of 0.05 M.

3.2.2 - Standard solutions

The general synthetic procedure is illustrated here, while in the next subsections, all the modifications are reported. Unless otherwise stated, the procedures were carried out at

room temperature although the Cd precursor was heated to approximately 50 °C prior to addition because it is a solid at room temperature.

Five different solutions were prepared using a 2:1 Cd/Te ratio and different volumes of octylamine: 0.00 mL, 0.01 mL (0.02 M), 0.1 mL (0.2 M, low amine concentration solution), 0.4 mL (0.8 M, intermediate amine concentration solution), 1.0 mL (2 M, high amine concentration solution). In the general synthesis protocol, the amount of toluene needed to obtain a total volume of 3 mL was added to a 20 mL clear reaction vial, followed by the desired volume of octylamine, 0.1 mL of TOP-Te (0.05 M in TOP, 0.005 mmol) and 0.1 mL of Cd(oleate)$_2$ (0.1 M in ODE, 0.01 mmol). The components were transferred into the vial using Finn pipettes. The vial was then lightly shaken to favor the mixing of the components. One hour later, the samples for UV-Vis absorption measurement were prepared in sealable quartz cuvettes, with an optical path length of 10 nm, by adding 200 µL of each solution to 2.5 mL of toluene and measured within 5 minutes after sample preparation.

	Low amine concentration (0.2 M)	Intermediate amine concentration (0.8 M)	High amine concentration (2 M)
Toluene (mL)	2.7	2.4	1.8
Octylamine (mL)	0.1	0.4	1.0
TOP-Te 0.05 M (mL)	0.1	0.1	0.1
Cd(oleate)$_2$ 0.1 M (mL)	0.1	0.1	0.1

Table 3.1. Solution compositions for the three standard solutions. These solutions have a 2:1 Cd:Te ratio. As the solution volumes are consistently 3 mL, the final amine concentration increases from 0.2 M to 0.8 M to 2 M at the cost of the amount of solvent.

3.2.3 - Diluted solutions

To investigate the effect of dilution, the samples in the cuvettes corresponding to the low, intermediate and high amine concentration solutions, prepared as described above, were left in the glovebox and new UV-Vis absorption spectra were measured one hour later and again 20 hours later.

3.2.4 - Temperature ramps

To investigate the effect of increasing the temperature, the samples with intermediate octylamine concentration (0.8 M), 0.01 mL of octylamine (0.02 M), and no amine were heated with the following temperature ramp (unless otherwise stated in the text). The reaction vial was placed inside an Al-block on a heating plate and the temperature was increased stepwise, by ~15 °C every 40 minutes (50°C, 65°C, 80°C, 95°C and 105°). The temperature was checked using a probe in a vial that was placed inside the same Al-block and that contained approximately the same volume of solvent as the analyzed solution. Absorption spectra were measured at each temperature interval, preparing the optical cuvettes as previously described.

3.2.5 - Increasing amounts of amine addition

To a sample containing 2.5 mL of toluene, 0.1 mL of TOP-Te (0.05 M in TOP, 0.005 mmol) and 0.1 mL of Cd(oleate)$_2$ (0.1 M in ODE, 0.01 mmol) as in the standard procedure, increasing amounts of octylamine were added, every 45 minutes, in order to reach a final volume of amine in solution equal to: 0.01 mL, 0.03 mL, 0.07 mL, 0.1 mL, 0.4 mL, 1.0 mL, respectively. Absorption spectra were measured after each addition, preparing the cuvettes as described above. Additionally, two spectra were measured after 4 hours and after 18 hours following the last amine addition. The sample was then heated following a temperature ramp, as described in subsection 3.4.3.

3.2.6 - Solutions with varying Cd/Te ratios

For each of the octylamine concentrations outlined in Table 3.1 (low (0.02 M), intermediate (0.08 M) and high (0.2 M)), five solutions were prepared with varying amounts of TOP-Te 0.05M and Cd(oleate)$_2$ 0.1M, in order to obtain a Cd/Te ratio equal to 4:1, 2:1, 1:1, 1:2, 1:4, as outlined in Table 3.2. Absorption spectra were measured one hour after the preparation of the solutions, as described above.

Cd:Te ratio	Cd(oleate)$_2$ (mL)	TOP-Te (mL)
4:1	0.2	0.1
2:1	0.1	0.1
1:1	0.1	0.2
1:2	0.1	0.4
1:4	0.1	0.8

Table 3.2. Composition of the Cd and Te precursors (mL) in the samples with different Cd/Te ratio.

3.2.7 - Different amines solutions

To investigate the effect of using non-primary alkylamines, two solutions with the low amine concentration (0.2 M) were prepared, substituting n-octylamine with the same volume (0.1 ml) of di-n-octylamine and tri-n-octylamine (a secondary and tertiary amine, respectively). 45 minutes after mixing, diluted samples for UV-Vis absorption were prepared and measured, as described above.

To investigate the effect of varying the length of the alkyl chain, six solutions with the low amine concentration (0.2 M) were prepared, adding different volumes of the following alkylamines (corresponding to the same molar amount of octylamine as in the standard solution): butylamine (0.06 ml), amylamine (0.07 ml), hexylamine (0.08 ml), heptylamine (0.09 ml), dodecylamine (0.14 ml), oleylamine (0.2 ml). 45 minutes after mixing, diluted samples for UV-Vis absorption were prepared and measured as described above.

3.2.8 - Different phosphines solutions

Seven reaction vials were prepared adding 0.1 mL of octylamine, 0.1 mL of *stoichiometric* TOP-Te 1:1 (0.05 M in toluene), and 0.1 mL of Cd(oleate)$_2$ 0.1 M to 2.7 mL of toluene. The solutions remain clear and colorless, not displaying the bright yellow color observed a few minutes after mixing in the case of the solutions with *non-stoichiometric* TOP-Te 0.05 M in TOP. After some minutes, 0.224 mmol of triphenylphosphine (TPP), tributylphosphine (TBP), triphenylphosphite (TPT), trioctylphosphine (TOP), diphenylphosphine (DPP), diterbutylphosphine (DTP) and chlorodiphenylphosphine (ClDPP) were added to each vial. The vials were then slightly

shaken. After one hour, the samples for UV-Vis absorption spectra were prepared and measured as described above.

3.2.9 - Different non-stoichiometric Te precursors solutions

Three solutions with the low amine concentration (0.2 M) were prepared adding to each vial 2.7 mL of toluene, 0.1 mL of octylamine, 0.1 mL of respectively TOP-Te, TBP-Te or DPP-Te 0.05 M, and $Cd(oleate)_2$ 0.1 M. DPP-Te precursor was filtered prior to addition to eliminate unreacted DPP powder. The vials were then slightly shaken. After one hour, the samples for UV-Vis absorption spectra were prepared and measured as described above.

3.2.10 - Addition of Superhydride ®, SH

One drop of Superhydride ® (SH) was added to three solutions with the low (0.2 M), intermediate (0.8 M), and high (2 M) amine concentration, prepared adding the respective amount of octylamine, 0.1 mL of TOP-Te 1:1 and 0.1 mL of $Cd(oleate)_2$ 0.1 M to 2.7 mL of toluene. Absorption spectra were measured as described above.

In a different reaction vial, one drop of SH was added to 0.1 mL of TOP-Te 1:1 and 2.7 mL of toluene. A milky suspension formed. Subsequently, 0.1 mL of octylamine and 0.1 mL of $Cd(oleate)_2$ 0.1 M were added, leading to a dark yellow, clear solution. After one hour, the sample for UV-Vis absorption spectroscopy was prepared and measured as described above.

3.2.11 - Different Cd precursors solutions

Three solutions with the low amine concentration (0.2 M) were prepared adding to each vial 2.7 mL of toluene, 0.1 mL of octylamine, 0.1 mL of TOP-Te 0.05 M, and 0.1 mL of either dimethyl cadmium ($CdMe_2$), 0.1 M in TOP, $Cd(oleate)_2$ 0.1 M in ODE or $Cd(stearate)_2$ 0.1 M in ODE. Absorption spectra were measured one hour after the preparation of the solution, as described above, for $Cd(oleate)_2$ and $Cd(stearate)_2$, while for $CdMe_2$ spectra were measured after one hour, after 20.5 hours and after 83 hours.

A solution with the low amine concentration (0.2 M) was prepared adding 2.7 mL of toluene, 0.1 mL of TOP-Te 0.05 M, and 0.1 mL of $Cd(acetate)_2$ 0.1 M in octylamine as the Cd precursor; to prepare the intermediate and high amine concentration solutions, an

additional 0.3 mL and 0.9 mL of octylamine were also added, respectively. UV-Vis absorption spectra were measured after 30 minutes and after 2 hours from mixing.

3.2.12 - Addition of organic charged species

Ten solutions with the low amine concentration (0.2 M) were prepared: in the first five reaction vials, 0.605 mmol of didodecyldimethylammonium bromide (DDAB, 279.9 mg), ammonium bromide (NH_4Br, 59.2 mg), hexadecyltrimethylammonium bromide (HTAB, 220.5 mg), hexadecyltrimethylammonium chloride (HTAC, 193.6 mg), and sodium myristate (151.5 mg) were added to 2.7 mL of toluene, followed by 0.1 mL of octylamine, 0.1 mL of TOP-Te 0.05 M, and 0.1 mL of Cd(oleate)$_2$ 0.1 M; in the second five reaction vials, DDAB, NH_4Br, HTAB, HTAC and sodium myristate were added as last reagents. After one hour, the samples for UV-Vis absorption spectra were prepared and measured as described above.

3.2.13 - Different solvents

The solution with the low amine concentration (0.2 M) was prepared as described for the standard solution above in 2.7 mL of different solvents, specifically tetrahydrofuran, ethyl acetate, dibutyl ether, dioctyl ether, tetrachloroethylene, toluene, 1-octadecene, hexadecane, n-hexane. UV-Vis absorption spectra were measured after 30 minutes and after 3 days from the preparation of the samples.

3.2.14 - Solutions leading to superstructures

All the samples discussed in Section 4.2 were prepared following the standard procedure for the low amine concentration solution, varying some parameters such as the alkylamine, the Cd precursor and the solvent. The amines used are octylamine (OTA, 0.1 mL, 0.605 mmol), oleylamine (OLAm, 0.2 mL, 0.605 mmol), dodecylamine (DDA, 112 mg, 0.605 mmol) octadecylamine (ODA, 163 mg, 0.605 mmol) and were all added in the same molar amount, unless otherwise stated. As the Cd precursor, 0.1 mL of either Cd(acetate)$_2$ 0.1 M in octylamine (OTA), in oleylamine (OLAm) or in a 1:1 mixture of the two amines (OTA/OLAm) was used. Toluene (Tol), 1-octadecene (ODE) or n-hexane (Hex) were used as solvents. Before TEM imaging, the samples were precipitated by centrifugation at 4000 rpm for 10 minutes and resuspended in toluene.

In case the samples did not show any turbidity, 1 ml of ethyl acetate (antisolvent) was added, to help destabilizing the colloidal suspension, before the centrifugation.

3.3. Characterization

3.3.1 - UV-Vis Absorption Spectroscopy

UV-Vis absorption spectra were acquired on a double beam PerkinElmer Lambda 950 UV/VIS Spectrometer. Sealable quartz cuvettes with path lengths of 10 mm were used. The spectra were recorded in the range of 300-600 nm. For the blanks, 2.5 mL of toluene were added to 10 mm cuvettes. For the measurements themselves, 2.5 mL of toluene were added to each cuvette followed by 200 µL of reaction solution. The cuvettes were wiped with ethanol prior to measuring. Before reusing, they were cleaned by rinsing with toluene, ethanol, and acetone.

For *in situ* UV-Vis Absorption Spectroscopy, the low, intermediate, and high concentration solutions were prepared and 300 µL of each solution was transferred into a sealable quartz cuvette with 1 mm optical path length and measured without dilution. The intermediate amine concentration solution was measured first after 7 minutes, then 15 minutes, and then every 5 minutes until 60 minutes after mixing. One last measurement was taken 80 minutes after mixing. The high amine concentration solution was measured starting at 4 minutes after mixing. UV-Vis spectra were acquired every 2 minutes until 30 minutes after mixing, then every 5 minutes until 60 minutes after mixing. Finally, the low amine concentration solution was measured starting at 4 minutes after mixing, every 2 minutes until 32 minutes after mixing. From 35 minutes after mixing, the solution was measured every 5 minutes until 60 minutes after mixing.

3.3.2 - Transmission Electron Microscopy (TEM)

Samples for TEM imaging were prepared by drop-casting the solutions onto a carbon-coated 200 mesh copper TEM grid. In the case of the samples discussed in Section 4.1, no previous washing treatments were performed. The samples discussed in Section 4.2 were centrifuged at 4000 rpm for 10 minutes, to allow precipitation of the superstructures, and then resuspended in toluene, before drop-casting on the TEM grids.

Conventional Transmission Electron Microscopy (TEM) images and High Angle Annular Dark Field Scanning TEM (HAADF-STEM) images were acquired on a Thermo Fisher Scientific Talos F200X microscope, operating at 200 kV.

Cryo-TEM images were made by preparing frozen films of the solutions on holey carbon-copper grids. The films were prepared by placing a droplet of solution on the grid and using a VITROBOT to automatically blot the grid. Subsequently, the films were instantly frozen by plunging the grids into liquid nitrogen. The grids were transferred to a FEI Tecnai20F microscope operating at 120kV, using a Gatan 626 cryo-transfer holder.

4. Results and Discussion

The aim of this work is to shed light on the formation process of CdTe magic-sized clusters (MSCs), and 1D and 2D superstructures thereof at low temperatures. A thorough analysis of experimental data combined with the comparison with previous results from literature will allow to propose a model involving non-classical pathways of nucleation and growth. Starting from an overview of the synthesis performed during the experimental work (Section 4.1), the characteristic sharp absorption peaks observed in the UV-Vis spectra are then investigated in terms of their growth in intensity over time (Section 4.1.1) and spectral shift as a consequence of changing temperature, dilution and concentration of ligands (Section 4.1.2). The different parameters involved in the process are addressed in the following sections, starting from the Cd:Te ratio (Section 4.1.3), the role of the alkylamine (Section 4.1.4), the effect of changing the phosphine-Te precursor (Section 4.1.5) and the Cd precursor (Section 4.1.6). In Section 4.1.7, the consequences of perturbating the system through the addition of organic charged species are examined.

The second part of this chapter (Section 4.2) is focused on the 2D superstructures and larger assemblies following the CdTe MSCs evolution, with a particular consideration for the influence of Cd precursor, amine chain length, solvent polarity and the interplay between these factors in the kinetics of formation and tendency to self-assembly of ultrathin CdTe nanosheets.

4.1. Room Temperature Synthesis of CdTe magic-sized clusters

The following general synthesis protocol was used to investigate the formation of CdTe magic-sized clusters at room temperature. The reaction system includes four components: solvent, primary alkylamine, chalcogenide precursor and metal precursor. In the standard solutions toluene was used as solvent, Cd(oleate)$_2$ and TOP-Te (trioctylphosphine-Te) as metal and chalcogenide precursors, respectively. Octylamine (OTA) was used as primary amine, unless otherwise stated. The molar ratio between Cd and Te was kept at 2:1; the quantity of amine in solution was increased progressively and different amounts of toluene were added in order to reach a final volume of 3.0 mL in every sample (Table 4.1). The reagents were mixed in a vial in the following order: solvent, amine, chalcogenide precursor and metal precursor. Altering the order of the reagents did not lead to any observable change in the results.
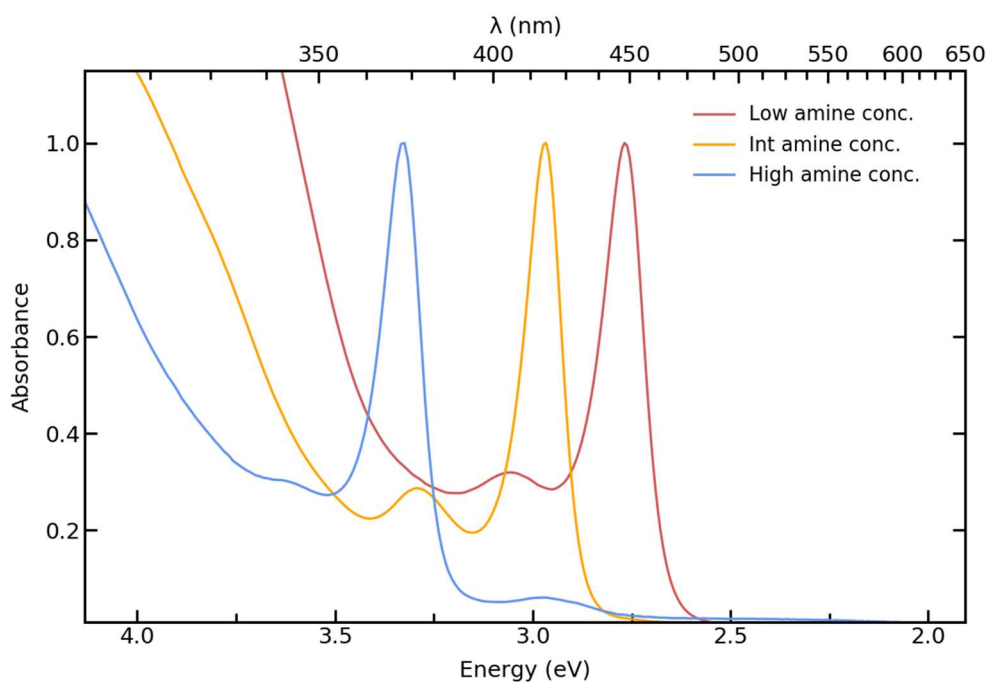
Figure 4.1. Normalized UV-Vis spectra of the three different amine concentration solutions, plotted in terms of wavelength(nm) and energy(eV).

UV-Vis absorption spectra of the solutions (Figure 4.1) were measured one hour after mixing and display sharp absorption peaks at well-defined wavelengths, depending on the concentration of amine. Similar features have been previously attributed to the

formation of magic-sized clusters in solution, [10][13][23] which, due to their well-defined stoichiometry, size and shape, exhibit comparatively narrow absorption peaks relative to those of quantum dots, which are affected by inhomogeneous broadening due to size and shape polydispersity.

#	Cd precursor	Te precursor	Amount of OTA (mL)	Concentration of OTA (M)	Absorption Peaks (nm)	Appearance
	Cd(oleate)$_2$	TOP-Te	0.00	-	420 (broad, overtime)	Colorless; turns yellow after 10 days
	Cd(oleate)$_2$	TOP-Te	0.01	0.02	440 (broad)	Bright yellow
1	Cd(oleate)$_2$	TOP-Te	0.10	0.2	449	Yellow
2	Cd(oleate)$_2$	TOP-Te	0.40	0.8	417	Pale yellow
3	Cd(oleate)$_2$	TOP-Te	1.00	2	373	Colorless

Table 4.1. Overview of the standard solutions used in this work. The Cd and Te precursors were added in the same amount in each solution, precisely 0.1mL (0.01 mmol) of Cd(oleate)$_2$ and 0.1 mL (0.005 mmol) of TOP-Te. The samples marked as 1, 2 and 3 correspond to the lower, intermediate, and higher amine concentration solutions respectively.

4.1.1 - Peaks growth

It was immediately evident that the presence of an alkylamine is necessary to observe narrow peaks, and that there is a lower limit of concentration under which only broad peaks are observed (viz. 0.01 mL, 0.02 M). Nevertheless, even the solution in which no amine was added turned bright yellow after ten days from its preparation. The broad absorption peak at ~420 nm, arising from [CdTe]$_x$ units present in solution, demonstrates that the reaction between Cd and Te precursors still occurred, despite the absence of amines. With the addition of volumes of octylamine $\geq$ 0.1 mL ($\geq$ 0.2 M), sharp peaks are observed, and the wavelength of their maxima is determined by the amount of amine. In other words, each narrow peak is selectively "stabilized" by a precise quantity of amine in solution and using concentrations in between the ones reported in Table 4.1

still produces the same peaks, but in different ratios. In particular, solutions prepared with the lower, intermediate, or higher amount of amine (0.2, 0.8, 2 M, as summarized in Table 4.1) exhibit three distinctive absorption spectra, characterized by an intense and narrow peak at 449, 417 and 373 nm, respectively (full width at half maximum, fwhm, of 12.8, 11.7 and 12.8 meV). These peaks are accompanied by weaker bands at 405, 378, and 341 nm respectively, which were assigned to the second absorption transition (Figure 4.2).

No additional peaks were observed at higher energy, instead the samples in which the amine concentration was further increased above 2 M still gave rise to the 373 nm absorption peak, as well as the samples in which neat amine was used as the solvent.
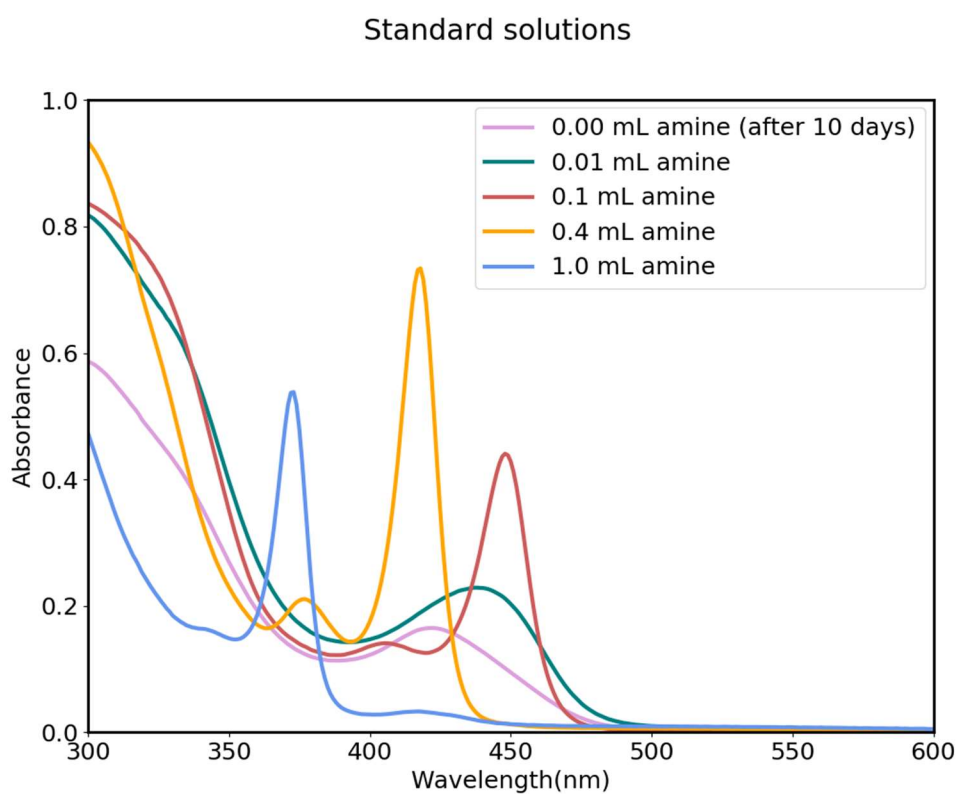
Figure 4.2. UV-Vis absorption spectra of the standard solutions. Quartz cuvettes with path length of 10 mm were used, in which 200 µL of reaction solution were added to 2.5 mL of toluene. The spectra were acquired shortly after diluting the samples, since longer waiting times between dilution and measurements result in (discontinuous) redshift of the peaks for the solutions with the higher amine concentrations, as described in Section 4.1.2.

To monitor the growth of the peaks over time, *in situ* UV-Vis absorption spectra of the solutions were acquired during the first hour following their preparation (Figure 4.3).
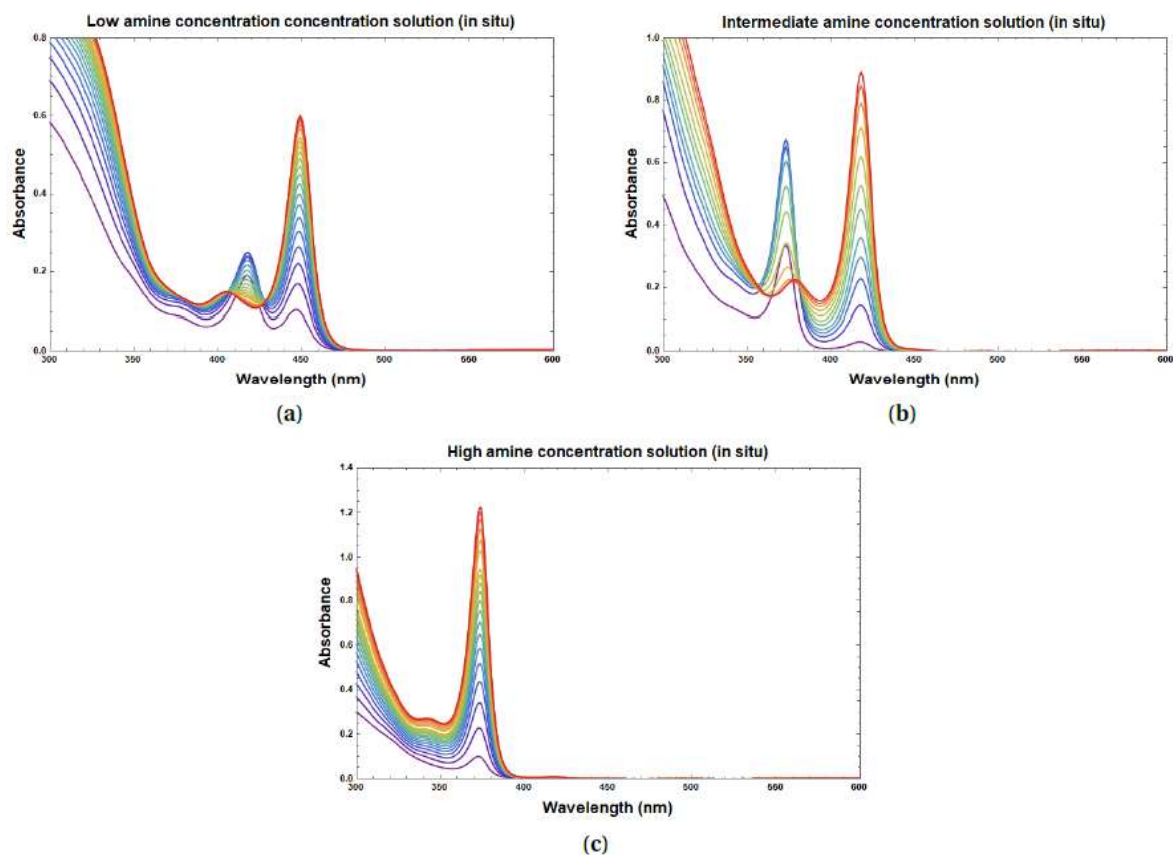
Figure 4.3. In situ UV-Vis absorption spectra over time (see Section 3.3) of the standard solutions with low(a), intermediate(b), and high(c) amine concentration. For this experiment, optical quartz cuvettes with 1 mm optical path were used, instead of the usual 10 mm. In this way, the samples did not need to be diluted ~10 times to get values of absorbance ~0.5 at the wavelength of the absorption peaks. In this experiment, dodecylamine (DDA) was used instead of octylamine, knowing that this does not lead to any change in the outcome (see Section 4.1.4 below).

In the spectra of the low amine concentration solution (Figure 4.3a, Figure 4.4), a higher-intensity peak initially appears at 417 nm with a lower-intensity peak at 449 nm. As the reaction progresses, the intensity of the 449 nm peak increases while that of the 417 nm peak initially increases but then quickly decreases. Eventually, the peak at 417 nm disappears and, together with the peak at 449 nm, a second lower-intensity peak appears at 405 nm, which is assigned to the second absorption transition of the species with first absorption peak at 449 nm. A similar process occurs for the intermediate amine

30

concentration solution (Figure 4.3b): initially a higher-intensity peak at 373 nm dominates the spectrum, while the peak at 417 nm has very low intensity. Over time, the peak at 373 nm first increases and then decreases in intensity while the peak at 417 nm continuously grows, together with a lower-intensity peak at 378, assigned to the secondary absorption transition of the species with first absorption peak at 417 nm. In the case of the high amine concentration solution (Figure 4.3c), no shift in peak position occurs, as the narrow signal at 373 nm is present from the beginning and continuously increases in intensity, together with the second transition at 341 nm.
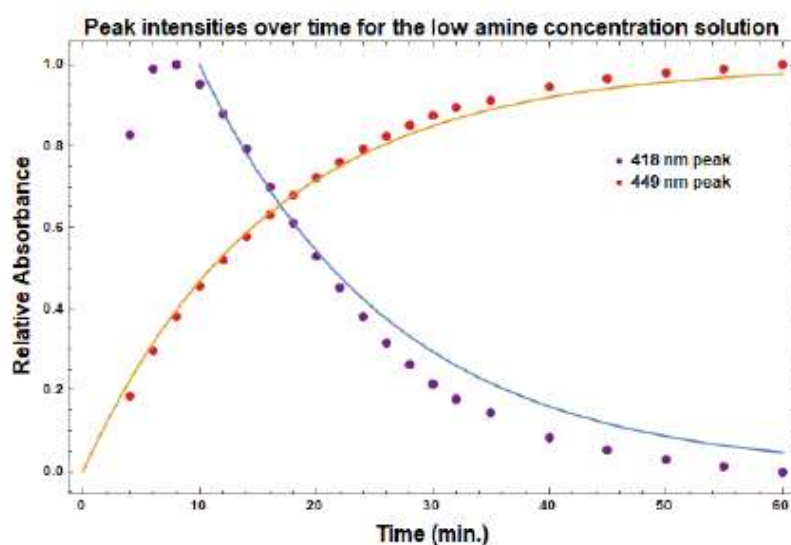
Figure 4.4. Peaks intensity over time for the *in situ* measurements of the low amine concentration solutions is plotted in terms of relative absorbance. These values were obtained using a polynomial function in a non-linear fit to approximate the UV-Vis absorption data and then determining the local maxima for each dataset. The decrease of the 417 peak and increase of the 449 peak can be approximated reasonably well by the exponential functions e^-(0.063*t) and 1-e^(-0.063*t), respectively, suggesting that the species with absorption peak at higher energy directly convert into the species with absorption peak at lower energy.

To further investigate the nature of the species present in solution, the sample with low amine concentration was drop-casted on a Transmission Electron Microscopy (TEM) grid without any washing treatment. It is worth mentioning that due to the higher amount of "organics" that would burn under the electron beam, contaminating the specimen, conventional TEM of the samples with higher concentrations of amine would not be

reliable to describe the nature of the species originally present in solution, because it would require washing and therefore strongly perturbing the system.

In the sample with low amine concentration, TEM images reveal the presence of 1D nanostructures with a string-like appearance. The strings are organized to form bundles of different thickness and length, and are very sensitive to electron beam damage, becoming segmented into smaller domains (bead-like) upon exposure (Figure 4.5).
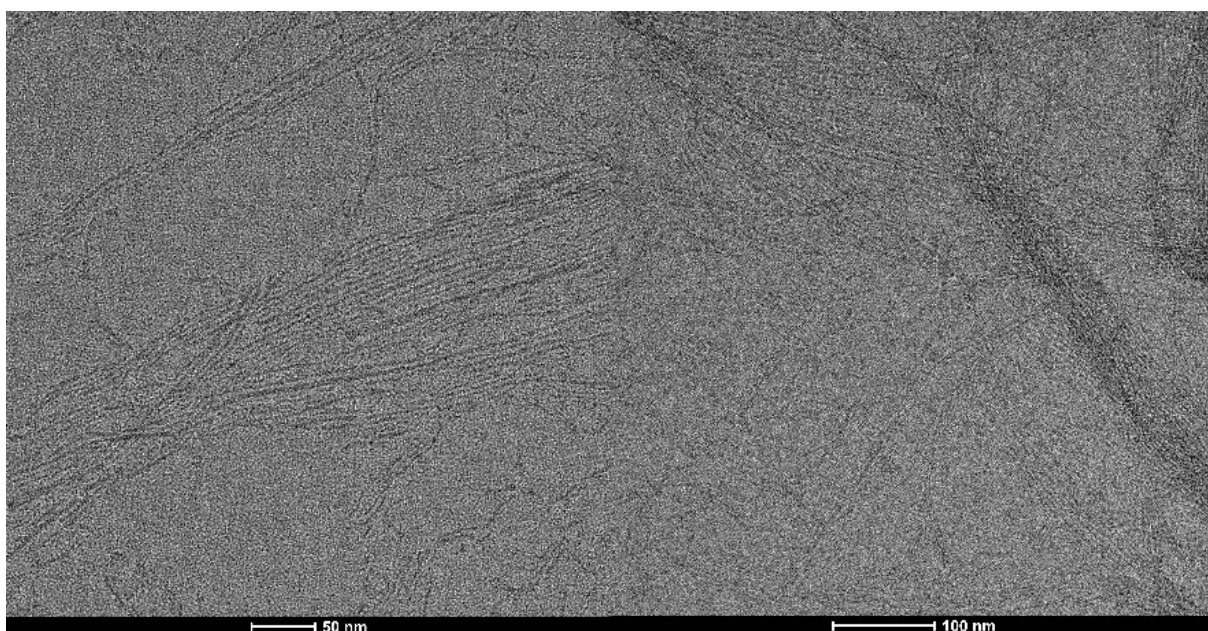
Figure 4.5. TEM image of the low amine concentration solution, displaying bundles of strings, of different lengths and thickness.

To exclude the possibility that these strings resulted from aggregation during the drying of the droplet on the TEM grid, the same sample was analyzed with cryo-TEM, a technique that ensures the observation of the species as they are in solution, since a droplet of sample is quickly frozen with liquid N_2 and the entire imaging is performed at cryogenic temperature.
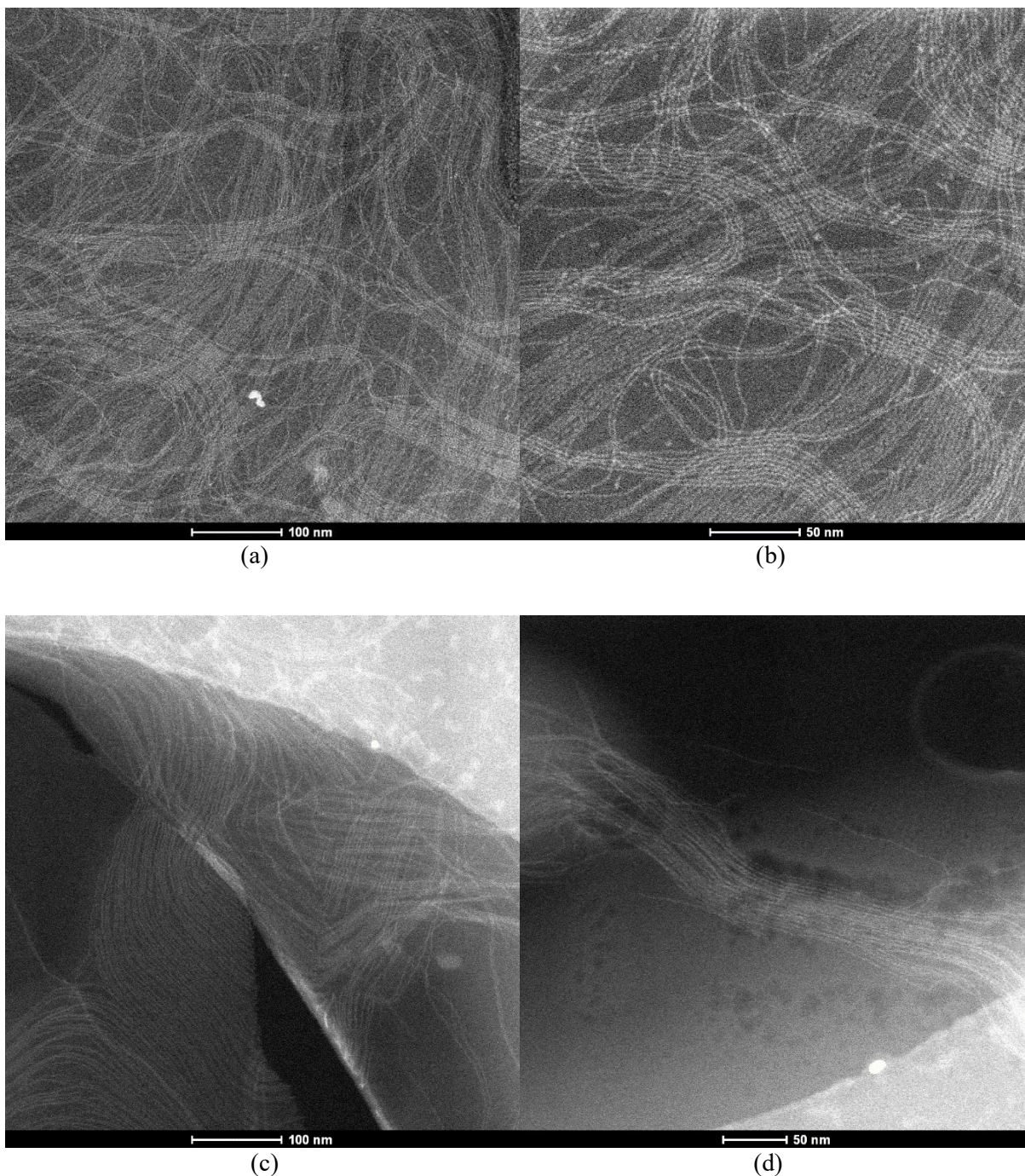
Figure 4.6. Cryo-TEM images taken in STEM mode of the standard solutions with low (a, b), and high (c, d) amine concentration.

Cryo-TEM images (Figure 4.6a, b) show the same bundles, demonstrating that these string-like structures are indeed present in solution and are not formed on the TEM grid during the drying process. The same high sensitivity of the nanostrings towards the electron beam was also observed, to the point that it cannot safely be concluded that the segmentation into bead-like structures is caused by the imaging, or if rather the 1D strings are already composed of distinct subunits (CdTe clusters), which increase their

separation due to atomic rearrangement as a consequence of ligand evaporation induced by the electron beam.

Similar extended bundles of long 1D nanostructures were observed in the solution with high amine concentration (Figure 4.6c, d). The average thickness of a 1D nanostrings in the low and high amine concentration solutions were determined to be approximately 2.40 ± 0.19 nm and 2.88 ± 0.27 nm, respectively. These values were estimated assuming that adjacent strings are separated by fully interdigitated monolayers of alkylamines. It is interesting to note that the high amine concentration sample gives rise to an absorption peak at shorter wavelengths than the low-concentration sample (maxima at 373 nm and 449 nm, respectively), and would thus be expected to have narrower diameter, if the spectral shift were to be ascribed only to the effect of quantum confinement.

To investigate whether the species giving rise to the three different absorption peaks are "nanostrings" differing in the diameter, a solution with 0.25 ml of OTA (0.5 M), an amount of amine in between the low and intermediate amine concentration solutions reported in Table 4.1 was prepared. The corresponding UV-Vis spectrum displays both the 417 nm and the 449 nm peak (Figure 4.7b, inset). The TEM images of the sample (Figure 4.7) again display long bundles of strings, but two different species are recognizable: denser bundles showing periodical twisting (high contrast in Figure 4.7a) and, in the background, less aggregated strings (low contrast in Figure 4.7a), more similar to those observed in the samples analyzed with cryo-TEM. The average thickness of the strings (including a monolayer of interdigitated ligands) in Figure 4.7b was estimated to be 2.11 ± 0.07 nm. The two absorption peaks could be assigned to these two different species, although a difference in thickness could not be estimated due to the low resolution of the images.
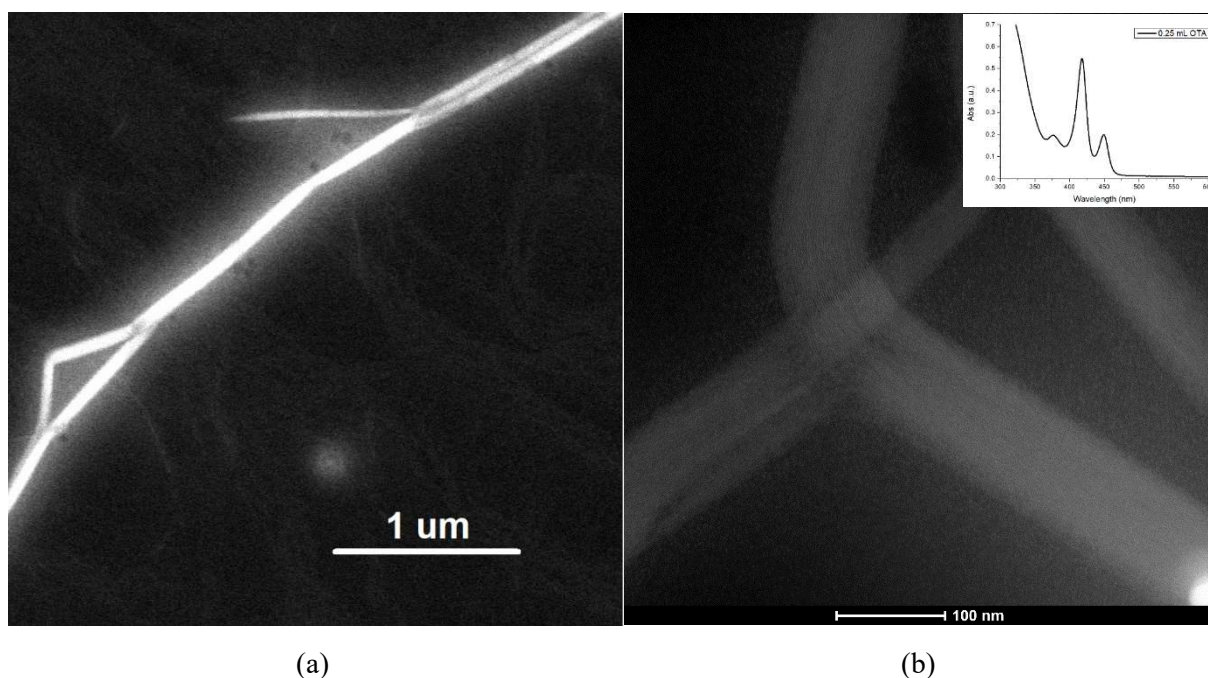
Figure 4.7. HAADF-STEM images and UV-Vis spectrum of the sample containing 0.25 mL of OTA. Both the species corresponding to the 417 nm and 449 nm peak are present in solution.

Similar structures to those shown in Figures 4.5-4.7 have been previously reported in literature for other Cd-chalcogenides, and have been interpreted in different ways, such as magic-sized clusters embedded in spontaneously formed amine-tubular templates [18] or Cd-amine mesophases,[22] fibrillar $(Cd_2Se)_x$ polymeric species, [20] as well as nanowires. [24] Different wavelengths of the absorption peaks, in most cases, have been attributed to nanoclusters of different sizes, shifting to higher energy with decreasing cluster size, as an effect of stronger quantum confinement.

In the present experimental work, the observed shifts in the UV-Vis spectra (Figure 4.1) are of 35.1 meV from the 373 nm to the 417 nm peak and of 21.2 meV from the 417 nm to the 449 nm peak. Such large spectral shifts, if solely due to different strength of quantum confinement should translate in significant differences in the thickness of the strings, which is in remarkable contrast what was observed in the TEM images above (Figure 4.6).

Based on the UV-Vis spectra, which demonstrate the formation at room temperature of $[CdTe]_x$ clusters in solution, and on the TEM images, which show variously organized 1D structures, it can be proposed that the latter originates from the connection of several

CdTe nanoclusters, probably directed and stabilized by a tubular mesophase, which forms in the presence of higher concentrations of primary alkylamine. Multiple evidences for such a mesophase to be present at low temperatures are provided in previous works, from Small-Angle X-Ray Scattering (SAXS) of similar solutions.[10][19] The observed assembly of the nanostrings into bundles, could be due to the van der Waals interactions between amine layers on neighboring nanostrings.

For comparison, Figure 4.8 shows a HAADF-STEM image of the sample containing 0.01mL of amine (0.02 M), for which no sharp peaks in the UV-Vis spectra are observed, but rather a broad peak at 440 nm. In this case, no string-like structures, but very small individual [CdTe] nanoclusters are recognizable, demonstrating that higher concentrations of amine are not necessary for $[CdTe]_x$ units to nucleate at room temperature, but instead in their presence, a different "growth" path with a lower energy barrier becomes available, leading to the formation of 1D nanostrings of interconnected clusters. The average diameter of the clusters in Figure 4.8 was estimated to be approximatively 1.8 ± 0.2 nm, which is comparable to the diameter of the nanostrings observed under high amine concentrations.
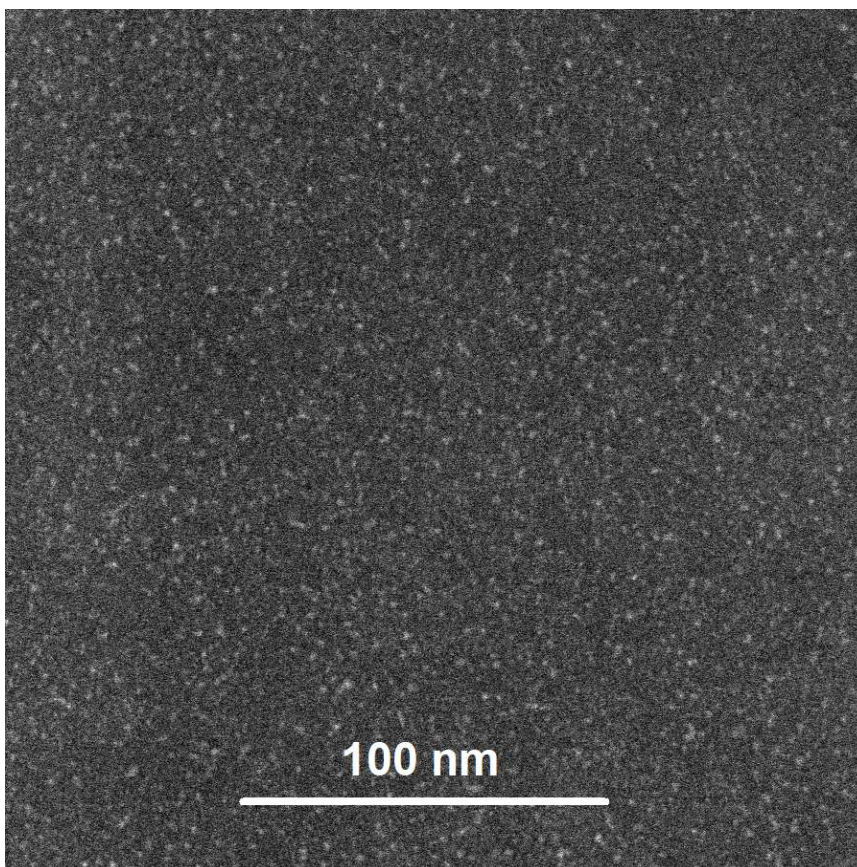
Figure 4.8. HAADF-STEM image of the sample containing 0.01 mL of octylamine, in which no bundles are observed. The average diameter of the clusters was estimated to be approximatively 1.8 ± 0.2 nm.

4.1.2 - Peaks shift

Peaks shift from higher to lower energy was observed to occur in a stepwise manner (no intermediate peaks are detected) and can be induced either by dilution or by an increase in temperature. Reverse peak shift (from lower to higher energy) was achieved by adding increasing amounts of amine. In the following subsections, these three cases will be discussed in detail.

4.1.2.1 - Peaks shift induced by dilution

In the case of the solution with high amine concentration, UV-Vis spectra measured 60 minutes and 20 hours after dilution in toluene display first the disappearance of the 373 nm peak and the rise of the 417 nm and 449 nm peaks, followed by a decrease in intensity

of the former and an increase of the latter, which remains stable over time. For the intermediate amine concentration solution a decrease in intensity of the 417 nm peak and an increase and stabilization of the 449 nm peak are observed, while the low amine concentration solution does not show any spectral shift, the 449 nm peak remaining stable over time (Figure 4.9). It is worth mentioning that dilution does not affect the fwhm of the absorption peaks.
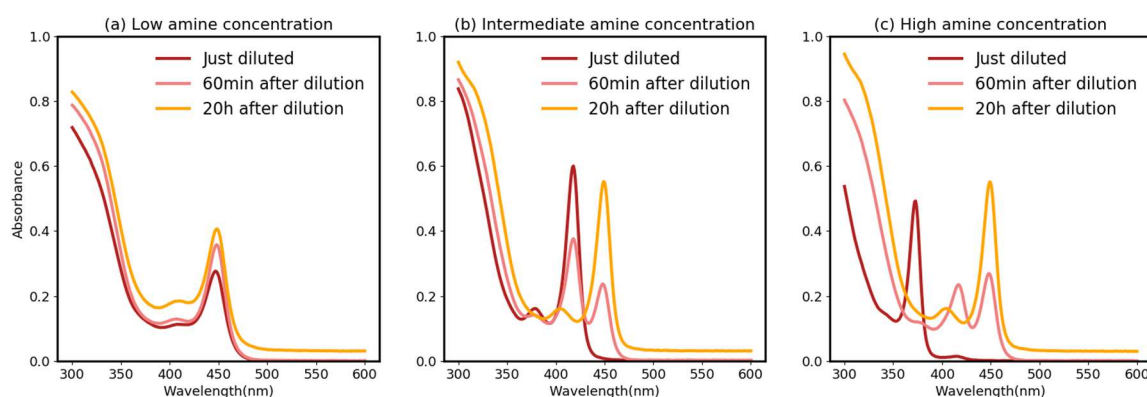
Figure 4.9. UV-Vis spectra of the low (a), intermediate (b), and high (c) amine concentration solution upon dilution, when 200µL of solution in 2.5 mL of toluene were left in quartz cuvettes over time.

This observation strongly supports the tubular mesophase model, since the diameter of crystalline CdTe nanowires cannot be affected by dilution. What could be affected by dilution, or better, by the decrease in the amine concentration caused by dilution are (a) the association of different nanostrings into bundles, promoted by interdigitation of the "coating" amine layers and (b) the way in which CdTe nanoclusters are interconnected inside the nanostrings, which determines the degree of electronic coupling between them. Nanoclusters loosely connected to each other would experience a weaker coupling and therefore absorb light of higher energy. On the other hand, if the degree of electronic coupling increases, the absorption peak would shift to lower energies. If the nanoclusters had only a few well-defined ways to interconnect (i.e. sharing corners or edges or alternating the connections) then the spectral shifts between the different conformations would occur stepwise. A high concentration of amine ligands could stabilize a conformation of the strings in which the nanoclusters are loosely connected to each other, while a lower concentration could force the nanoclusters to strengthen the

interconnections inside the 1D structures, as a response to the lower availability of ligands (stronger coupling, redshift of the peak).

If on the other hand, the electronic coupling responsible for the spectral shifts of the peaks would be between different nanostrings associated in a bundle, then dispersing the bundles by diluting the samples should lead to a shift to higher energies, contrary to what is experimentally observed.

Therefore the model proposed for the species present in solution is that of a hybrid organic-inorganic polymer-like structure, composed by nanostrings of interconnected [CdTe] nanoclusters inside an amine tubular mesophase, that can assemble into bundles to maximize the van der Waals interactions between the alkylamine chains. These [CdTe] units can twist and change their relative conformations and orientations in response to the concentration of amine ligands in solution, leading to varying degrees of electronic coupling, which are responsible for the changes in band gap manifesting as the different energies of the absorption transitions.

4.1.2.2 - Peaks shift induced by temperature

Peaks shift with increasing temperature was monitored by analyzing the temporal evolution of the absorption spectra in the case of the intermediate amine concentration solution between room temperature and 105°C. At temperatures above 50°C, a decrease in intensity of the 417 nm peak was observed while the intensity of the peak at 449 nm increased. When reaching a temperature of 90°C ca. a new peak started arising at lower energies (483 nm), which displays a sharp increase in intensity when the temperature was brought up to 105°C. The overall absorbance of the solution increased when keeping the sample at higher temperature for 90 minutes (Figure 4.10). Due to the low boiling point of toluene, used as the solvent, it was not possible to further increase the temperature.
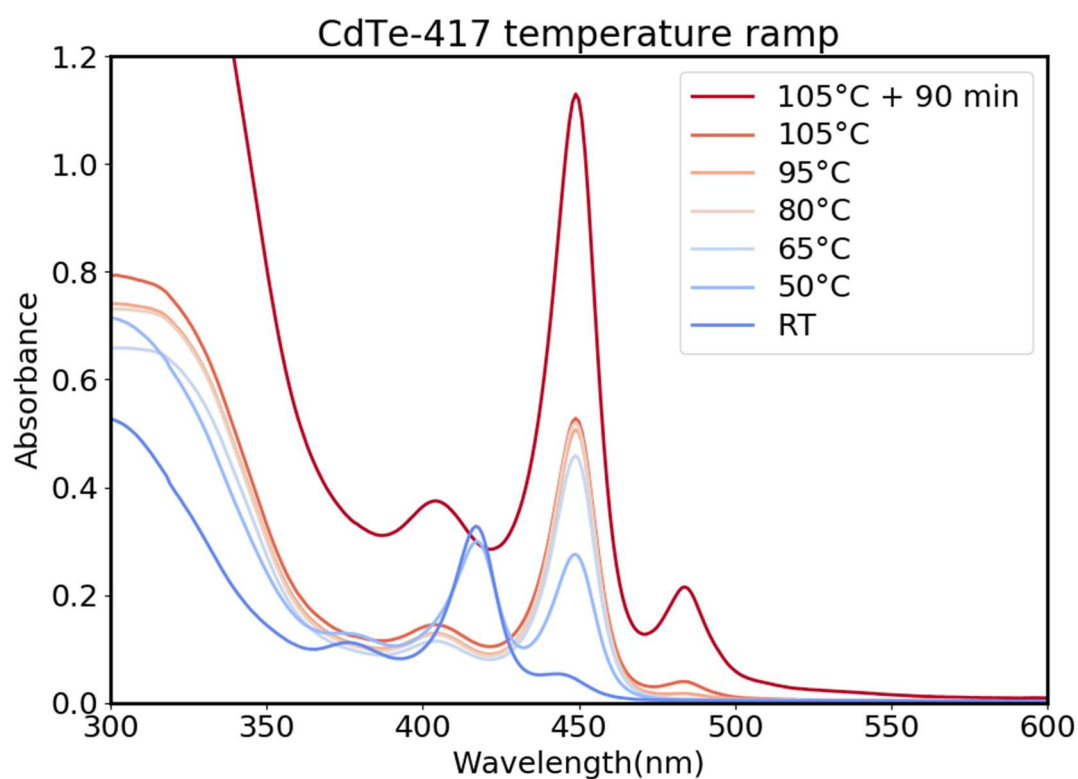
Figure 4.10. Temperature ramp performed on the intermediate amine concentration solution. Each UV-Vis spectrum was measured 45 minutes after the previous one, with exception of the last one, measured after 90 minutes.

The sample was analyzed with TEM some days after the temperature ramp treatment (Figure 4.11). The images display the coexistence of two species: long bundles made of thinner nanostrings and short stacks of thicker nanobelts. Thinner bundles are the main component of the sample, thus the very intense 449 nm peak can be attributed to this species (average thickness 2.20 ± 0.08 nm), while the thicker and shorter stacks give probably rise to the signal at 483 nm (average thickness 2.72 ± 0.17 nm). Both species are extremely sensitive to the electron beam, which is observed to induce the formation of CdTe nanoparticles. It is worth to notice that neither from the absorption spectra, nor from the TEM images any evidence of regular quantum dots is seen. This means that at these temperatures the presence of the nanostrings represent a constraint that inhibits isotropic growth, allowing rather the fusion between a small number of (segmented) strings to form thin 2D nanobelts.
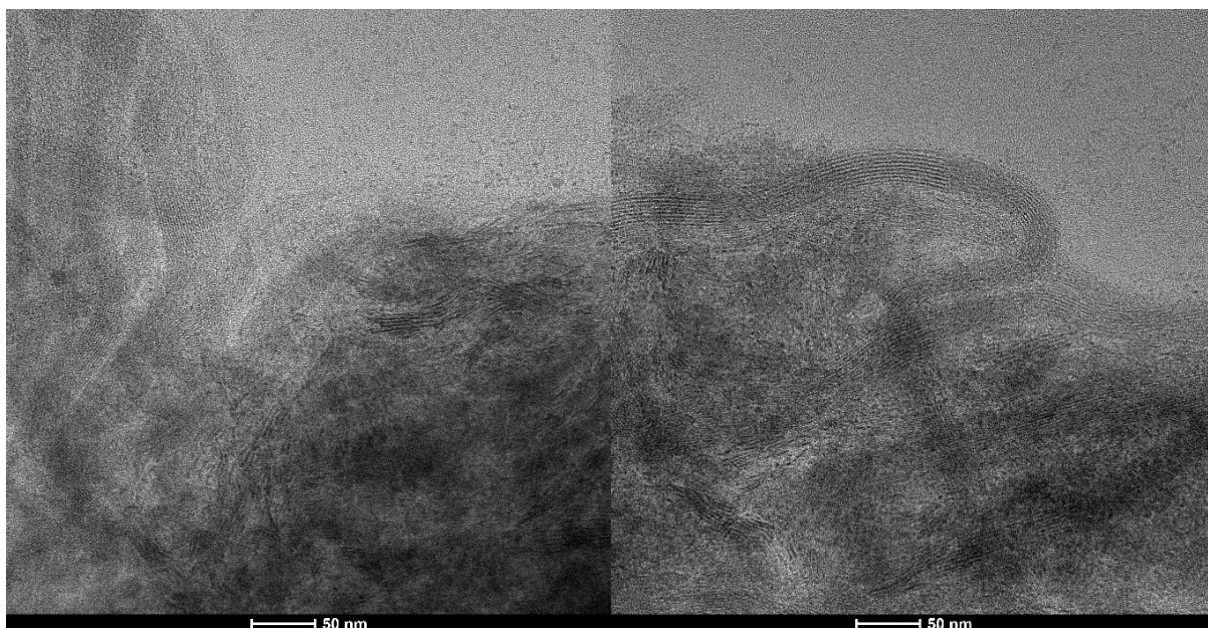
Figure 4.11. TEM images of the CdTe-417 species after the temperature ramp, when the sample was kept at 105°C for 90 minutes. Bundles of strings of different thicknesses are displayed.

The same sample was prepared and heated up to 57°C aiming to visualize at TEM the species of both the 417 nm and 449 nm peak. Interestingly, bundles are still present but appear to be segmented and periodically denser; additionally, stacks made of bundle pieces of the same length and thickness are also recognizable (Figure 4.12). The structures observed in the middle image could be the "precursors" of the thicker stacks visible in Figure 4.11.
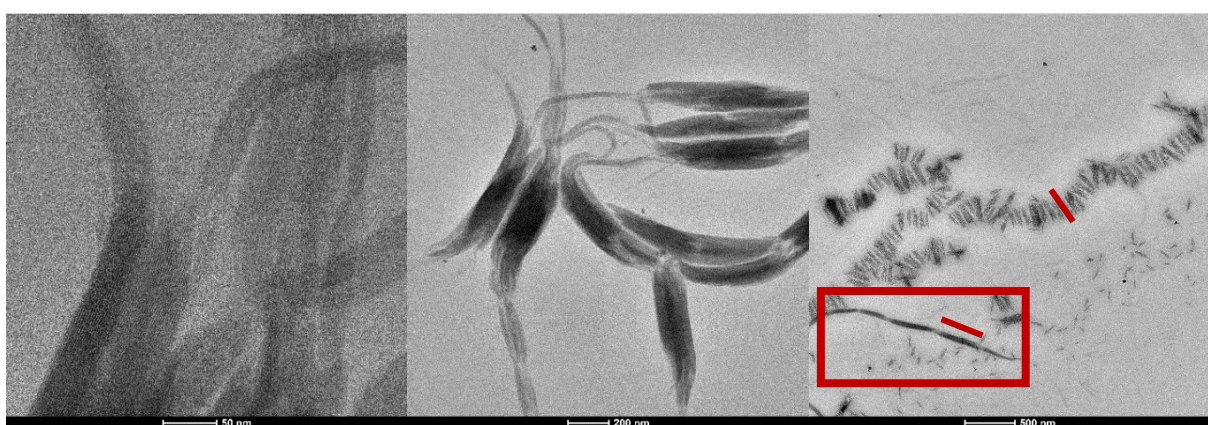
Figure 4.12. TEM images of the intermediate amine concentration solution heated to 57°C.

For comparison, the evolution with increasing temperature of a system in which CdTe nanoclusters are not interconnected into 1D strings was also monitored (solution with

0.01 mL of amine (0.02 M), broad peak at 440 nm, Figure 7) , by treating it with the same temperature ramp previously described. In this case, no stepwise peak shift to lower energy was observed, but rather an increase in intensity of the 440 nm band. Starting from 80°C, a new peak arose, displaying a continuous shift towards the red spectral region, from 509 nm to 551 nm at 105°C, when the solution turned finally orange and luminescent (Figure 4.13). From the sizing curve for CdTe quantum dots reported by Koole *et al*, the absorption peak at 570 nm was attributed to quantum dots of 3.3 nm. [9] TEM images confirmed the presence of nanocrystals of average size 4.0 ± 0.3 nm (Figure 4.14).

This result demonstrates that, at the temperatures at which nucleation and growth of isotropic nanocrystals would occur, the presence of amine-stabilized nanostrings of interconnected CdTe nanoclusters inhibits it, constraining the system to follow a different reaction path.
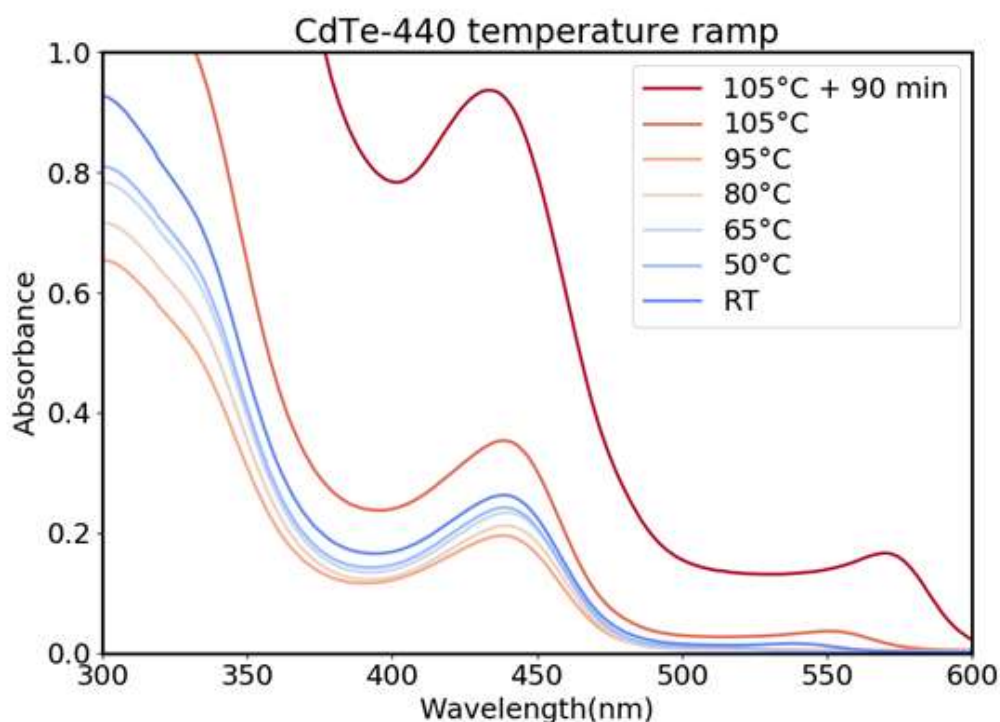
Figure 4.13. Temperature ramp of the CdTe-440 species, displaying and increase of intensity of the peak and QDs formation at high temperatures.

(a)   (b)
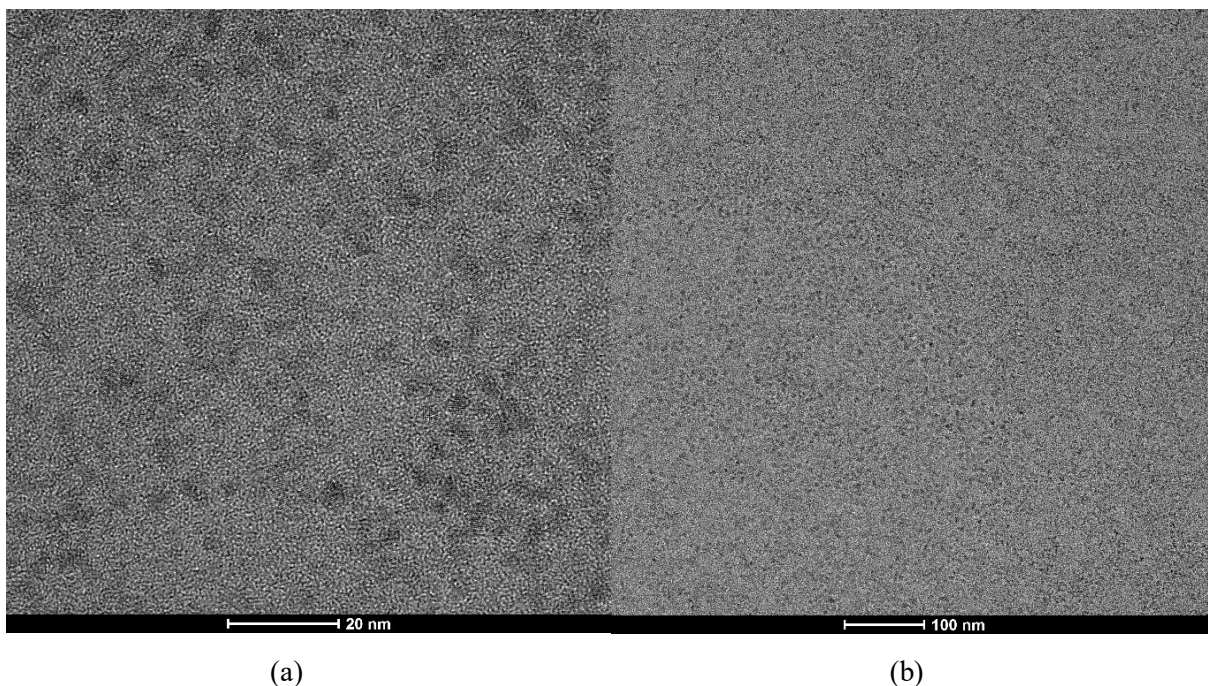
Figure 4.14. TEM images of CdTe-440 after the temperature ramp display QDs (a) that easily aggregate over beam exposure (b).

A different behavior was noticed for the solution that did not contain any amine: a broad peak at 420 nm slowly arises at room temperature, about 10 days after the precursors were mixed. Treating the solution with the same temperature ramp leads to an increase in intensity, but the absorption feature that was attributed to quantum dots in Figure 4.13 in this case was not observed (Figure 4.15).

This result is consistent with previously reported interpretation in which small amounts of amines lower the nucleation temperature of Cd-chalcogenide quantum dots, by weakening the Cd-carboxylate bond. [25] In their absence, the nucleation temperature is higher and was not reached in this experiment.
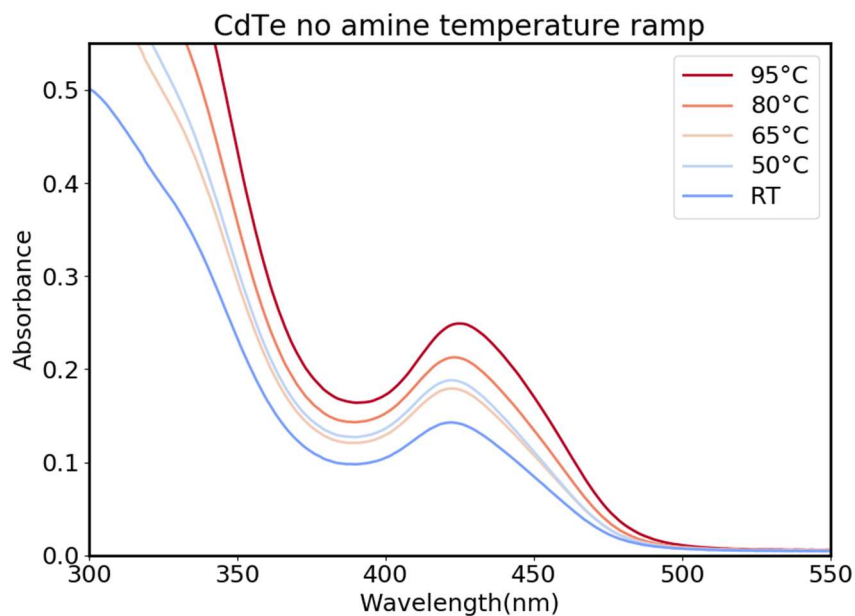
Figure 4.15. Temperature ramp of the amine free sample, which displays an increase in intensity of the peak but no additional peaks from 509 nm to 551 nm, as observed in Figure 4.13.

As shown above, in the case of samples where CdTe nanoclusters are interconnected in nanostrings, stepwise shift from higher to lower energy can be easily promoted by changing parameters such as dilution and temperature: the higher energy narrow peaks (373 and 417 nm) obtained with the higher concentrations of amine converts to the lower energy narrow peak (449 nm). These different absorption features have been previously attributed to CdTe MSCs of increasing sizes, characterized by progressively red-shifted peaks corresponding to smaller band gaps, as a consequence of weaker quantum confinement. [11][26] This assignment is mostly based on data acquired from laser-desorption-ionization (LDI) mass spectrometry. In particular, the peak at 373 nm has been assigned to the $(CdTe)_{13}$ cluster, while the peak at 449 nm to $(CdTe)_{34}$ cluster. In the LDI mass spectrum of the latter, the fragments $(CdTe)_{13}$, $(CdTe)_{33}$ and $(CdTe)_{34}$ are observed, while the $(CdX)_{13}$ cluster has only been isolated in the case of CdSe and also its LDI mass spectrum interestingly show several (also bigger) fragments, namely $(CdSe)_{13}$, $(CdSe)_{19}$, $(CdSe)_{33}$, $(CdSe)_{34}$. This characterization technique, however, is highly destructive, and does not ensure that the units detected after laser ionization were originally present in the sample. Furthermore, the fact that the same fragments are detected in mass spectra attributed to MSCs of different size is consistent with an

alternative interpretation, which relates the different energies of the narrow absorption peaks not to isolated nanoclusters of different sizes, but to changes in the degree of interconnection of nanoclusters associated into nanostrings.

The results presented above support the hypothesis that the redshift reflects a strengthening of the electronic coupling between the nanoclusters, since both in the case of a decreased concentration of amine caused by dilution and of a higher temperature, the amine mesophase (dynamic bonds) becomes more labile, favoring the formation of stronger *intra*-string interactions. The stronger electronic coupling is recognized in UV-Vis spectra as a shift to lower energies of the absorption transitions.

4.1.2.3 - *Reverse peak shift with increasing amine concentration*

Reverse peak shift (from lower to higher energy) was observed to occur in a stepwise manner when increasing amounts of amine were added overtime to a toluene solution initially containing only the Cd and Te precursors. Each addition was performed 45 minutes after the previous one, and the UV-Vis spectra were recorded over time (Figure 4.16).
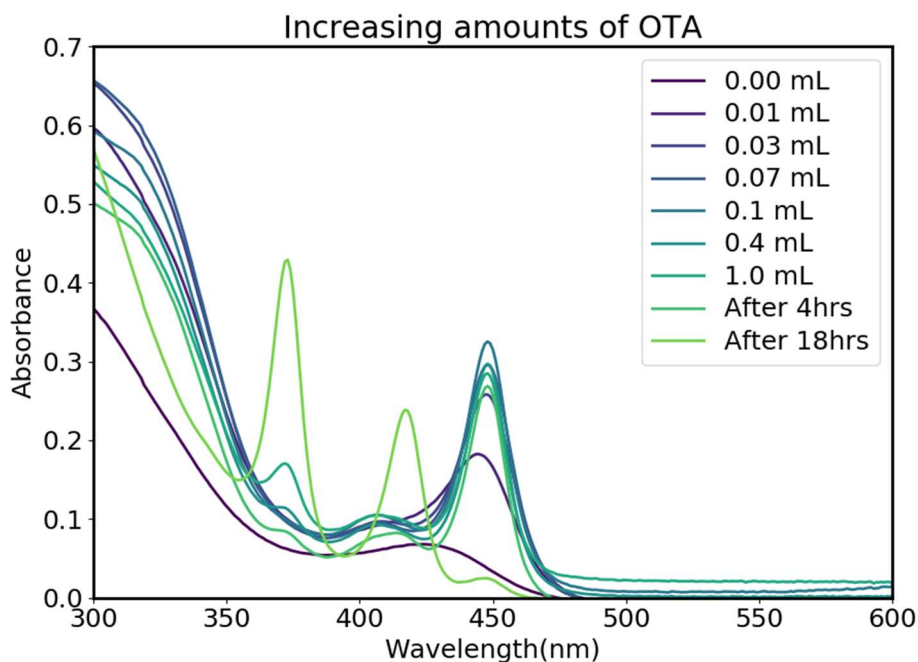
Figure 4.16. UV-Vis spectra of the sample in which increasing amount of octylamine were added (every 45 min) to a toluene solution containing only the Cd and Te precursors.

When the sample did not contain any amine, only a broad peak at ~ 420 nm was present, as observed in Section 4.1.1, while the addition of 0.01 mL of amine originated a less broad band centered at ~ 444 nm. A sharp absorption peak at 449 nm, characteristic of the low amine concentration solution arose when 0.03 mL of amine were added. The 449-nm sharp peak is the only feature observed with ≤ 0.1 mL (0.2 M) of amine in solution, while from 0.4 mL (0.8 M) the 373 nm peak started to rise, and increased in intensity when the concentration of amine was brought to 2 M (1 mL). Interestingly, the 417 nm peak, which was expected to appear before the highest energy one, appears and intensifies only over time.

If the peaks corresponded to MSCs of different sizes, this spectral shift from lower to higher energy with increasing concentration of amine, would imply the unlikely scenario of larger nanoclusters partially dissolving and becoming smaller over time. The results are, on the other hand, fully consistent with the model described above of nanoclusters interconnected to form nanostrings stabilized by amine ligands, in which the degree of *intra*-string coupling is dictated by the interactions with the amines. Even the slower kinetics of the "reverse" spectral shift with respect to the forward one promoted by temperature or dilution, could be rationalized in terms of how energetically easier it is to strengthen the interconnections between the clusters instead of loosening them.

Performing a temperature ramp on the same sample, which after 24 hours at room temperature only displays the 373 nm peak and a broader band around 425 nm, leads to a stepwise shift to lower energy peaks as observed above for the standard solutions samples. Also in this case, the 417 nm peak does not grow high in intensity, suggesting that the species originating this absorption peak readily interconverts in the higher or lower energy ones (Figure 4.17).
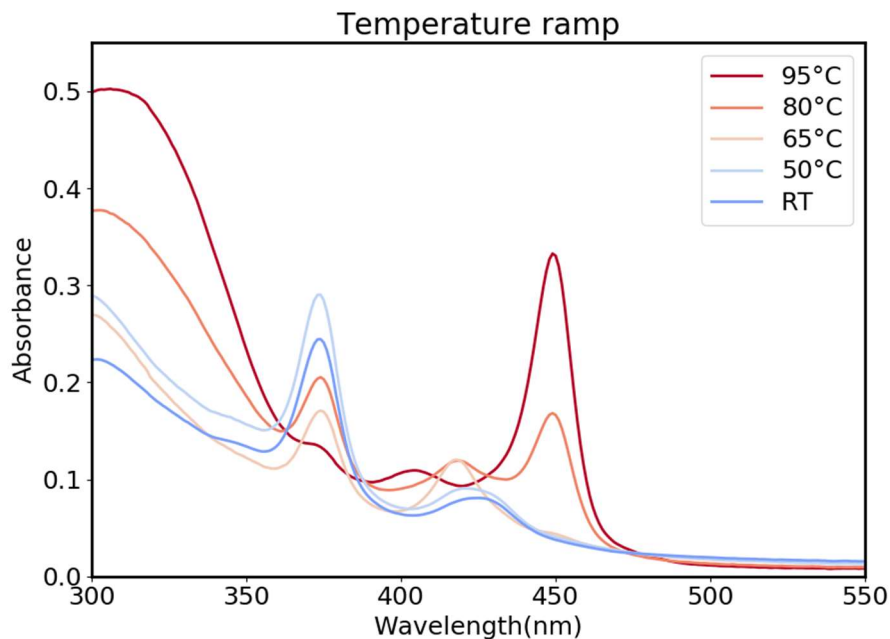
Figure 4.17. UV-Vis spectra of the temperature ramp performed on the sample obtained after the addition of increasing amounts of amine.

4.1.3 - Cd:Te ratio

The standard lower, intermediate and higher amine concentration solution were obtained using a Cd:Te ratio equal to 2:1. In this section, it is described how the same solutions were prepared with different volumes of precursors, in order to obtain different Cd:Te ratios (Table 4.2).

Cd:Te ratio	Cd(oleate)$_2$ (mL)	TOP-Te (mL)
4:1	0.2	0.1
2:1	0.1	0.1
1:1	0.1	0.2
1:2	0.1	0.4
1:4	0.1	0.8

Table 4.2. Metal and chalcogenide amount used to obtain different Cd:Te ratio solutions.
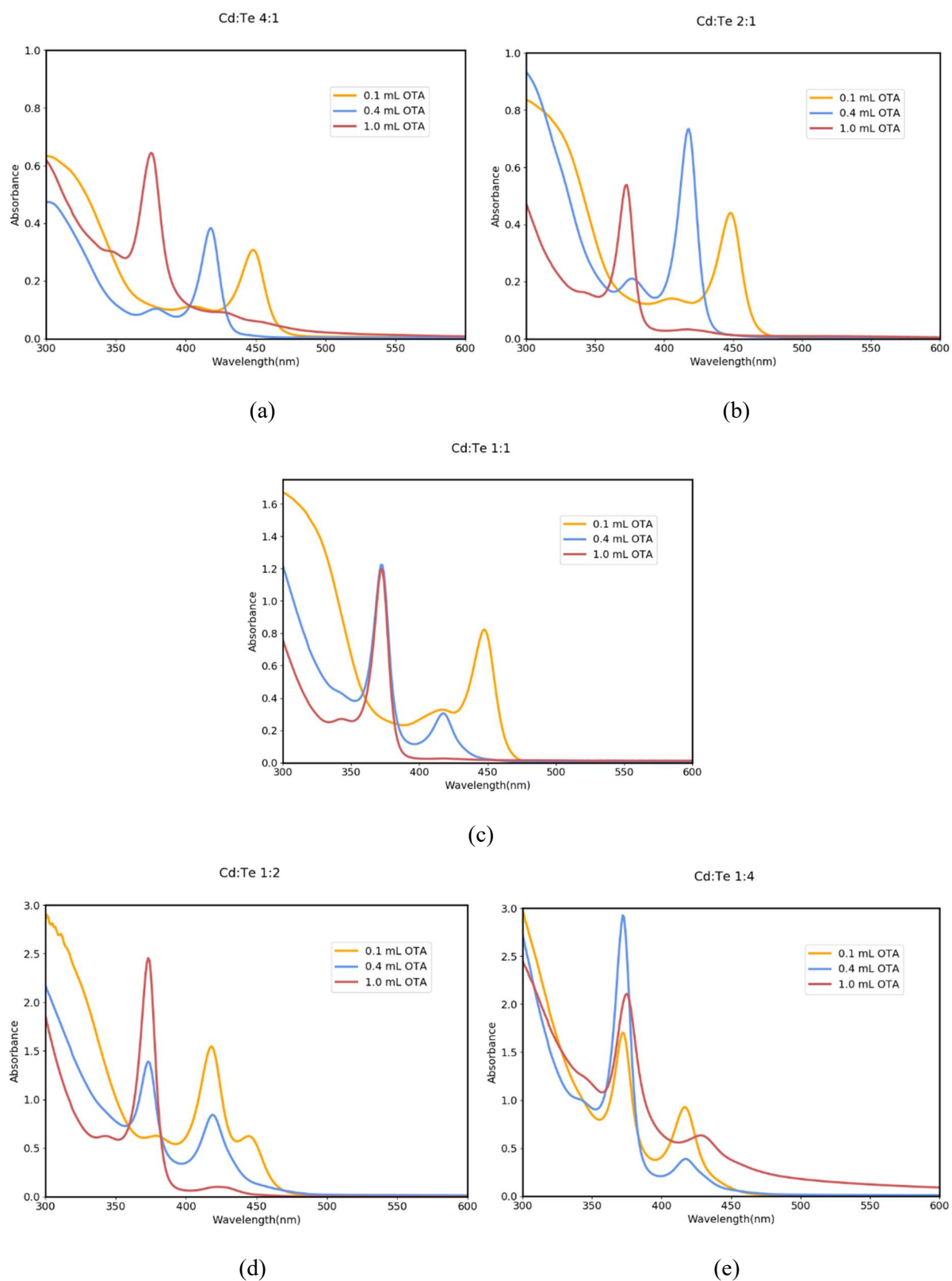
Figure 4.18. UV-Vis spectra of the low, intermediate and high amine solutions prepared with different Cd:Te ratio, specifically 4:1 (a), 2:1 (b), 1:1 (c), 1:2 (d), 1:4 (e). The relative intensity of the peaks is different in each case, relatively to the absorbance scale.

The UV-Vis spectra (Figure 4.18) show how the intensity of the peaks increases with the amount of Te precursor added, meaning that the reaction with $Cd(oleate)_2$ proceeded further and a larger quantity of [CdTe] units was formed, since the intensity of the absorption transitions is proportional to the number of [CdTe] units. This leads to the conclusion that $Cd(oleate)_2$ is the rate limiting reagent, since a higher amount of it can react when the quantity of Te in solution is increased. Regarding the relative intensities of the peaks, it is worth to notice that, compared to the samples outlined in Table 4.1, different peaks are stabilized by the same amine amount used in the standard solutions: for example, in presence of a Cd:Te ratio of 1:4, in addition of 0.1 mL of octylamine the peaks at 417 and 373 nm are visible, while for the standard solution only the peak at 449 nm was observed (Figure 4.2). In general, the species giving rise to the 373 nm peak seems to be more and more easily stabilized when the reaction proceeds further (*i.e.* when a higher amount of Te is present in solution), and more [CdTe] units are formed.

4.1.4 - Role of amine

To better understand the role of the amine in the stabilization of narrow absorption peaks, different amines were compared. First, to investigate the differences between primary and secondary or tertiary amines, UV-Vis absorption spectra were recorded for the low amine concentration solution, in which n-octylamine, di-n-octylamine, and tri-n-octylamine were used respectively (Figure 4.19). In case of the secondary and tertiary amines, low-intensity, broad peaks appear, having maximum intensity at 420 nm and 426 nm, respectively. Interestingly, the peaks are similar to the broad peak obtained when no amine is present in solution. This allows to conclude that the reaction leading to the formation of [CdTe] units still occur, but narrow absorption peaks are formed at room temperature only when primary amines are present in solution.
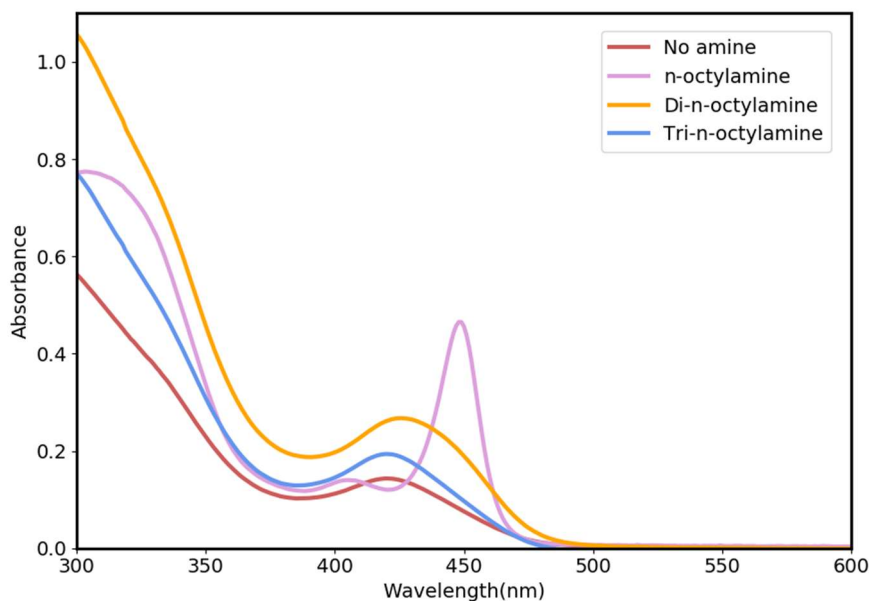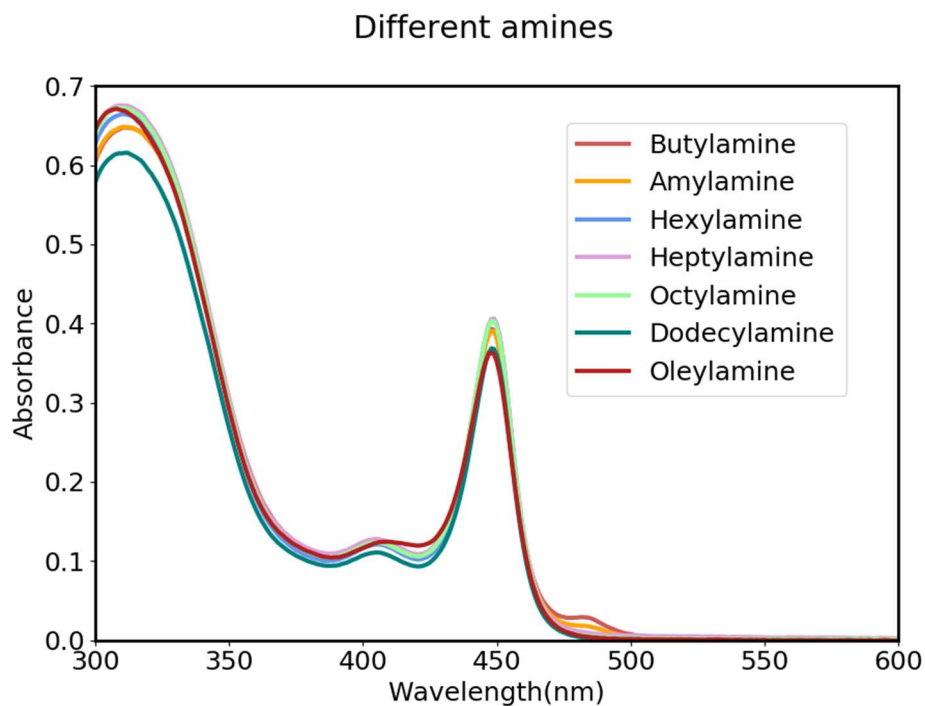
Figure 4.19. UV-Vis spectra of the low amine concentration solution prepared with different amines.

TEM images of the sample containing di-n-octylamine were obtained, in order to better investigate the nature of the broad peak. As observed above for the samples containing broad absorption peaks, no bundles are observed in the TEM images, but the species present in solution appears as very short and thin wires, separated between each other in a disordered way (Figure 4.20). Whilst it cannot be safely concluded that these species were already present in solution and do not form on the TEM grid during the drying process, it is evident how the string-like bundles assigned above to the sharp absorption peaks are not observed in this case.
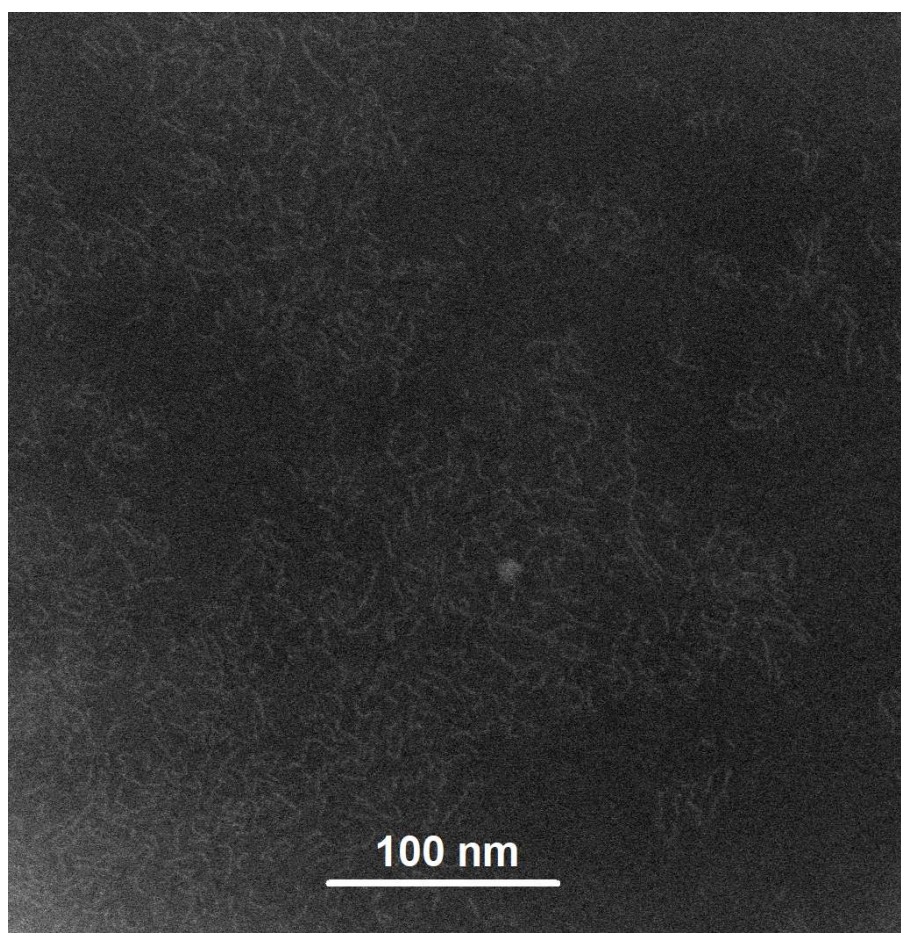
Figure 4.20. HAADF-TEM image of the sample containing 0.1 mL of di-n-octylamine.

To determine the influence of the length and saturation of the chain of the primary amine, the low amine concentration solution was prepared with different amines: butylamine (C4), amylamine (C5), hexylamine (C6), heptylamine (C7), octylamine (C8), dodecylamine (C12), and oleylamine (C18, one double C=C bond at position 9,10). The UV-Vis absorption spectra show that the 449 nm peak initially arises unaffected by the difference in chain length, even though a faster kinetic was observed for shorter alkylamines. Concerning amine saturation, using a bent amine such as oleylamine did not lead to any change in the UV-Vis spectra. However, over time, solutions containing amines with chain length < C8 display an increase in turbidity, and a new lower-energy absorption peak appears at 483 nm (Figure 4.21). The same peak was observed in Figure 4.10 in Section 4.1.2, subsequent to the heating of the sample up to 105°C, and was attributed to the formation of thicker nanobelts.
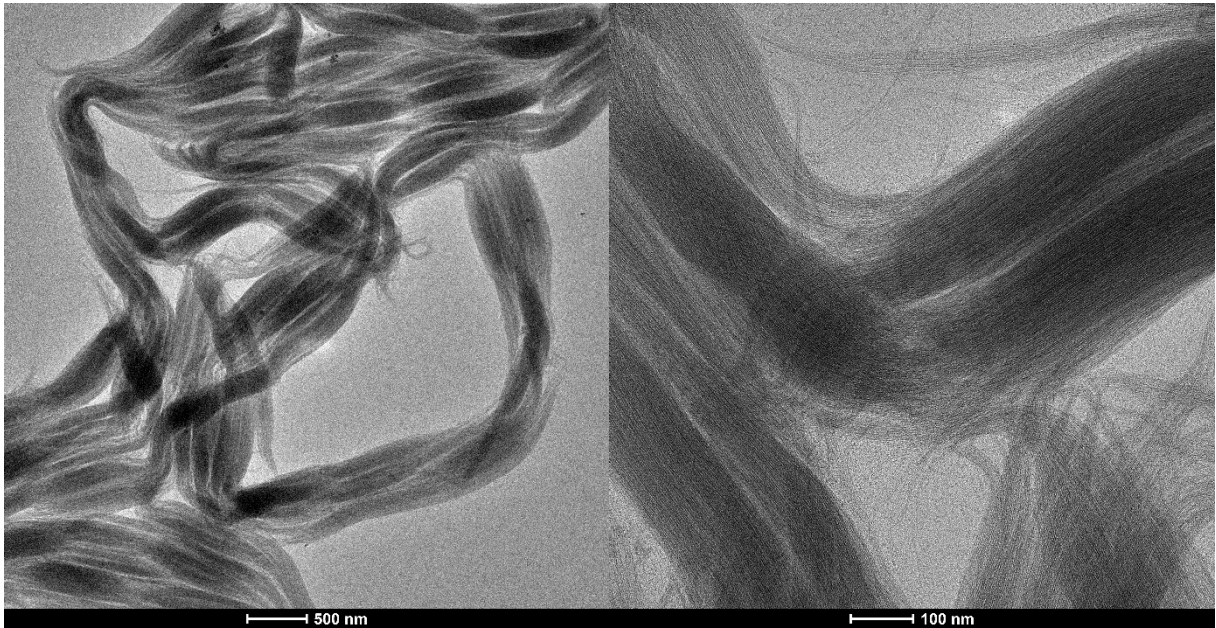
Figure 4.21. UV-Vis spectra of the low amine concentration solution prepared with amines of different length and nature.

TEM images were obtained for the samples containing butylamine, amylamine, hexylamine, heptylamine, octylamine and dodecylamine, and display strings in every case, with different thickness and twisting of the bundles (Figure 4.22).
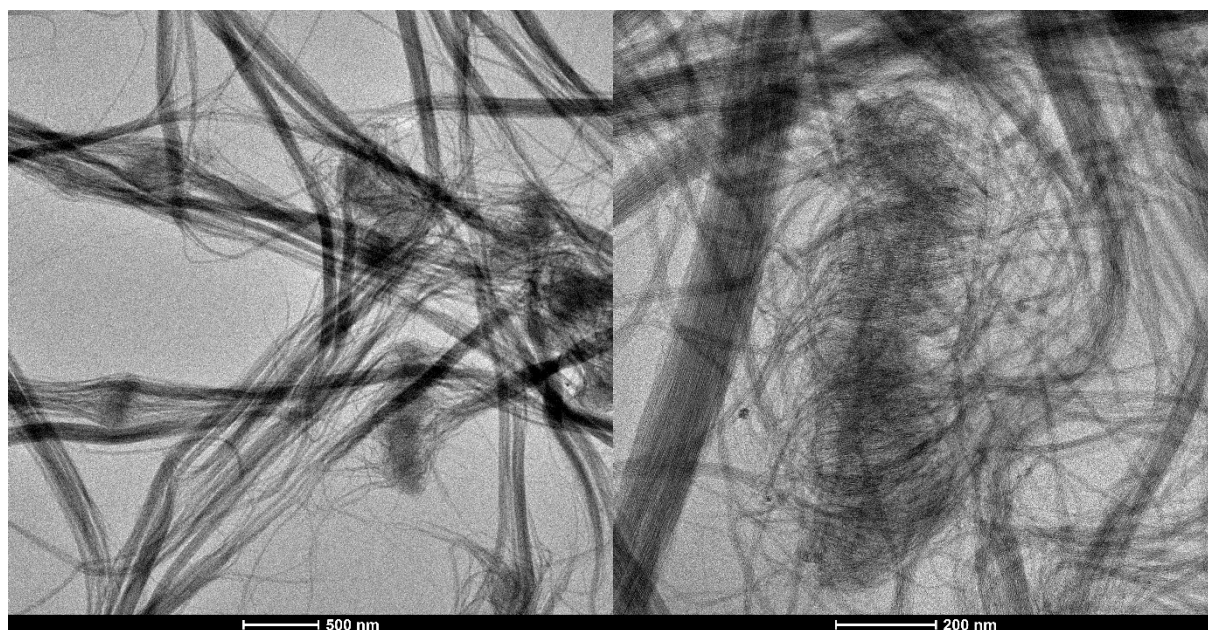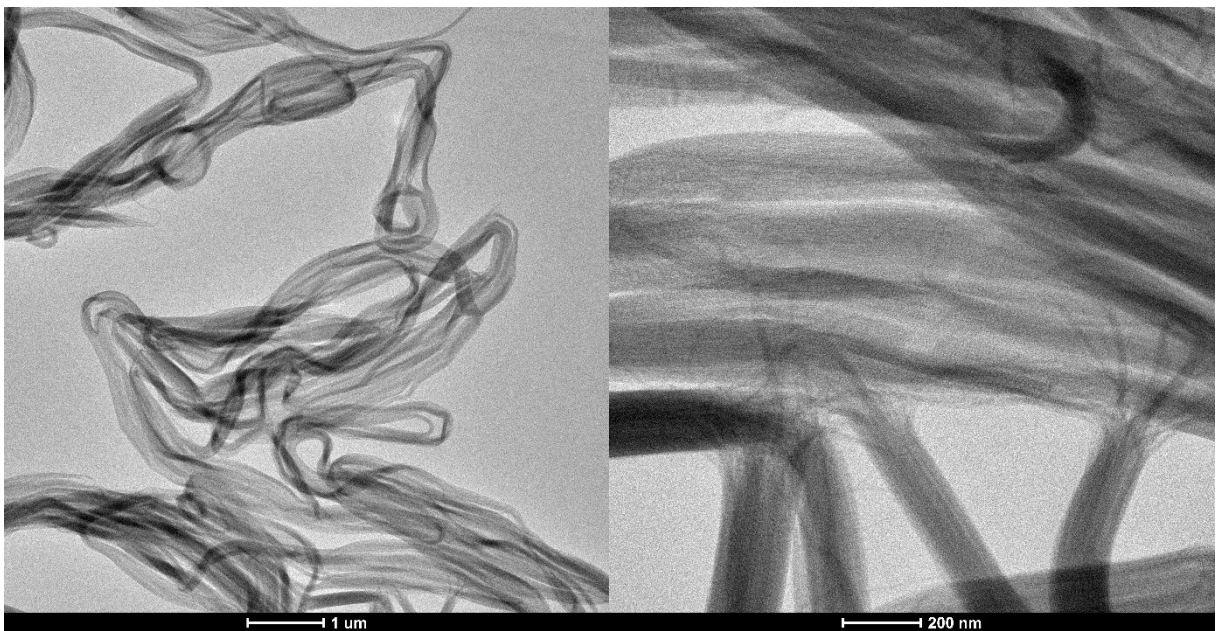

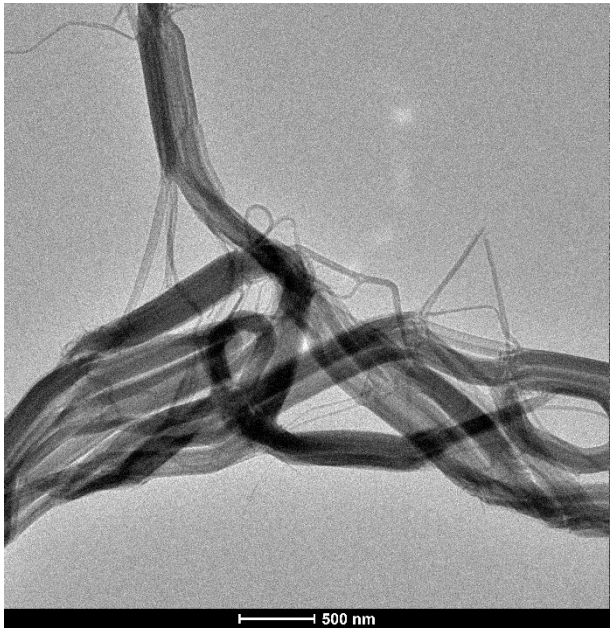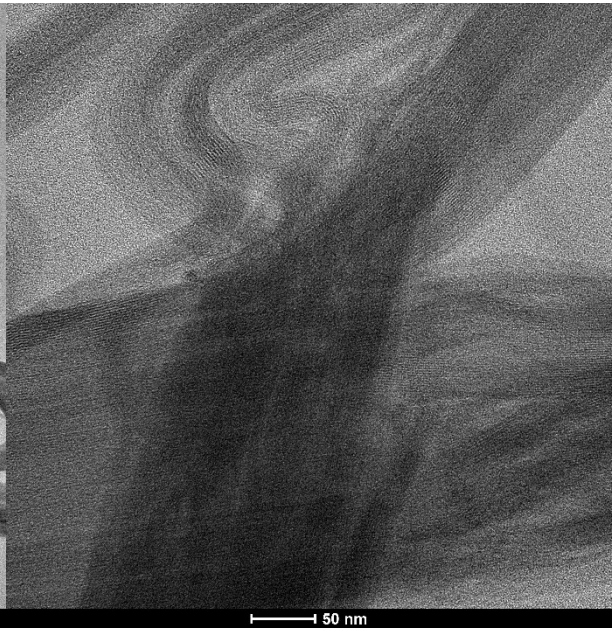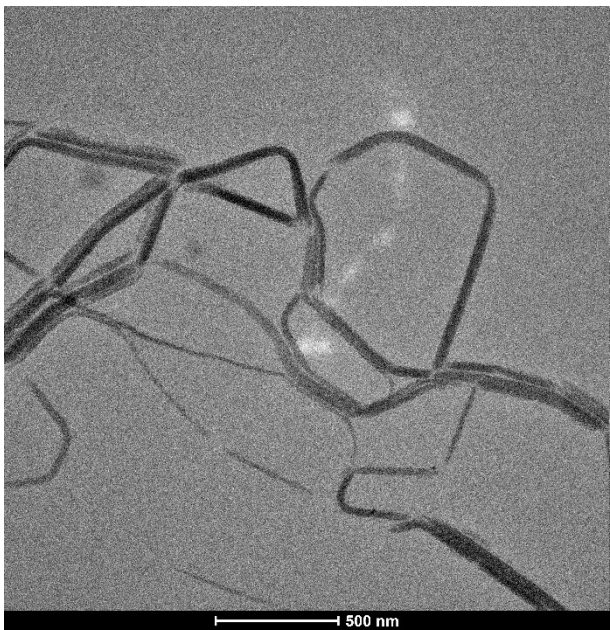(a)   (b)

(c)

(d)

(e)

(f)
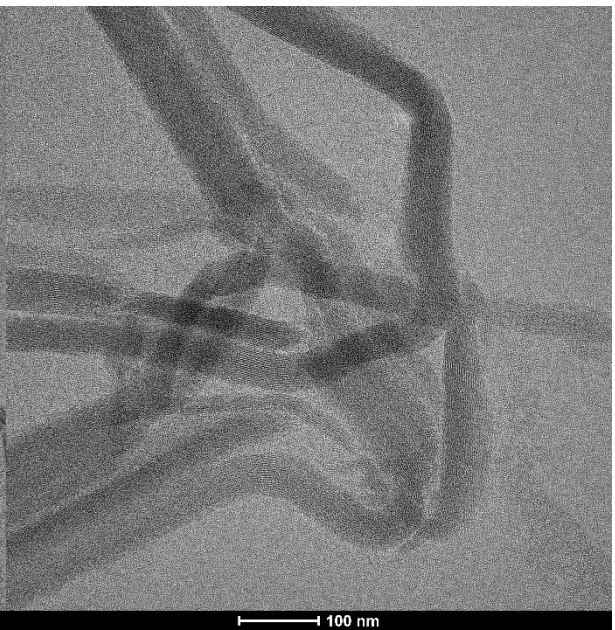
(g)

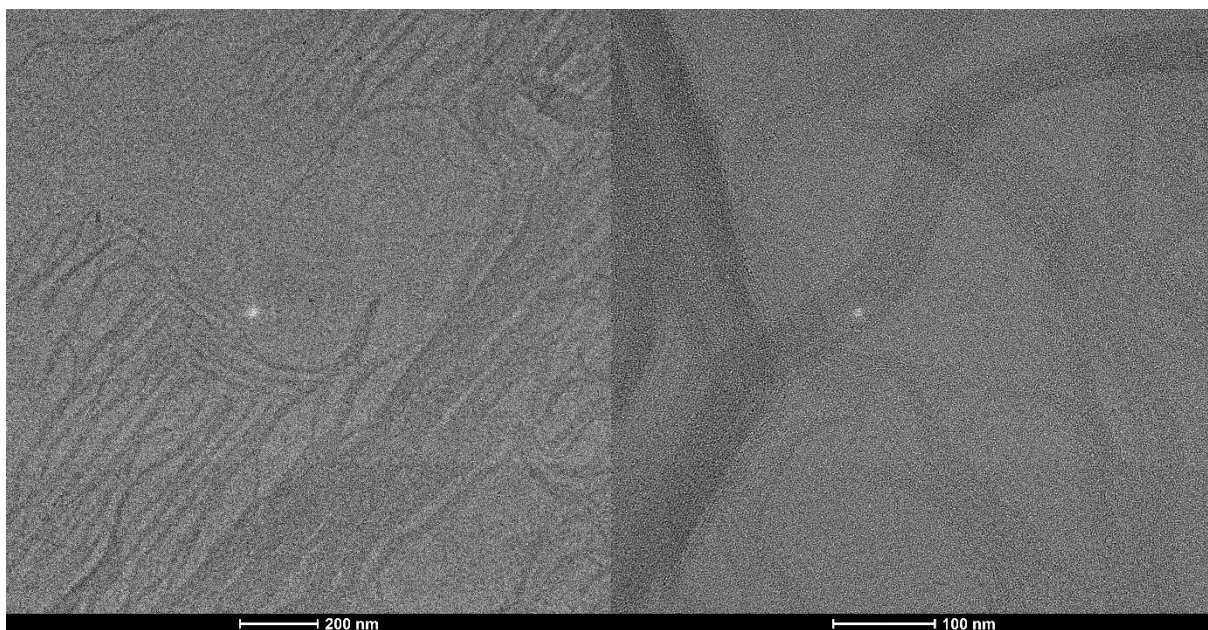
(h)

(i)

(j)

<div align="center">(k)   (l)</div>

Figure 4.22. HAADF-TEM and TEM images of the samples obtained using butylamine (a, b), amylamine (c, d), hexylamine (e, f), heptylamine (g, h), octylamine (i, j), dodecylamine (k, l).

For alkylamines with $C \geq 8$, the TEM images displays twisted bundles which start breaking periodically. In these samples, the formation of a precipitate was observed only after two/three days from preparation.

These results clearly indicate that chain length is not directly involved in the formation of sharp absorption peaks, which were attributed in Section 4.4.1 to the presence of nanostrings in solution, formed in every case. However, different kinds of interactions can be held responsible for their different thickness and twisting periodicity: in case of shorter alkylamines, on-off binding dynamics are faster, strength of interchain van der Waals interactions is weaker and diffusivity in solution is higher, leading to a faster formation of large aggregates or superstructures. It is worth to notice also that the presence of charged species in the system cannot be excluded, contributing to the observation of the different bundles conformations in the TEM images.

In general, these results also support the notion that the sharp absorption peaks require the formation of a tubular mesophase in which the concentration of the primary alkylamines play an important role, while the relative conformations and orientations of

the $[CdTe]_x$ cluster units inside the strings are not affected by the amine length and saturation, since no shifts in energy of the peaks was observed.

4.1.5 - Te precursor

The syntheses previously described were performed using a Te precursor solution containing a large excess of phosphine, namely an amount of TOP 45 times greater than the amount of Te. To analyze the role of the free phosphine in the formation process of [CdTe] units, the low amine concentration solution was prepared using a stoichiometric TOP-Te precursor. Under these conditions, the change in color which was observed for the samples displaying the absorption peak at 449 nm was not observed, and the solution remained transparent, demonstrating that the excess of phosphine is essential for the reaction to occur.

Starting from the solutions prepared with stoichiometric TOP-Te, the *same molar amount* of different phosphines was added in order to investigate the effects of the excess of phosphine and of its type (Table 4.3). The phosphines chosen for this study were: triphenylphosphine (TPP), tributylphosphine (TBP), triphenylphosphite (TPT), trioctylphosphine (TOP) and diphenylphosphine (DPP). In the UV-Vis spectra of the resulting solutions, a narrow peak at ~ 449 nm was observed in each case except with TPP, which gives a transparent solution and a corresponding featureless spectrum.

| Phosphine	Volume (mL)	Mass (g)	Moles (*10-4)	Peak position (nm)
TPP	-	0.0997	2.24	-
TBP	0.055	-	2.24	447
TPT	0.059	-	2.24	450
TOP	0.1	-	2.24	449
DPP	0.039	-	2.24	449

Table 4.3. Composition of different solutions obtained adding the same molar amount of free phosphine to the low amine concentration solution, containing stoichiometric TOP-Te as precursor.
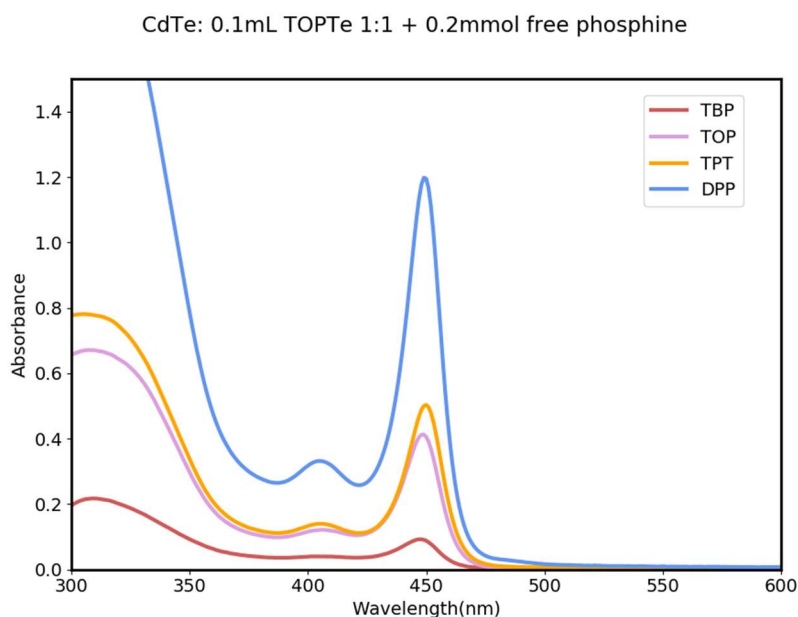
Figure 4.23. UV-Vis spectra of the different solutions obtained adding the same molar amount of free phosphine to the low amine concentration solution, containing stoichiometric TOP-Te as precursor.

Nevertheless, the peaks display slightly different positions and different intensities: the least intense peak was found when TBP was used, followed by TOP and TPT, while DPP displays an extremely high intensity peak compared to the other phosphines.

The trend in peaks intensity is reported in Figure 4.24:
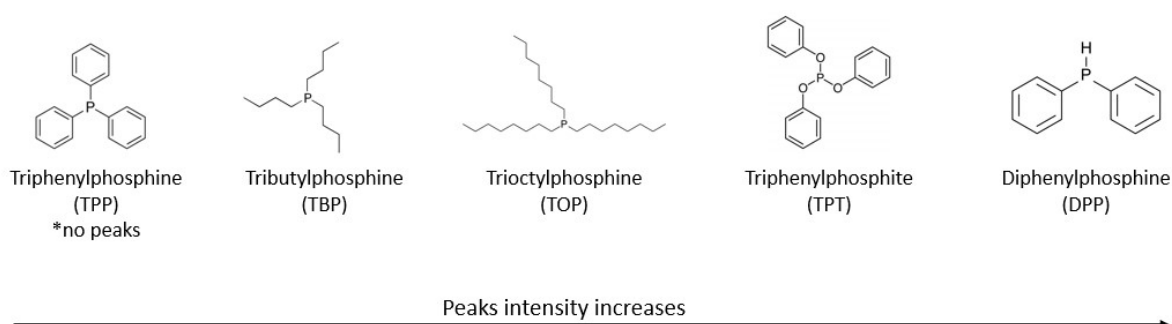
Figure 4.24. Trend in peak intensity as observed from the UV-Vis spectra reported in Figure 4.23.

Interestingly, in the preparation of the phosphine-Te precursor solutions, TBP, TOP and DPP show the inverse trend in reactivity towards Te than the one observed for the peaks' intensity, with TBP having the higher affinity to Te and quickly forming the complex at

room temperature, while DPP required longer reaction times and higher temperatures to react (40-50°C for 1 hour). The overall intensity of the narrow peaks obtained in the UV-Vis absorption spectra (Figure 4.25) appears to be lower compared to the ones reported in Figure 4.23 and 4.24, even if the trend in intensity is retained, suggesting the phosphine is more effective in the reaction mechanism when it is present in excess in solution rather than when directly added as the Te precursor.
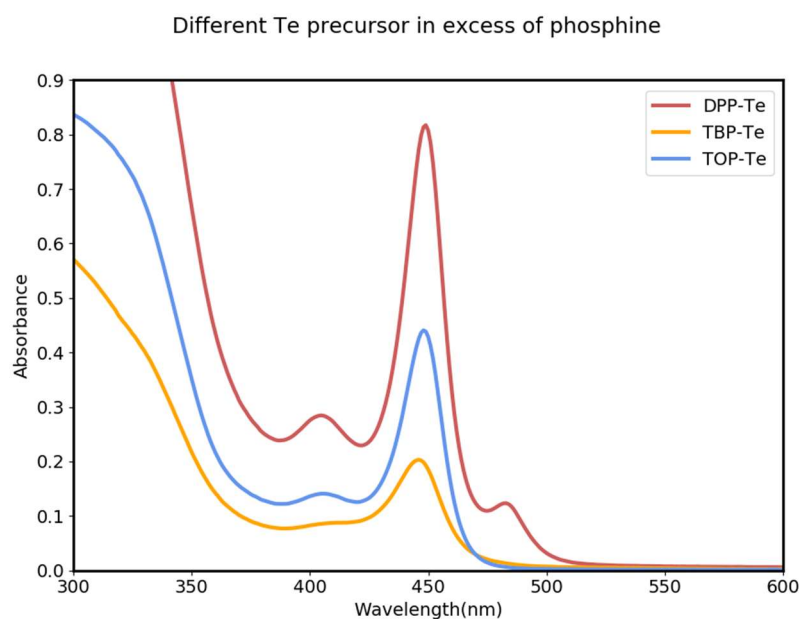

Figure 4.25. UV-Vis spectra of the low amine concentration solutions obtained using different Te precursors.

These results suggest that phosphines have an important role in obtaining narrow peaks, with the phosphine-chalcogenide bond strength being an important parameter in allowing the reaction to proceed further, thus forming a greater number of [CdTe] units (more intense peaks). The trend in peaks intensity can also be rationalized in terms of bulkiness of the substituents connected to the P atom of the phosphines: TPP is a tertiary phosphine in which the phenyl rings mobility is strongly costrained, while for TPT, the presence of the O atoms leads to much more freedom and the π-systems of the rings can easily stack on top of each other; on the same line, TBP and TOP contain alkyl chains as substituents, which create a greater steric hindrance around the P atom, which translates into a lower reactivity. In all cases, DPP was found to be the most reactive

phosphine, providing faster kinetics and more intense narrow peaks. Compared to the other phosphine tested, DPP is the only secondary phosphine and, as a consequence, the steric hindrance is remarkably reduced. Another peculiarity of DPP is its strong reducing power, suggesting this can also have an important role in the formation mechanism: the Te atom, present in its oxidation state (0) in the precursor, needs to be reduced to (-2) when bonded to Cd^{2+} in the $[CdTe]_x$ units. For this reason, one of the elementary steps of the reaction must be the reduction of Te, which can be accomplished by the excess of phosphine, that appeared to be necessary for the reaction to occur.

In order to test the importance of reduction as one of the elementary steps in the formation mechanism of $[CdTe]_x$ units, solutions with the three concentrations of amine reported above (Table 4.1) were prepared, in the presence of stoichiometric TOP-Te, and one drop of lithium triethylborohydride (Superhydride ®, SH), a strong reducing agent of different nature compared to the phosphines. Interestingly, the reaction takes place and proceeds with a much faster kinetic, as evidenced by a quicker change in color, accompanied by an increase in turbidity. In the UV-Vis absorption spectra, shown in Figure 4.26, the expected peaks were observed, even if they display lower intensities and a higher scattering background compared to the standard solutions reported in Figure 4.1. Moreover, in the case of the Superhydride, for the solution with low amine concentration, a weak peak at 483 nm can be noticed; the same peak was observed for the analogous "standard" solution when the temperature was increased above 90°C or at room temperature when shorter amines (hexylamine or butylamine) were used (Section 4.1.2, Section 4.1.4).
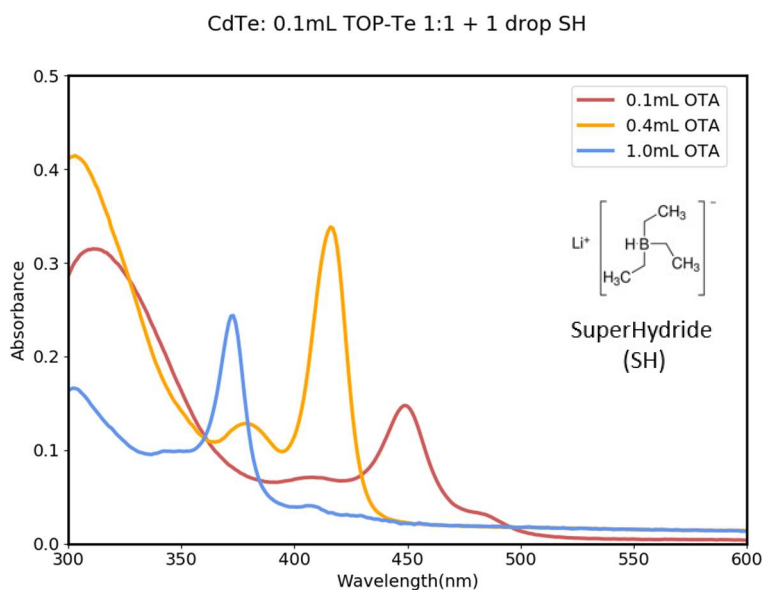
Figure 4.26. UV-Vis spectra of the solutions in which SH was added to solutions containing stoichiometric TOP-Te as precursors.

A marked difference in the reactivity was observed when SH was added to a solution containing only toluene and stoichiometric TOP-Te (Figure 4.27): under these conditions, a milky suspension was initially formed, which cleared up after 0.1 ml of octylamine and finally turned dark yellow when the Cd precursor was added. The absorption spectra in this case displays a more intense peak, comparable to the one obtained using an excess of TOP, suggesting the reaction occurs more quantitatively. Nevertheless, two different effects were observed: using a phosphine with a stronger reducing power leads mostly to an increase in intensity of the peaks, together with a faster reaction rate, while the use of SH as reducing agent mostly affects the kinetic of the reaction rather than the peaks' intensities.
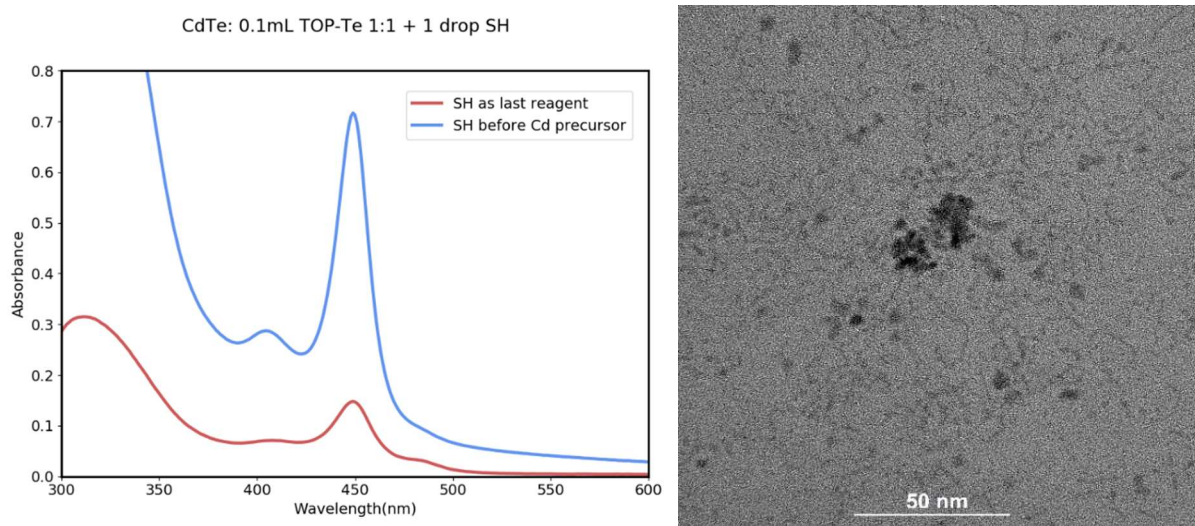
Figure 4.27. On the left, UV-Vis spectra of the low amine concentration solution in which SH was added before the addition of the Cd precursor (red line), and after (blue line). On the right, TEM image corresponding to the red spectrum.

In conclusion, the reducing agent (an uncomplexed phosphine or the SH) is directly involved in the reaction mechanism. In particular, its effect is clearly related the Te precursor, and can therefore be rationalized as the reduction of Te^0 to Te^{2-}, which can subsequently react with Cd^{2+} to form $[CdTe]_x$ units.
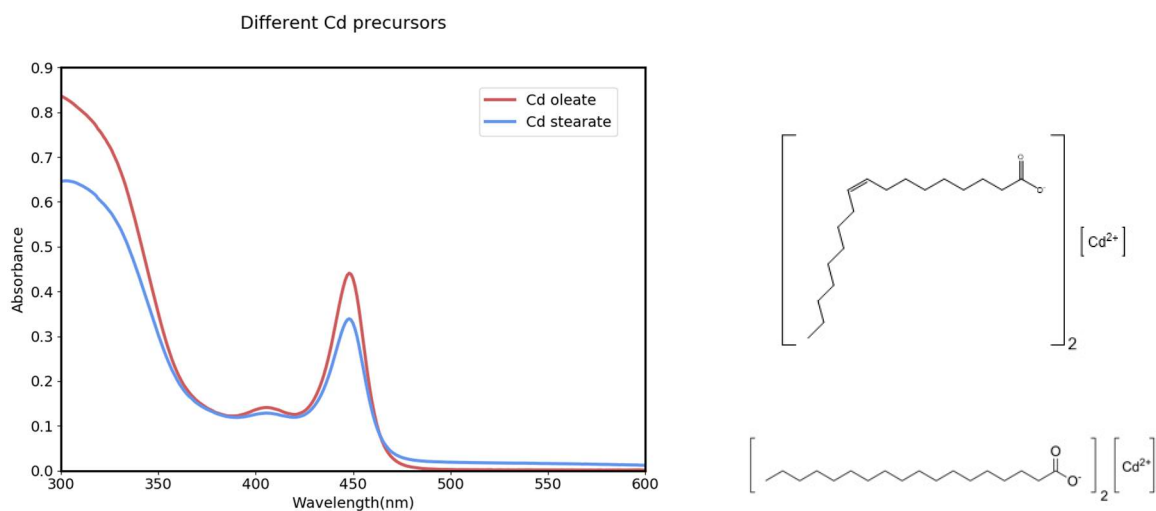
4.1.6 - Cd precursor

Another aspect to demand further investigation is the nature of the cadmium precursor. At first, Cd(oleate)$_2$ was compared to CdMe$_2$ (Figure 4.28), which is an unstable and reactive compound. Nevertheless, the UV-Vis absorption spectra over time for the low amine concentration solution showed that the 449 nm absorption peak appears for the CdMe$_2$ solution only over a long period of time and with a remarkably broader fwhm, whereas the use of a Cd carboxylate leads to faster kinetic as well as more well-defined peaks. The oxidation state of Cd in the CdTe clusters (or QDs) must be (2+), thus a faster kinetic could be expected using Cd(oleate)$_2$ as precursor, in which Cd is already in the (2+) oxidation state, while it is formally (0) in CdMe$_2$, which needs to be oxidized first.
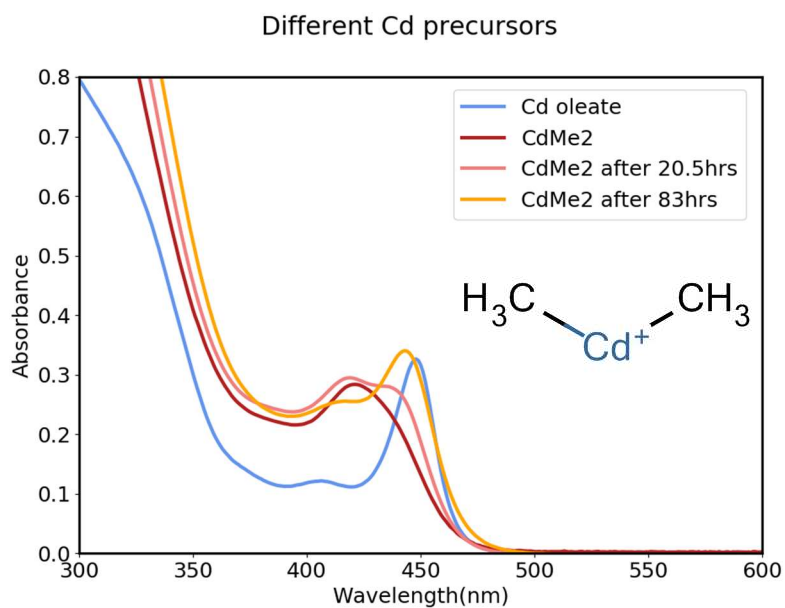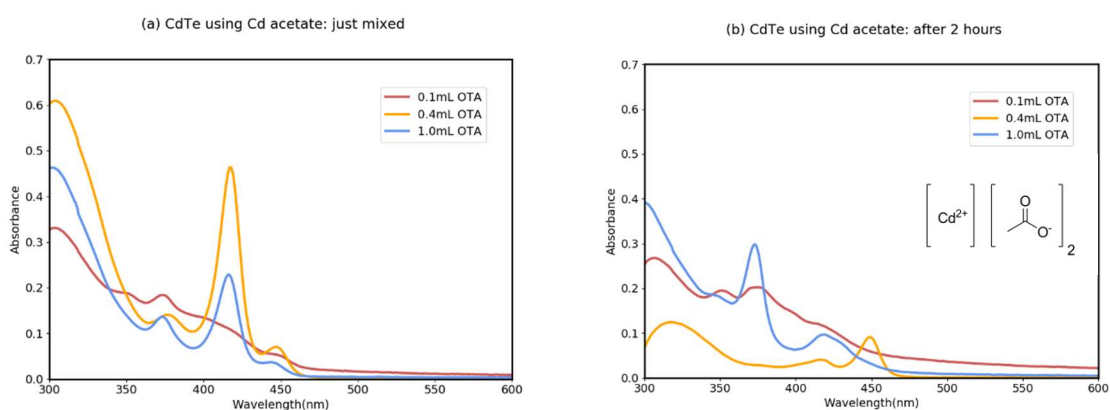
Figure 4.28. UV-Vis spectra of the solution in which the use of Cd(oleate)$_2$ was compared to CdMe$_2$ as the metal precursor.

Testing a Cd precursor containing a saturated carboxylate, namely Cd stearate, led to the conclusion that the absence of an insaturation in the alkyl chain does not have any effect on the stabilization of the peaks, since the 449 nm peak was still observed in the low amine concentration solution (Figure 4.29). This suggests that packing of the Cd precursor does not affect the formation of [CdTe] units, and that the relevant interaction between the amine, Cd and Te precursors does not directly involve the carboxylate chain. Moreover, the formation of the tubular template, verified by the presence of the sharp absorption peaks, requires the presence of both Cd and Te bound in [CdTe]$_X$ units, while the oleate is dispersed in.

Figure 4.29. UV-Vis spectra in which the use of Cd(oleate)$_2$ was compared to Cd(stearate)$_2$ as the metal precursor.

The next Cd precursor tested was Cd(acetate)$_2$. In this case, due to its insolubility in toluene, stock solutions of the precursor were prepared dissolving anhydrous Cd(acetate)$_2$ directly in octylamine, obtaining solutions with the desired molarity (0.1 M). The following results were obtained for the solutions prepared with different concentrations of amine (Figure 4.30).


Figure 4.30. UV-Vis spectra of the three amine concentration solutions in which Cd(acetate)$_2$ was used as precursor.

In the high amine concentration solution (2 M), a higher intensity peak at 417 nm arises after mixing, while the 373 nm peak which was observed in the standard solution (Section 4.1.1) only increases in intensity over time; in the sample containing 0.4 mL of

octylamine (0.8 M), the 417 nm peak observed above for solutions with the same amine concentration is the first to appear, but decreases in intensity while the 449 nm peak arises over time; in the low amine concentration solution (0.2 M), a strong scattering background is displayed, which increases even further after two hours from preparation, eventually disguising the formation of a doublet at 351-371 nm. In presence of the lower amine concentration, the solutions tend to show a stronger scattering background compared to the spectra previously taken, which can be ascribed to the formation of larger aggregates/superstructures, as confirmed in the TEM images shown in Figure 4.31.

(a)

<center>(b)   (c)</center>
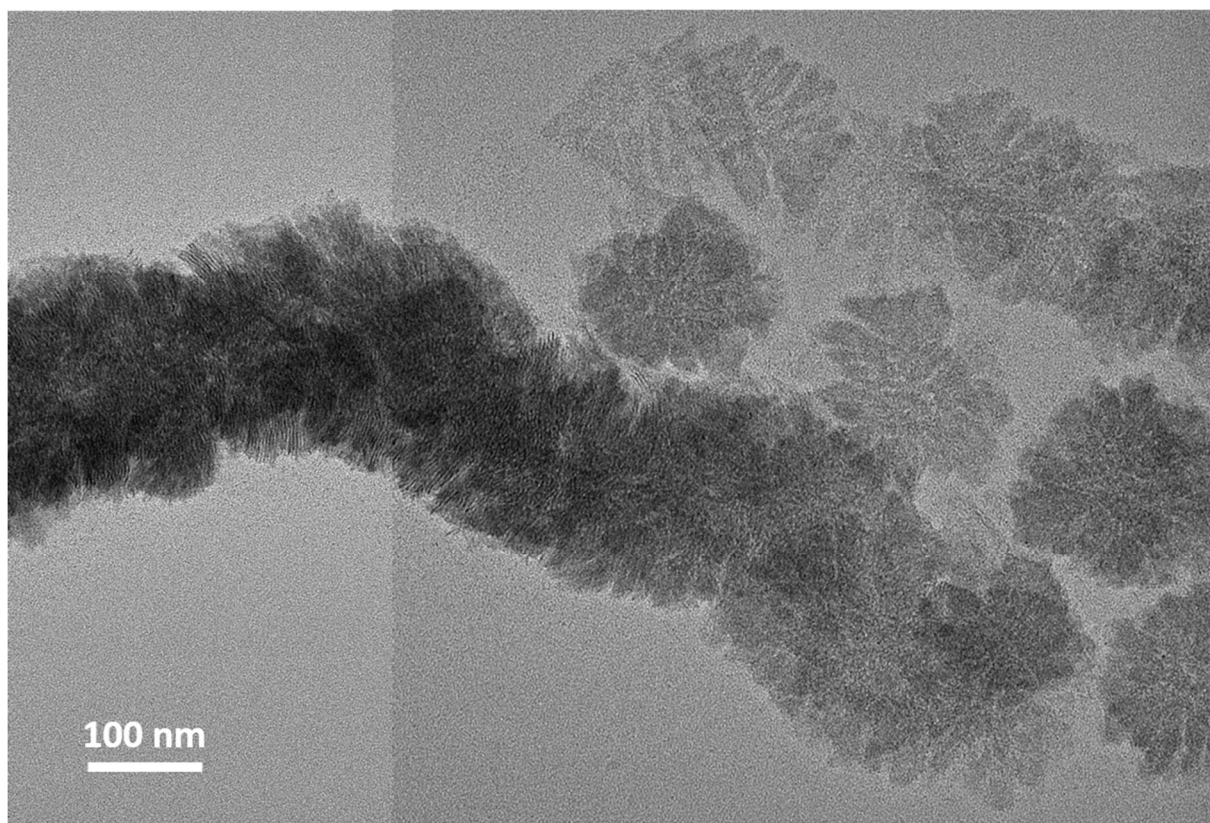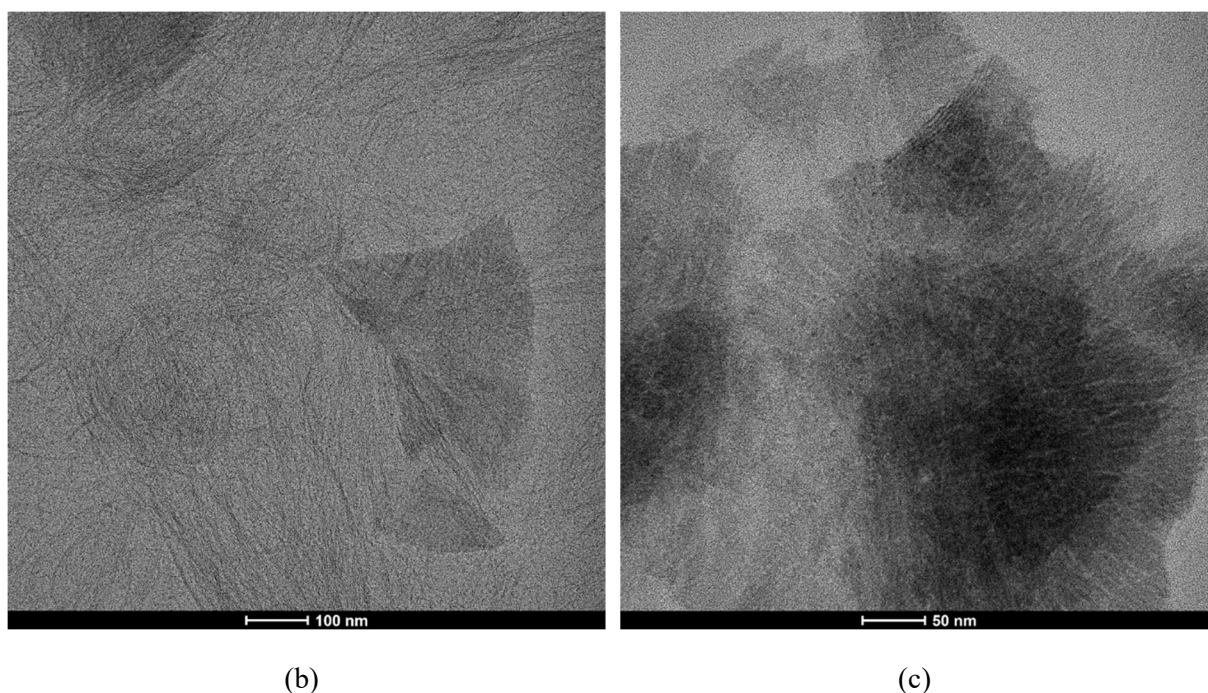
Figure 4.31. TEM images corresponding to the low (a) and high (b, c) amine concentration solution.

The sample with lower amine concentration appears as large superstructures ("nanobrushes") of stacked triangular nanosheets, arranged in flowers, then further assembled perpendicularly to the length of the superstructures. In the case of the sample with higher amine concentration, two species are recognizable from the TEM images: long bundled fibrils and large triangular nanosheets, partially assembled. The corresponding absorption spectrum can therefore be interpreted as a combination of the signals from these two species: two singlets at 373 and 417 nm (attributed to the fibrils and representing the only signal in the "just mixed" solutions) and the doublet at 351-371 (attributed to the nanosheets).

These results suggest that, besides having a shorter alkyl chain, in the case of $Cd(acetate)_2$, polarity and dielectric constant of the system play an important role in the stabilization of narrow peaks.

In conclusion, the use of $Cd(acetate)_2$ as precursor can bring interesting insights on how the clusters can assemble to form 2D nanosheets and superstructures. The former can be identified by a double peak in the UV-Vis spectra at ~ 351-373 nm, in combination with a strong scattering background, in the case of their self-assembly. Further results as well

<center>65</center>

as TEM images to confirm the formation of superstructures will be presented and discussed in Section 4.2.

## 4.1.7 - Addition of cations/anions

The addition of organic charged species to the reaction mixture were investigated, in order to better understand if a tubular/lamellar mesophase is present in solution that influences the formation of CdTe clusters. Didodecyldimethylammonium bromide (DDAB), ammonium bromide (NH$_4$Br), hexadecyltrimethylammonium bromide (HTAB) and hexadecyltrimethylammonium chloride (HTAC) were used as cations, while sodium myristate was used as anion, that could be possibly interfere with the formation of a mesophase. In all cases the ions were added to a solution containing the lower amine concentration (*viz.* 0.2 M), either before or after the addition of the Cd and Te precursors. The resulting UV-Vis spectra are reported in Figure 4.32.
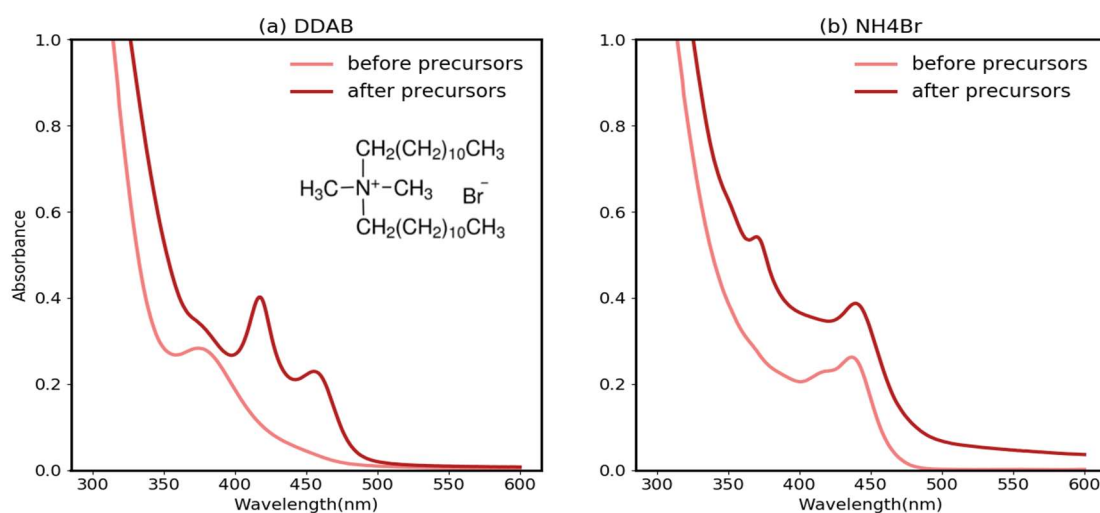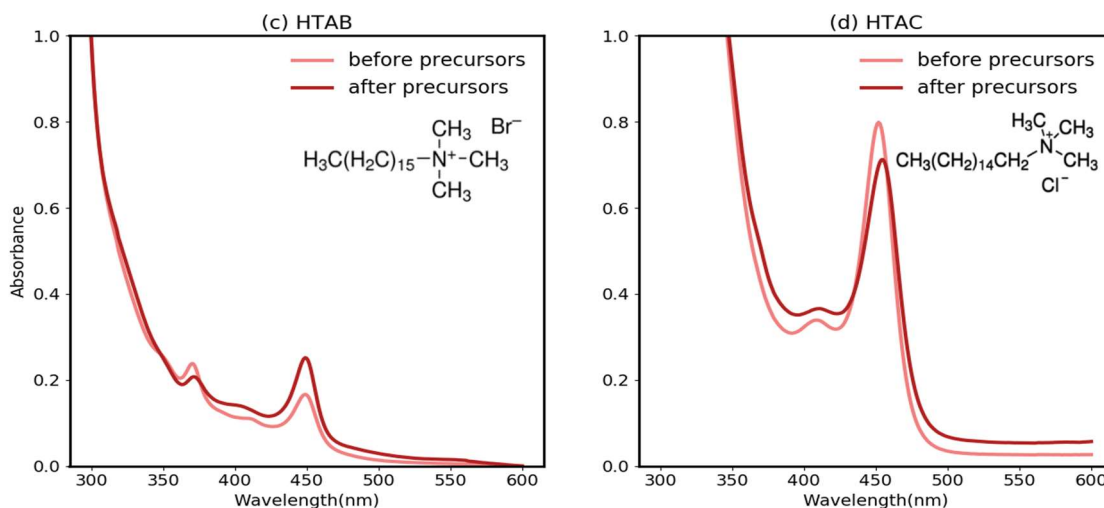
Figure 4.32. UV-Vis spectra displaying the effects of the addition of different organic cations before and after the addition of the Cd and Te precursor.

Analyzing the effect of cations, it is evident how in the case of DDAB, the addition of the salt before the metal and the chalcogenide precursors prevents the formation of the species that give rise to the 449 nm peak, which forms in the other cases. An intense scattering background is observed when using NH_4Br, possibly due to the scarce solubility of the salt in toluene. HTAC and HTAB do not display significant differences, confirming that the counterion associated to the ammonium ion does not affect the reactivity. Nevertheless, these ions present only one long alkyl chain compared to the two chains in DDAB: the steric hindrance of the latter might be the reason why it is the only cation able to interact with the system present in solution, preventing the formation of sharp peaks.
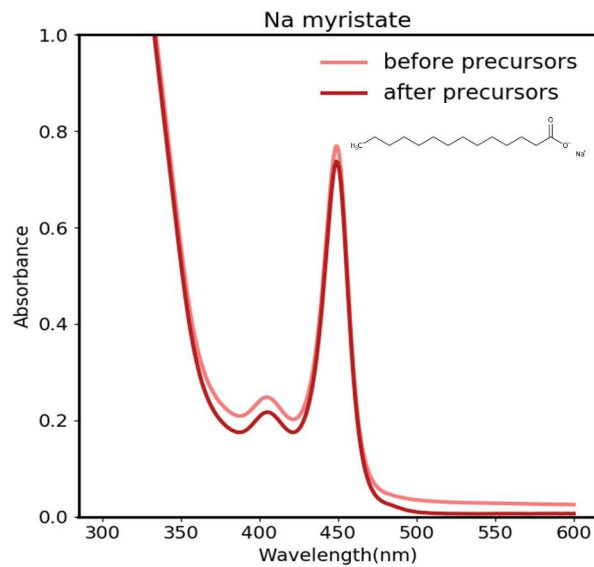
Figure 4.33. UV-Vis spectra displaying the effects of the addition of Sodium myristate before and after the addition of the Cd and Te precursor.

The addition of sodium myristate did not lead to any changes in the UV-Vis spectra, as reported in Figure 4.33. This suggests that the presence of an anion, specifically a free carboxylate, does not affect the formation of a mesophase in the system. The result is in line with what was observed above for the use of different carboxylates as Cd precursors, which did not lead to any difference (Section 4.1.6).

4.2. Superstructures

As previously observed in Section 4.1.6, the use of Cd(acetate)$_2$ as metal precursor led to different results compared to the use of Cd(oleate)$_2$. In particular, the arising of a double peak at high energies as well as an increase in scattering background in the UV-Vis spectra was attributed to the formation of 2D structures or larger assemblies.

To better understand which are the parameters leading to the formation of superstructures, three different Cd(acetate)$_2$ precursors were compared, obtained by dissolving anhydrous Cd(acetate)$_2$ in either octylamine (OTA), oleylamine (OLAm) or a 1:1 mixture of the two amines. The use of oleylamine allows to investigate how the co-presence of amines of different lengths would affect the formation of superstructures: [17] Buhro et al. previously reported the use of OLAm as the agent responsible for the "unbundling" of CdSe quantum belts, which were obtained by the group in presence of only octylamine.

Cd precursor	Amine	Peaks
Cd(acetate)$_2$ in OTA +	-	353-373 nm (broad)
	OTA	353-373 nm (broad)
	OLAm	351-373 nm
Cd(acetate)$_2$ in OLAm +	-	449 nm
	OTA	449 nm; 351-371 nm
	OLAm	449 nm
Cd(acetate)$_2$ in OTA:OLAm +	-	351-373 nm
	OTA	353-373 nm (broad)
	OLAm	351-373 nm

Table 4.6. Composition of the solutions obtained using different Cd(acetate)$_2$ precursors. In each sample, 0.1mL of TOP-Te 0.01M in TOP were used as the chalcogenide precursor. The same molar amount of amine was added in each case (0.605 mmol). The color code indicating which amine was added refers to the UV-Vis spectra shown in Figure 4.34.

The samples were prepared using the same procedure described for the low amine concentration solution (see Section 4.1.1), varying the amine that was added every time.
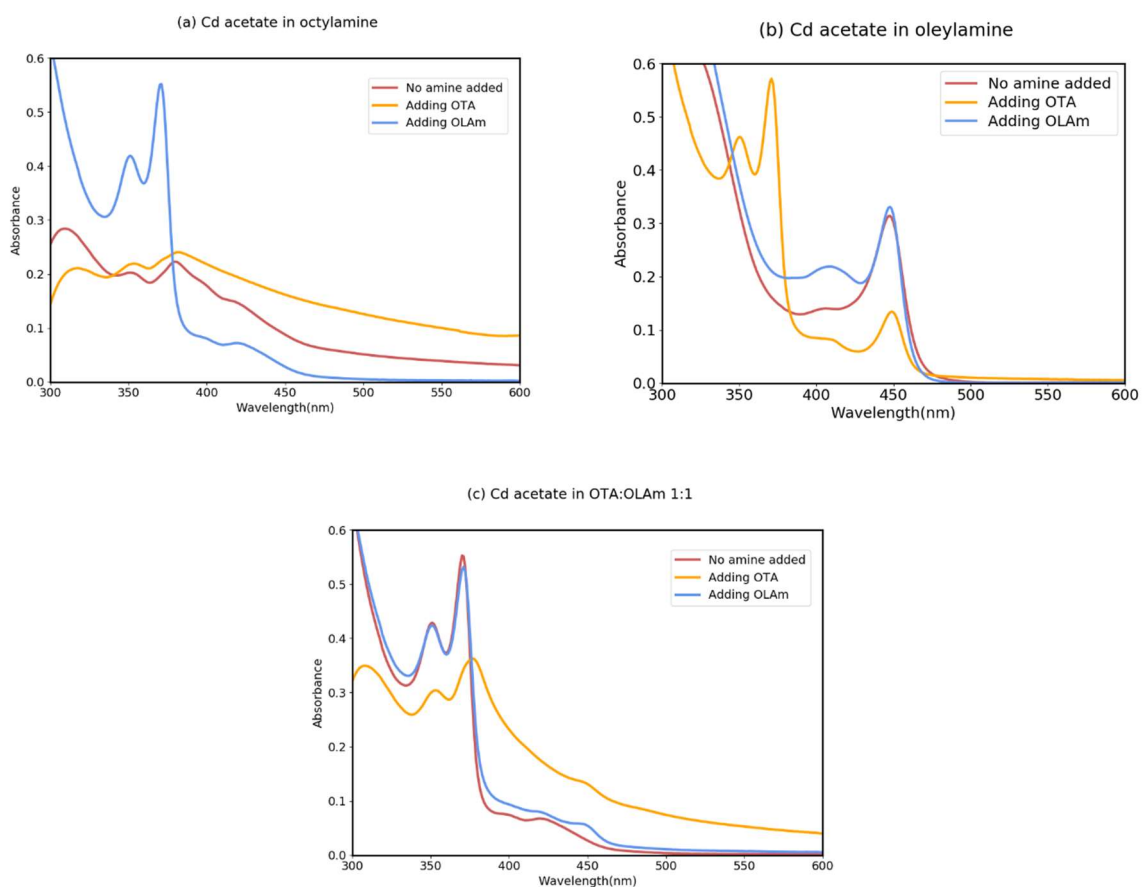
Figure 4.34. UV-Vis spectra obtained using different Cd acetate precursors and adding different amines, as reported in Table 4.6. They were acquired after 48 hours from preparation, since soon after mixing all samples displayed the same single peak at 449 nm.

In all cases, the peak at 449 nm, observed in Section 4.1.1 with the low amine concentration in solution, is the first to arise in the UV-Vis spectra, while the features displayed in Figure 4.34 evolve only over time, with different kinetics depending on the precursor or amine added. It is evident how the presence of *both* octyl- and oleylamine is necessary in order to observe a doublet of two sharp peaks at ~ 351-373 nm, while in the samples containing only octylamine, the same feature is disguised by a strong scattering background. Interestingly, the presence of exclusively oleylamine in solution prevents the formation of the sharp double peak, as confirmed in the red and blue UV-Vis spectra in Figure 4.34b, which only display the feature at 449 nm.
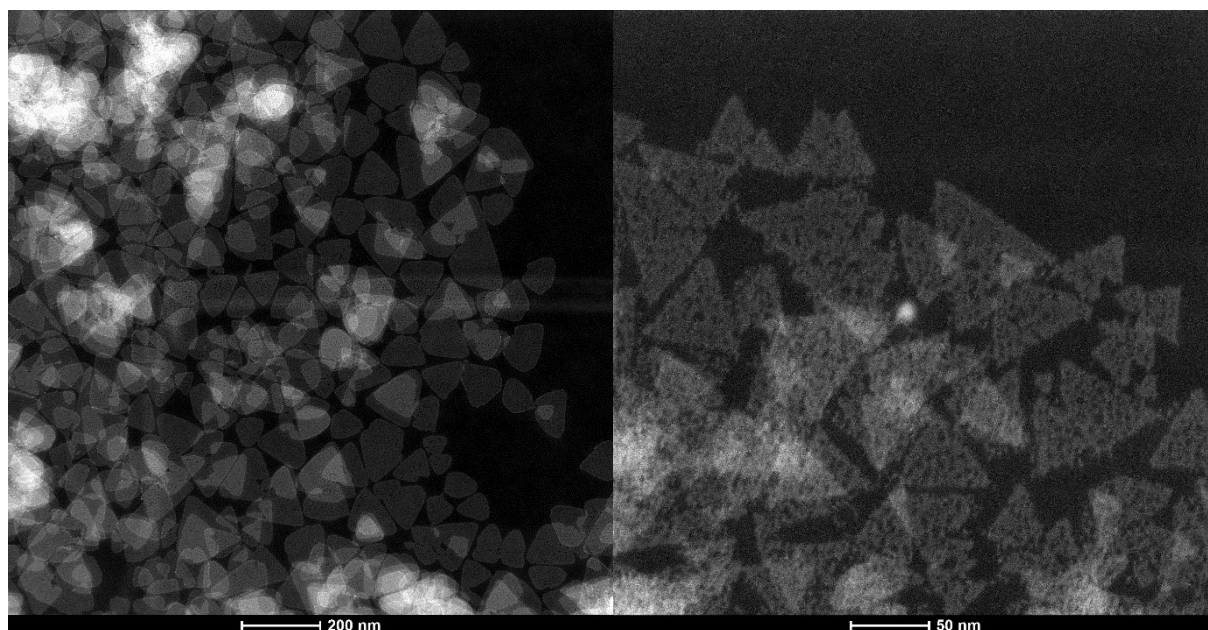
When Cd(acetate)$_2$ dissolved in octylamine was used, the addition of another 0.1 mL of octylamine (Figure 4.34a, orange spectrum) originates in the UV-Vis spectrum a strong scattering background and only a slightly visible double peak at 353-373 nm. In Section 4.1.6, this was attributed to the formation of large superstructures of stacked triangular nanosheets, arranged in flowers which further assemble in "nanobrushes" (Figure 4.35; see also Figure 4.31a, Section 4.1.6)
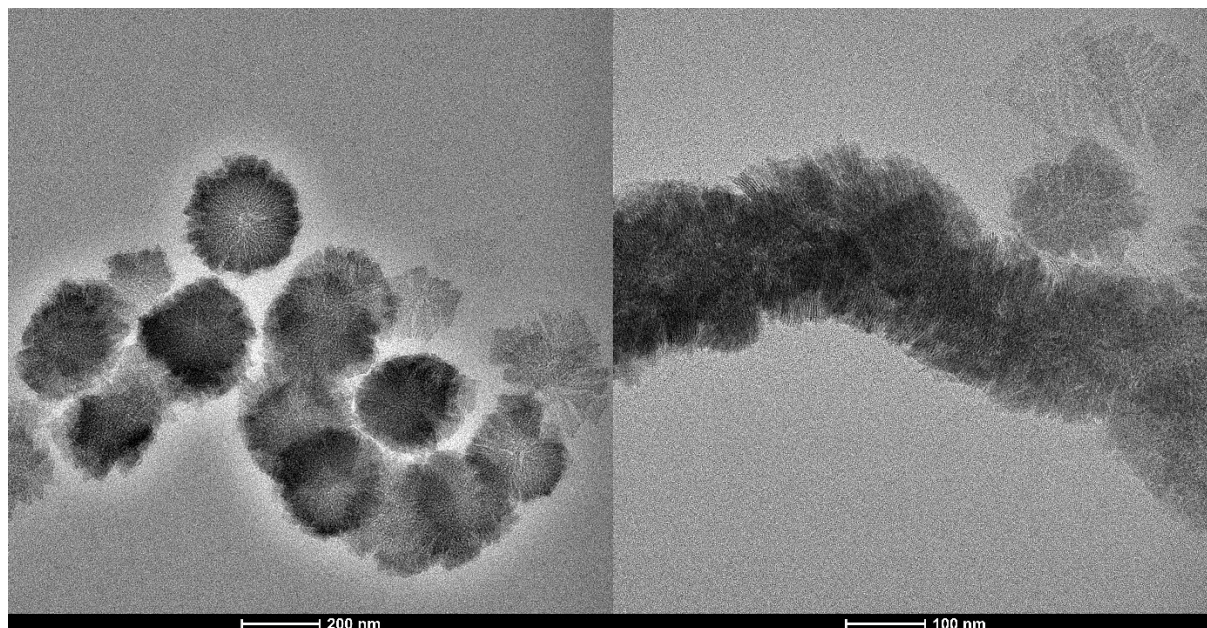

Figure 4.35. TEM images of the sample containing Cd(acetate)$_2$ dissolved in octylamine, in addition of octylamine (orange spectrum, Figure 4.34a).

A sample containing the same Cd precursor (Cd acetate dissolved in octylamine) was prepared, but adding 0.1 mL of oleylamine, to check if the spontaneous assembly of the nanosheets into nanobrushes could be prevented by the unfavorable packing interactions between the different amine ligands. The resulting solution appears clear and has a pale yellow color; its corresponding UV-Vis spectrum (Figure 4.34a, blue spectrum) displays a more evident double peak, around 371-351 nm, without any scattering background. The TEM images reveal that the sample is composed of separated triangular nanosheets, all lying flat on the grids, showing very high e-beam sensitivity. The azimuthally integrated electron diffraction (ED) pattern of the nanosheets can be assigned to CdTe wurtzite crystal structure, although the principal reflections fall at slightly higher q-

values, indicating that the interplanar distances are smaller than in bulk wurtzite CdTe (Figure 4.37).

Figure 4.36. TEM images of the sample containing $Cd(acetate)_2$ dissolved in octylamine, in addition of oleylamine (blue spectrum, Figure 4.34a).
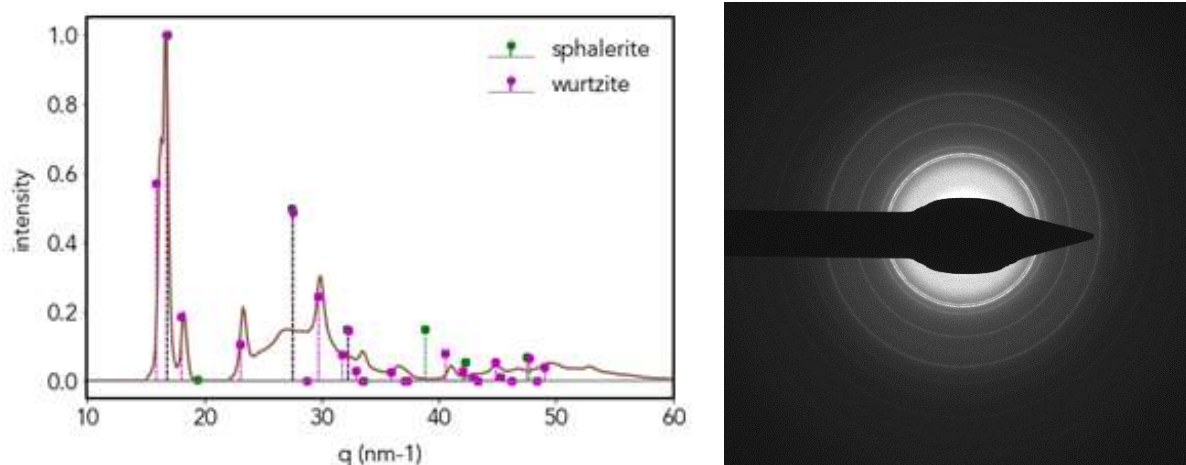
Figure 4.38. Azimuthally integrated electron diffraction (ED) pattern of the nanosheets shown in Figure 4.36.

The sample corresponding to the red spectrum in Figure 4.34a was prepared without further addition of amine, besides the amount present with the Cd precursor. It still displays a strong scattering background in the region in which the double peak attributed

to the nanosheets arises, displaying a broader feature. In the same way as it was observed in Figure 4.35, the TEM images obtained from the sample (Figure 4.38) show the presence of nanobrushes, in which the singular triangular nanosheets composing them are even less distinguishable.
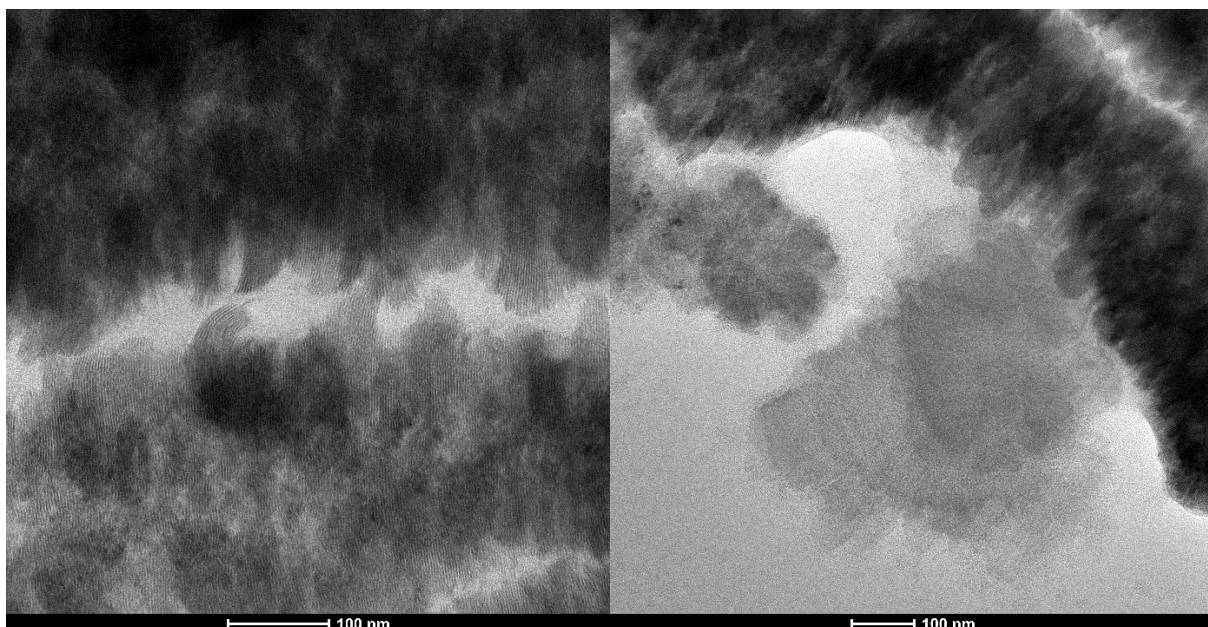

Figure 4.38. TEM images of the sample containing Cd(acetate)$_2$ dissolved in octylamine, without any further addition of amine (red spectrum, Figure 4.34a).

These results clearly indicate that in the presence of only octylamine in solution, the nanosheets readily aggregate, while in addition of oleylamine, they are clearly visible and spaced between each other.

In conclusion, with all three Cd acetate precursors used, the sharp double peak at ~ 351-373 nm in the UV-Vis spectra attributed to the triangular nanosheets, is clearly visible only when both octylamine and oleylamine are present in solution. In particular, using an excess of octylamine seems to further increase the intensity of the nanosheets feature, as shown in Figure 4.39.
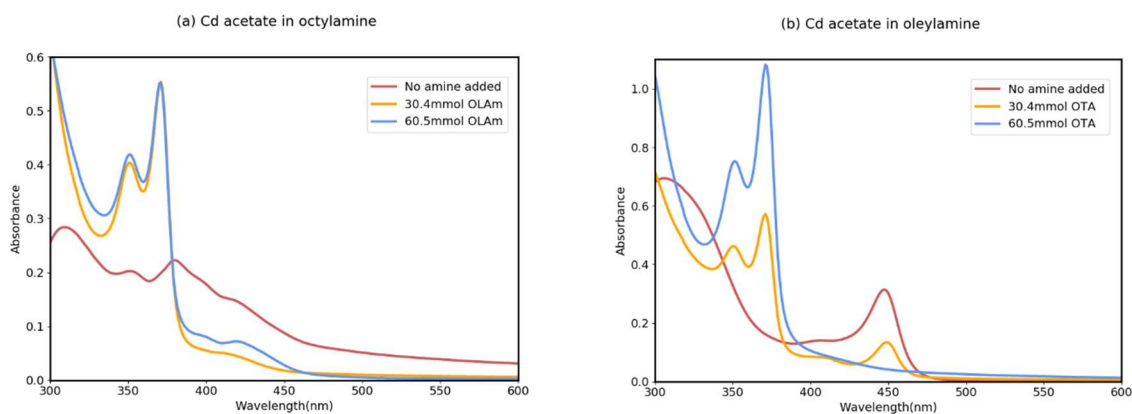
Figure 4.39. UV-Vis spectra showing the effects of the addition of increasing amounts of amine to the two samples displaying the nanosheets feature.

In order to verify that the effect of oleylamine on the evolution of 2D structures is to be attributed to its different length compared to octylamine, and not to the presence of a double C=C bond at position 9,10 of its alkyl chain, the same solution corresponding to the blue spectrum in Figure 4.34a was prepared, but in addition of octadecylamine (ODA), a saturated alkyl amine with the same chain length (C18) as octylamine. The UV-Vis spectra displayed in Figure 4.40 confirm the same behavior observed above, in which the 449 nm single peak arises shortly after preparation and evolves in a sharp doublet at ~ 351-373 nm only over time. This result demonstrates that the formation of separated nanosheets is to be ascribed to the presence of amines of different length, rather than to the nature of the alkyl chain thereof.
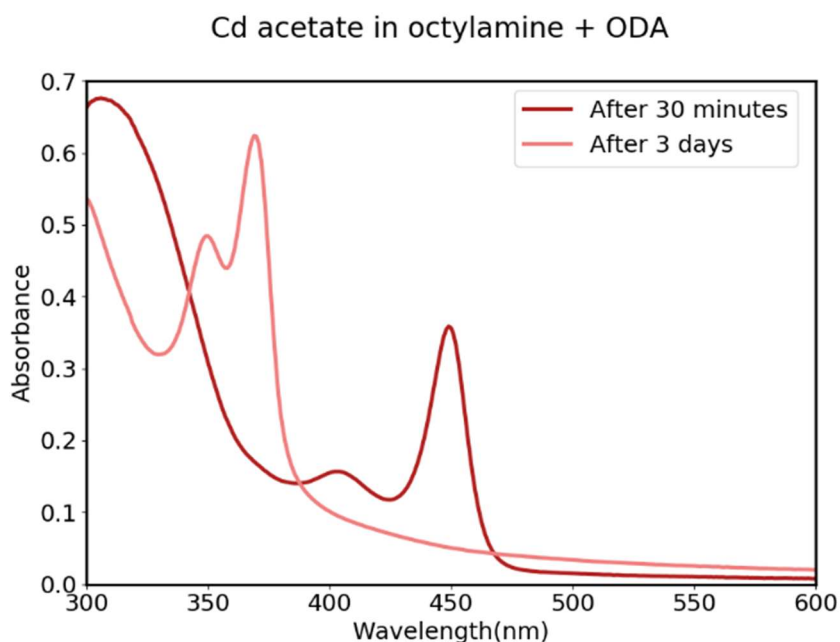
Figure 4.40. UV-Vis spectra of the solution corresponding to the blue spectrum in Figure 4.34a, in addition of octadecylamine instead of oleylamine.

To further support what was discussed in Section 4.1.6 regarding the polarity of the system, which plays an important role in determining the formation of 2D structures, three solutions corresponding to the red spectra in Figure 4.34 a, b, c (no amine added) were prepared in different solvents. In comparison to toluene (dielectric constant 2.38 at 25°C), octadecene (ODE) and hexane were chosen due to their lower polarity (dielectric constants 2.14 (22°C) and 2.09 (25°C) respectively). In both cases, the evolution into superstructures, identified by an increase in turbidity of the solutions, was found to happen more quickly. As reported in Figure 4.41, performing the reaction in ODE gives rise to a double peak with all the three Cd precursors, with a slower kinetic in presence of only oleylamine. In the case of hexane, a remarkable difference can be noticed when only octylamine is present compared to the sample containing both octylamine and oleylamine: in the first case, an increase of scattering background is visible, demonstrating that the nanosheets are preferably assembled in bigger structures, while the addition of oleylamine causes a drastic decrease in scattering background and the double peak appears very sharp, to indicate a lower tendency of the nanosheets to form stacks. Interestingly, in presence of only oleylamine, the nanosheets feature is only slightly visible in the light red spectrum, requiring probably even longer reaction times

to be clearly distinguishable. It is worth to notice that, when toluene was used as solvent, the corresponding solution did not display the double peak feature (Figure 4.34b, red spectrum).
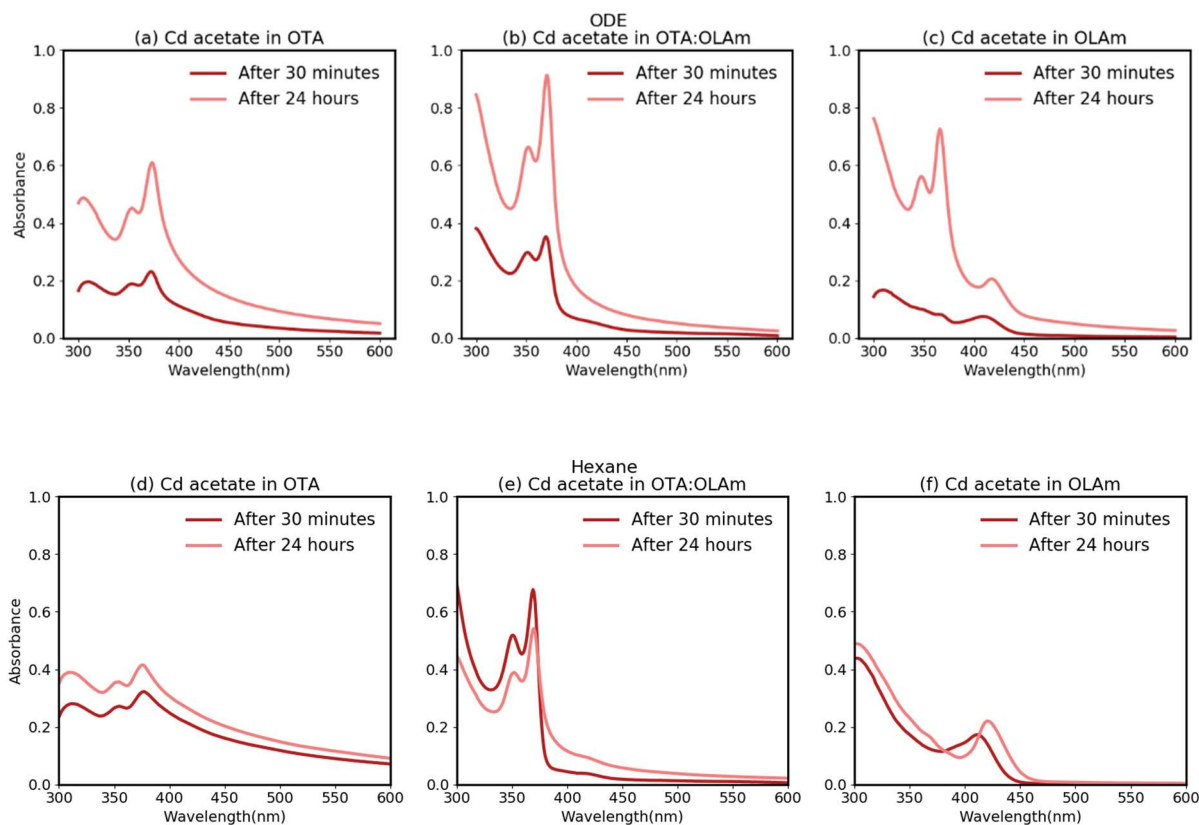
Figure 4.41. UV-Vis spectra displaying the effects of using ODE (a, b, c) and hexane (a, b, c) as solvents for the solutions with the different Cd precursors.

TEM images of the samples in Figure 4.43d and e were obtained, in which hexane was used as the solvent in presence of only octylamine and of both octyl- and oleylamine, respectively (Figure 4.42).
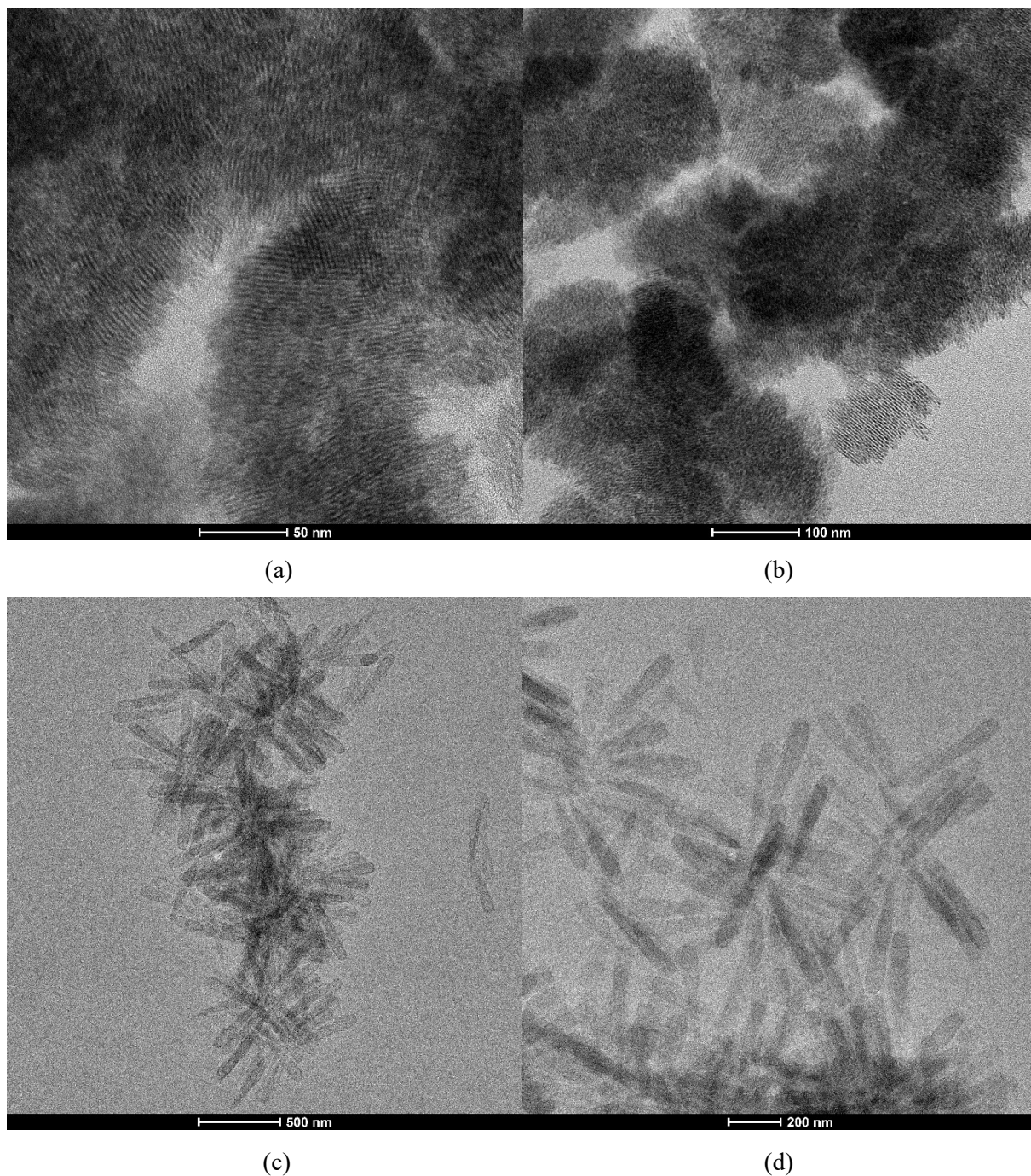
Figure 4.42. TEM images of the sample in which hexane was used as the solvent, in presence of only octylamine (a, b) and of both octyl- and oleylamine (c, d).

Similar to was observed above for toluene, large assemblies are observed in the sample containing only octylamine (Figure 4.42a, b), but in this case the stacked nanosheets seem to further aggregate in many different directions. In presence of both octyl- and oleylamine, the TEM images display separated nanosheets with a more elongated shape compared to the triangles observed in toluene (Figure 4.42c, d). They tend to connect

towards the tips, forming "nanoflowers" which eventually further assemble into bigger structures.

In conclusion, 2-dimensional structures were observed to evolve with a faster kinetic in less polar solvents compared to toluene, nevertheless giving rise to the same absorption features. Large aggregates were still found responsible for an increase of scattering background in presence of octylamine, while the addition of oleylamine led to the formation of separated nanosheets of a different morphology, but featuring the same sharp double peak at ~ 371-373 nm.

5. Conclusions

In this Thesis, a facile room temperature synthesis procedure was employed to gain new insights into the formation mechanism of CdTe magic-sized nanoclusters, as well as into their evolution into 1D and 2D structures. In the reaction system, which includes toluene as solvent, octylamine as primary alkylamine, TOP-Te as chalcogenide precursor and $Cd(oleate)_2$ as metal precursor, concentrations of octylamine ≥ 0.2 M were proved to be essential to observe well-defined, narrow absorption peaks in the UV-Vis absorption spectra. Depending on the concentration of alkylamine, samples giving rise to absorption spectra with peaks maxima at 373, 417 and 449 nm were selectively synthesized, these absorption features having been previously attributed to different CdTe magic-sized clusters.[13] TEM images revealed the presence of 1D nanostructures with a string-like appearance, organized to form bundles of different length and thickness. On the other hand, at lower concentrations of octylamine (*viz.* 0.02 M), the formation of separated $[CdTe]_x$ units is substantiated by broad peaks in the UV-Vis spectra, centered at 440 nm and HAADF-STEM images showing isolated clusters.

Upon dilution, the sharp absorption peaks of the aforementioned samples displayed a stepwise shift to lower energies, which allowed to exclude the attribution of the 1D structures to crystalline CdTe nanowires, and supported instead the previously proposed model of interconnected $[CdTe]_x$ nanoclusters in a tubular, amine-capped mesophase.[18][19][20] The same stepwise redshift was observed when the samples were heated up to 105°C, and even at these temperatures, no formation of quantum dots was observed, which was however noticed to take place from 80°C in the solution containing isolated CdTe clusters. This led to regard the 1D nanostrings of interconnected $[CdTe]_x$ nanoclusters as metastable products resulting from non-classical nucleation and growth pathways, that become available in the presence of high concentrations of alkylamines and allow to circumvent the high energy barrier of classical nucleation of QDs. Reverse peak shift to higher energies, still occurring stepwise if the concentration of alkylamine is progressively increased, further corroborated the hypothesis of interconnected [CdTe] nanoclusters in a tubular mesophase. Therefore, the model proposed for the species

present in solution is that of a hybrid organic-inorganic polymeric-like structure, in which interconnected $[CdTe]_x$ units can modify their structure, relative conformation and orientation in response to the concentration of alkylamine ligands in solution, in order to optimize a complex balance of interactions between: (i) the amine alkyl chains organized in a tubular mesophase, (ii) the amines polar heads and the (possibly variable) surface atoms of the nanoclusters, (iii) the nanoclusters interconnected in the nanostrings. The hypothesis advanced is that, due to the interconversion between optimal configurations of the $[CdTe]_x$ clusters in the nanostrings, they experience different degrees of electronic coupling, which is responsible for the change of band gap manifesting as the shift to different energies of the absorption transitions.

Based on the proposed model, the many parameters involved in the synthesis procedure were investigated, starting from the Cd:Te ratio, which was equal to 2:1 in the standard protocol: it was demonstrated how the addition of increasing amounts of Te precursor leads to the formation of a larger quantity of [CdTe] units in solution, translating in more intense absorption peaks, and that different peaks are stabilized with the same amine concentrations, if different Cd:Te ratios are present in solution. The role of a primary alkylamine was demonstrated to be essential to observe narrow peaks, since secondary and tertiary amines only gave rise to broad peaks; differences in the alkylamine chain length did not appear to have a remarkable effect on the absorption spectra, although they strongly influence the kinetics of formation and the colloidal stability of the nanostrings over time, as a consequence of variations in the strength of the van der Waals interactions. Testing different phosphines for the phosphine-chalcogenide complexes used as Te precursors, allowed to identify a trend in reactivity in which the strength of the bond between Te and the P atoms inversely correlates with the formation rate of CdTe nanoclusters. Additionally, the presence of an excess of non-complexed phosphine was found to be essential for the reaction to take place, demonstrating that one of the key elementary steps in the formation mechanism is the reduction of tellurium (substituting the excess of phosphine with a reducing agent of different nature still allowed the reaction to proceed). The use of different Cd precursors allowed to conclude that $Cd(oleate)_2$ is the most effective in obtaining intense and narrow absorption peaks,

while the use of Cd(acetate)$_2$ led to the formation of larger aggregates in solution, as indicated by the increase in scattering background in the UV-Vis spectra and by the TEM images. Additional experiments demonstrated that the polarity of the system plays a major role in the evolution of superstructures, and the use of less polar solvents accelerates the process. To further emphasize the importance of the solvent polarity, it was found that similar structures were obtained when Cd(oleate)$_2$ was used as precursor, and the synthesis was performed in solvents with lower polarity than toluene, such as octadecene or hexane. In any case, these superstructures consisted of self-assembled nanosheets (as unraveled by TEM) and their presence is always signaled by a doublet of narrow absorption peaks (351 and 373 nm), alongside an increased scattering background.

The formation of 2D structures and their tendency to self-assemble were then investigated using Cd(acetate)$_2$ in the presence of varying volumes of two amines of different alkyl chain length, octylamine (C-8) and oleylamine (C-18), in toluene. When only octylamine was present, the large aggregates of stacked nanosheets mentioned above were found in the TEM images, while with only oleylamine, the evolution of 2D structures was not observed. Interestingly, the co-presence of both amines led to the formation of free-floating triangular nanosheets, with wurtzite crystal structure, whose corresponding absorption spectrum showed a narrow doublet at ~ 351-373 nm.

In conclusion, the observations made in this experimental work allowed to propose a new model involving non-classical nucleation and growth pathways for the formation of interconnected CdTe nanoclusters, organized in 1D nanostrings and stabilized by a tubular alkylamine mesophase. Additional studies, such as theoretical simulations addressing the actual structure of the mesophase as a function of the concentration of alkylamine, the different possibilities of interconnections of $[CdTe]_x$ cluster units inside it, the consequences of different degrees of electronic coupling on the absorption spectra, would all contribute to strengthen this attribution. The role of the different parameters involved in the synthesis procedure requires to be further rationalized, to fully elucidate the elementary steps involved in the formation mechanism of MSCs. Moreover, since

one of the central unknown for MSCs is their exact size, analytical methods such as time-of-flight mass spectrometry (TOF-MS) could be useful, even if mild ionization methods would be needed to avoid fragmentation and/or decomposition of the samples. Taking advantage of the MSCs reduced size (molecule-like), nuclear magnetic resonance (NMR) techniques could offer important details on both the core and the surface of the MSC: unlike diffraction techniques, NMR does not require a crystalline material to obtain information regarding the cluster structure, although small-angle X-ray scattering (SAXS) has been already shown to be useful, especially when synchrotron radiation is available.[27]

The observed evolution of MSCs into triangular nanosheets at room temperature represents a promising research topic, which deserves further attention. The origin of this very unusual morphology for semiconductor nanosheets, and the reason behind the observed blueshift of the absorption features as a consequence of the conversion of 1D nanostrings into 2D nanosheets demand additional investigation and theoretical support. Their optoelectronic properties also need to be thoroughly investigated, for example by low temperature photoluminescence spectroscopy, since the nanosheets do not show radiative recombination at room temperature. This is possibly caused by the presence of surface trap states, that could be "passivated" by overgrowing the CdTe nanosheets with an epitaxial shell of a larger-band gap semiconductor.

References

[1] Kovalenko, M. V.; Manna, L.; Cabot, A.; Hens, Z.; Talapin, D. V.; Kagan, C. R.; Klimov, V. I.; Rogach, A. L.; Reiss, P.; Milliron, D. J.; et al. **Prospects of Nanoscience with Nanocrystals.** *ACS Nano* 2015, 9, 1012−1057.

[2] Novoselov, K. S.; Geim, A. K.; Morozov, S. V.; Jiang, D.; Zhang, Y.; Dubonos, S. V.; Grigorieva, I. V.; Firsov, A. A. **Electric Field Effect in Atomically Thin Carbon Films**. *Science* 2004, 306, 666−669.

[3] Peng, Z. A.; Peng, X. **Nearly Monodisperse and Shape-Controlled CdSe Nanocrystals via Alternative Routes: Nucleation and Growth.** *J.Am. Chem. Soc.* 2002, 124, 3343−3353.

[4] Harrell, S. M.; McBride, J. R.; Rosenthal, S. J. **Synthesis of Ultrasmall and Magic-Sized CdSe Nanocrystals** *Chem. Mater*. 2013, 25, 1199−1210.

[5] C. de Mello Donegà. **Nanoparticles.** Springer-Verlag Berlin Heidelberg, 2014.

[6] Groeneveld, E.: **Synthesis and optical spectroscopy of (hetero)-nanocrystals.** Ph.D. Thesis, Utrecht University, Utrecht, 2012.

[7] J. Lee, J. Yang, S. G. Kwon, T. Hyeon, **Nonclassical nucleation and growth of inorganic nanoparticles**. *Nature Reviews Materials*, 2016, 1, 16034.

[8] S. Kudera M. Zanella C. Giannini A. Rizzo Y. Li G. Gigli R. Cingolani G. Ciccarella W. Spahl W. J. Parak L. Manna. **Sequential growth of magic-size CdSe nanocrystals.** *Adv. Mater.* 19, 2007, 548–552.

[9] C. de Mello Donegá and R. Koole. **Size Dependence of the Spontaneous Emission Rate and Absorption Cross Section of CdSe and CdTe Quantum Dots.** *J. Phys. Chem. C* 2009, 113, 16, 6511–652.

[10] Y. Zhou, R. Jiang, Y. Wang, H. W. Rohrs, N. P. Rath, and W. E. Buhro. **Isolation of Amine Derivatives of $(ZnSe)_{34}$ and $(CdTe)_{34}$. Spectroscopic Comparisons of the $(II−VI)_{13}$ and $(II−VI)_{34}$ Magic-Size Nanoclusters.** *Inorg. Chem.* 2019, 58, 1815−1825.

[11] C. Palencia, K. Yu, and K. Boldt. **The Future of Colloidal Semiconductor Magic-Size Clusters.** *ACS Nano* 2020, 14, 2, 1227–1235.

[12] Schiener, A.; Magerl, A.; Krach, A.; Seifert, S.; Steinru¨ck, H. G.; Zagorac, J.; Zahn, D.; Weihrich, R. **In situ Investigation of Two-Step Nucleation and Growth of CdS Nanoparticles from Solution**. *Nanoscale*, 2015, 7, 11328−11333.

[13] C. Luan, J. Tang, N. Rowell, M. Zhang, W. Huang, H. Fan, and K. Yu. **Four Types of CdTe Magic-Size Clusters from One Prenucleation Stage Sample at Room Temperature**. *J. Phys. Chem. Lett.* 2019, 10, 4345−4353.

[14] C.B. Williamson, D.R. Nevers, A. Nelson, I. Hadar, U. Banin, T. Hanrath, R.D. Robinson, **Chemically Reversible Isomerization of Inorganic Clusters**. *Science* 363, 731, 2019.

[15] B. Zhang, T. Zhu, M. Ou, N. Rowell, H. Fan, J. Han, L. Tan, M. T. Dove, Y. Ren, X. Zuo, S. Han, J. Zeng and K. Yu. **Thermally-induced reversible structural isomerization in colloidal semiconductor CdS magic-size clusters.** *Nature Communications* 9, 2499, 2018.

[16] Nelson, P. N.; Taylor, R. A. **Theories and experimental investigations of the structural and thermotropic mesomorphic phase behaviors of metal carboxylates.** *Appl. Petrochem. Res*. 2014, 4, 253−285.

[17] Y.H. Liu, F. Wang, Y. Wang, P. C. Gibbons, and W. E. Buhro. **Lamellar Assembly of Cadmium Selenide Nanoclusters into Quantum Belts.** *J. Am. Chem. Soc*. 2011, 133, 42, 17005–17013.

[18] Nevers, D. R.; Williamson, C. B.; Savitzky, B. H.; Hadar, I.; Banin, U.; Kourkoutis, L. F.; Hanrath, T.; Robinson, R. D. **Mesophase Formation Stabilizes High-purity Magic-sized Clusters**. *J. Am. Chem. Soc.* 2018, 140, 3652−3662.

[19] Hsieh, T.-E.; Yang, T.-W.; Hsieh, C.-Y.; Huang, S.-J.; Yeh, Y.-Q.; Chen, C.-H.; Li, E. Y.; Liu, Y.-H. **Unraveling the Structure of Magic-Size (CdSe)$_{13}$ Cluster Pairs**. *Chem. Mater.* 2018, 30, 5468−5477.

[20] Wurmbrand, D.; Fischer, J. W. A.; Rosenberg, R.; Boldt, K. **Morphogenesis of Anisotropic Nanoparticles: Self-Templating via Non-classical, Fibrillar Cd$_2$Se Intermediates.** *Chem. Commun.* 2018, 54, 7358−7361.

[21] Y. Wang, Y. Zhang, F. Wang, D. E. Giblin, J. Hoy, H. W. Rohrs, R. A. Loomis, and W. E. Buhro. **The Magic-Size Nanocluster (CdSe)34 as a Low-Temperature**

Nucleant for Cadmium Selenide Nanocrystals; Room-Temperature Growth of Crystalline Quantum Platelets. *Chem. Mater*. 2014, 26, 2233−2243.

[22] F. Wang, Y. Wang, Y.H. Liu, P. J. Morrison, R. A. Loomis, and W. E. Buhro. **Two-Dimensional Semiconductor Nanocrystals: Properties, Templated Formation, and Magic-Size Nanocluster Intermediates.** *Acc. Chem. Res.* 2015, 48, 13−21.

[23] B. M. Cossairt and J. S. Owen. **CdSe Clusters: At the Interface of Small Molecules and Quantum Dots.** *Chem. Mater.* 2011, 23, 3114–3119.

[24] F. S. Riehle, R. Bienert, R. Thomann, G. A. Urban, and M. Kruger. **Blue Luminescence and Superstructures from Magic Size Clusters of CdSe.** *Nano Letters* 2009, Vol. 9, No. 2, 514-518.

[25] K. Yu, X. Liu, Q. Y. Chen, H. Yang, M. Yang, X. Wang, X. Wang, H. Cao, D. M. Whitfield, C. Hu, Y. Tao. **Mechanistic Study of the Role of Primary Amines in Precursor Conversions to Semiconductor Nanocrystals at Low Temperature.** *Angew Chem Int Ed Engl.* 2014, 53(27), 6898-6904.

[26] Y. Wang, Y.-H. Liu, Y. Zhang, F. Wang, P. J. Kowalski, H. W. Rohrs, R. A. Loomis, M. L. Gross, W. E. Buhro. **Isolation of the Magic-Size CdSe Nanoclusters [(CdSe)$_{13}$(*n*-octylamine)$_{13}$] and [(CdSe)$_{13}$(oleylamine)$_{13}$].** *Angew Chem Int Ed Engl*. 2012, 51(25), 6154–6157.

[27] Liu, M.; Wang, K.; Wang, L.; Han, S.; Fan, H.; Rowell, N.; Ripmeester, J. A.; Renoud, R.; Bian, F.; Zeng, J.; Yu, K. **Probing Intermediates of the Induction Period Prior to Nucleation and Growth of Semiconductor Quantum Dots.** *Nat. Commun.* 2017, 8, 15467.